AN ABSTRACT OF THE THESIS OF

Michael A. Delos-Reyes for the degree of Master of Science in Materials Science presented on September 20, 1995. Title: Microstructure and Mechanisms of Cyclic Deformation of Aluminum Single Crystals.

Abstract approved: Redacted for Privacy

Michael E. Kassner

Aluminum single crystals were cyclically deformed in single-slip at small strain amplitudes at 77 K to presaturation. The observed mechanical behavior is consistent with other recent work. The dislocation substructure was analyzed in detail. The structure can be described as consisting of dense bundles or veins of dislocation dipoles, separated by lower dislocation density regions where debris is evident. This debris was determined to be principally relatively short dipole segments. Screw dislocations with the same Burgers vector span the channels. Dislocations were essentially all of the same Burgers vector. *In-situ* cyclic deformation experiments were successfully performed by the X-Y technique where thin foils are stressed in alternating perpendicular directions. Screw dislocations span the channel and easily move and reverse direction with shear reversal. Our experiments indicate that loops frequently expand from the dipole bundles into the channels and the edge component is absorbed by nearby bundles leaving screw segments behind. Dipole "flipping" was not observed and these edges are relatively difficult to mobilize. There is no obvious evidence for internal backstresses that assist plastic deformation on reversal of the applied shear.

Microstructure and Mechanisms of Cyclic Deformation of Aluminum Single Crystals

by

Michael A. Delos-Reyes

A THESIS

submitted to

Oregon State University

in partial fulfillment of
the requirements for the
degree of

Master of Science

Completed September 20, 1995
Commencement June 1996

Master of Science thesis of Michael A. Delos-Reyes presented on September 20, 1995

APPROVED:

Redacted for Privacy

Major Professor, representing Materials Science

Redacted for Privacy

Chair of Department of Materials Science

Redacted for Privacy

Dean of Graduate School

I understand that my thesis will become part of the permanent collection of Oregon State University libraries. My signature below authorizes release of my thesis to any reader upon request.

Redacted for Privacy

Michael A. Delos-Reyes, Author

TABLE OF CONTENTS

TABLE OF CONTENTS (CONTINUED)

LIST OF FIGURES

LIST OF FIGURES (CONTINUED)

LIST OF APPENDICES

Appendix Page

Microstructure and Mechanisms of Cyclic Deformation of Aluminum Single Crystals

INTRODUCTION

Since the evolution of metals as important engineering materials, the expectation of worry-free performance has been high. Starting with train trusses made of iron, metal failures began to have a large economic impact. Consequently, research efforts were initiated in order to attempt to understand and prevent metal failures. Of the modes of failure studied, the least well understood is called fatigue.

The term fatigue comes from the Latin *fatigare*, meaning to weary. This was an appropriate name for the particular type of failure, because it was often evidenced after the material had been in service (under load) for a while (days or even years), i.e., after the material had become "tired". In addition, it was not possible to predict when a fatigue failure would occur. Thus, an increased understanding of fatigue behavior was needed.

The need for fatigue research is not *only* historical. For example, presently the airline industry is *very* interested in fatigue failure. The reason for this is that fatigue failure is the second leading cause of airline fatalities (Figure 1). Only pilot error causes more fatalities. This is only one of many current examples of the importance of fatigue today.

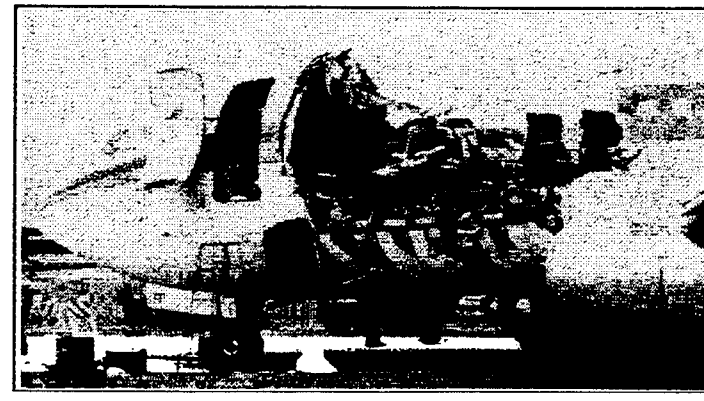

Figure 1. A catastrophic plane wreck that may have been due to fatigue failure of a fuselage joint.

One of the most direct means for gaining an

understanding of fatigue, is to study fatigued single crystals of metal. By understanding the simplest case of single-slip in a single crystal, we may extend our understanding to the more complicated case of slip in polycrystals. This type of study has yielded a lot of information about fatigue, especially with respect to understanding fatigue phenomenologically. For example, in the process of cyclically loading face centered cubic (FCC) metals, it is now understood that there is initially a rapid hardening followed by a "steady-state" deformation (very little change in applied stress for a strain controlled test), and then a gradual but (possibly) prolonged secondary hardening stage. This behavior is common to the FCC metals studied to date. Another phenomenon observed in fatigue studies is the "Bauschinger Effect," where a material exhibits an apparent "weakening" for stress in one direction after loading in the reverse direction.[1,2] It has also been noted that if the imposed plastic strain amplitude is large enough, and if deformation proceeds sufficiently, persistent slip bands (PSBs) may form in the material. These are believed to facilitate surface degradation, crack formation and ultimate failure. The above behaviors are some of the phenomena that require definite explanations.

An understanding of fatigue behavior must come from an analysis of dislocation behavior in reversed deformation.[3] Dislocations are the line defects that occur in crystalline materials. Motion of dislocations

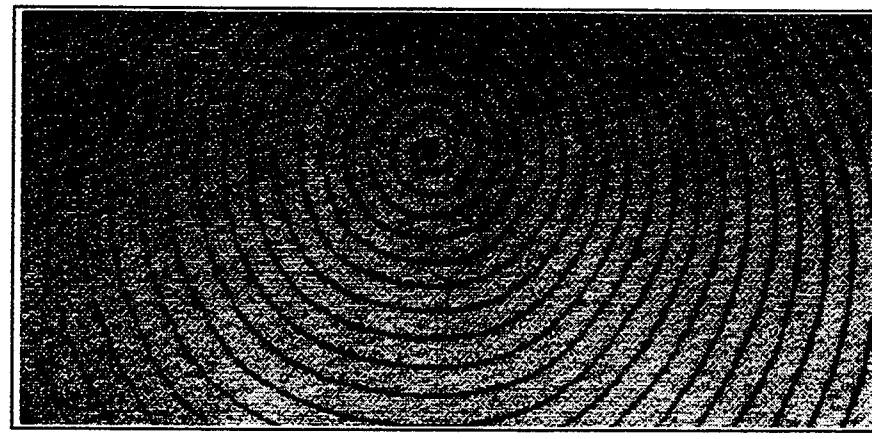

Figure 2. Transmission electron microscope (TEM) image of a growth screw dislocation in NaCl.

is permanent deformation (plasticity) in metals. Static micrographs of dislocation arrangements (by transmission electron microscopy, TEM) have been analyzed for static, monotonic, as well as cyclically deformed materials, such as in Figure 2 (for an example of a static TEM image). Much has been learned about the role of dislocations in fatigue from TEM. For example, the evolution of dislocation structures into dislocation tangles, walls, cells, ladders, and macrobands has been described phenomenologically (while the exact mechanisms are still being determined). While phenomenological descriptions based on static images are very useful, there *is* missing information. What happens between each frame? How did the dislocations rearrange from one photo to another? What is the *mechanism* that controls the dislocation motion? And, how can we attempt to reduce the likelihood of fatigue failure with the answers to these questions? What is needed, then, is to study the dislocation dynamics by in-situ experiments in which we will "watch" the dislocations move, and rearrange. One objective of this work is to better understand cyclic deformation by observing dislocation reversal *directly* (in-situ), in the high voltage electron microscope (HVEM).

The reason that definitive work of this type has not been done previously, is because of the difficulty in cyclically deforming an electron transparent thin film that allows effective imaging of dislocations in an HVEM. Difficulties have arisen from buckling of the sample with stress (or strain) reversal; complicated stress states due to sample perforation; and not being able to isolate the primary slip system. The in-situ "stage" (device which holds, and deforms the sample in the HVEM) which we used to overcome these difficulties was built by M.L. Tech, of Stockton, CA. The latest in-situ stage was an improvement of an earlier stage that uses the unique "X-Y" deformation. The X-Y technique will be described subsequently, and was successfully demonstrated using the HVEM at TNO, Apeldoorn, the Netherlands in our previous work.[4]

BACKGROUND

General Fatigue

As was mentioned in the introduction, the problem of fatigue is of substantial importance, and much has been learned in the last century. Fatigue generally refers to the repeated application of a relatively low load or stress to a material. This repeated, or cyclic loading may require anywhere from several hundred to several million cycles to cause fatigue failure. In most research of fatigue, the stress or strain is controlled, and is repeated exactly in each cycle--for example, pushing and then pulling on a sample with 500 MPa of stress in every cycle would be a "stress controlled" test. This is typically plotted on a cyclic hardening curve. Most metals exhibit a behavior similar to that in Figure 3, where they harden rapidly under the applied cyclic stress or strain for the first small fraction of its life; then a large portion of the fatigue life may be spent in a "saturation" regime where there is little hardening or softening; then, (if the material is still intact) the sample will undergo a second hardening stage until it finally breaks.

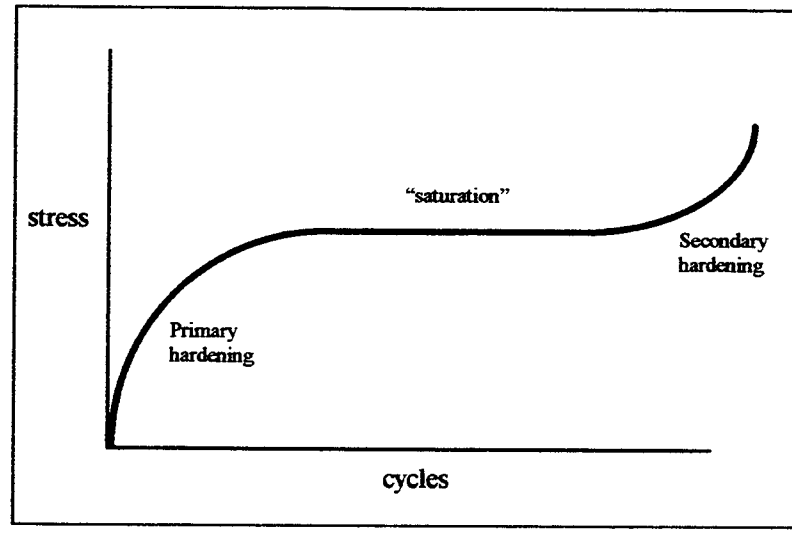

Figure 3. Schematic of a cyclic hardening curve (strain controlled test).

In the above cyclic hardening sequence, the deformation is accommodated in different ways in each of the three regimes described. Deformation in the primary hardening stage

is generally accommodated by dislocation motion where the dislocations arrange into ordered structures, and the deformation is uniform on a macroscopic scale throughout the sample. The beginning of the "saturation" stage is characterized by the onset of localization of deformation. At this point, the slip (deformation) may be occurring almost entirely in narrow slip bands. As the cycling continues, the initial slip bands harden, and other slip bands are created to accommodate additional slip. Once the entire sample is filled with these slip bands, the sample starts to harden again, i.e., secondary hardening begins. Slip during secondary hardening is generally characterized by slip occurring in systems other than the primary slip systems. As the material moves from slip on secondary slip systems to slip on tertiary slip systems etc., slip becomes much more difficult. Materials eventually fail in this secondary hardening stage if cycling is continued.

Metal failure in fatigue is usually associated with local surface imperfections. It has been observed that the slip bands may form "steps" (intrusions and extrusions) at the sample surface due to slip irreversibility.[5] These imperfections can lead to crack formation, and ultimately, to sample failure.

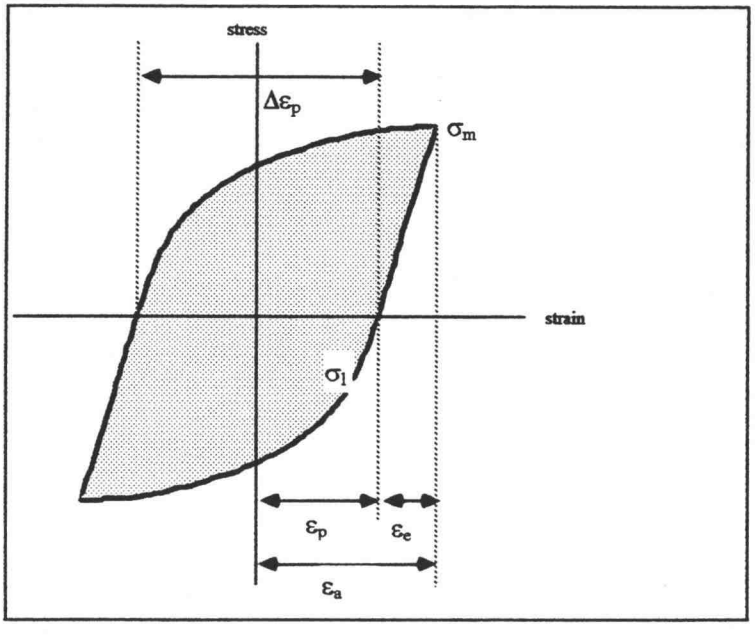

Figure 4. A typical hysteresis loop for response of a material to a plastic strain controlled fatigue test. ε_p is the plastic strain, ε_e is the elastic strain, ε_a is the strain amplitude, and $\Delta\varepsilon_p$ is the plastic strain range.

Descriptions of fatigue will invariably involve hysteresis loops. Hysteresis loops are a plot of a material's response

to a cyclic stress or strain. A typical hysteresis loop is shown in Figure 4. The hysteresis loop is useful for describing the mechanical response of a material because it offers a graphical representation of the stress and strain (or plastic strain) in a given cycle. As fatigue proceeds, changes may take place in the shape of the hysteresis loops which reflect microstructural changes in the material. The Bauschinger effect is also evident from the hysteresis loops. After the sample has been loaded in one direction up to a maximum stress σ_m we would expect (based on isotropic hardening) it to yield at σ_m in the reverse loading direction, but it does not. Instead, it yields at some stress σ_1 much less than σ_m. This is the Bauschinger effect, and is one important element of cyclic deformation that has been difficult to explain in terms of dislocation mechanics.

Face Centered Cubic Materials

Much of the pioneering work in understanding fatigue of FCC metals, has been performed on copper. In addition, there has been work performed on silver,[6] nickel[7], magnesium, zinc (hcp)[8,9] and aluminum[2]. While the behaviors of these materials are generally analogous, it has been

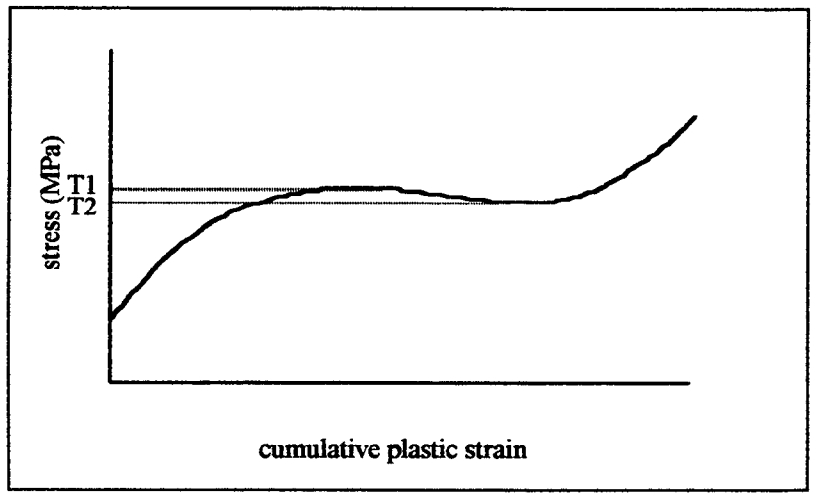

Figure 5. Cyclic hardening curve which demonstrates softening after the initial hardening.

noted that there are distinct differences.* For instance, under identical fatigue conditions, many of these metals exhibit a plateau stress (T1-T2 ≅ 0, in Figure 5), while others may not. Instead, they may exhibit a "secondary softening," with T1-T2 > 0 in Figure 5. Additionally, each metal has a different stacking fault energy (SFE): with copper having a relatively low SFE (40 erg/cm^2), and aluminum having a relatively high SFE (140 erg/cm^2).[18,19] The SFE is significant as it determines the material's propensity to cross-slip. A material, aluminum or nickel, with a high SFE, will be more likely to have slip occur on a secondary slip plane (cross-slip) in addition to the primary slip plane; while a material, copper or silver, with a low SFE, would be more likely to confine slip to the primary slip plane.[20] This will, in turn, affect the observed dislocation arrangements.[7,21] While some materials (e.g., copper) exhibit veins, walls, ladders cells, and labyrinths in their dislocation structures, others (e.g., aluminum) may have veins, walls, cells macrobands (no ladders) and "lattices."[22] Cumulative plastic strains at which these different microstructures occur is also different from material to material--see Figure 6.[23,24] One final difference worth noting, is the melting temperatures of each metal. This can be important when considering thermally activated processes.[18,25,26,27,28,29,30] For example, when a material is fatigued, and dislocation structures form (e.g., cells), there is a driving force for the dislocations to spontaneously rearrange (into a lower energy configuration), that is related to the temperature of the material relative to its melting temperature.[20,22] *

---

* (There are several good reviews of fcc fatigue deformation, e.g., Erber1993[10], Basinski and Basinski, 1992[11], Mughrabi 1985[12] and 1986[13], Laird 1983[14], Neumann 1983[15], Kuhlman-Wilsdorf and Laird 1977[16], Grosskreutz 1971[17].)

* Basinski and Basinski[31] have reviewed the effect of temperature on fatigue in copper single crystals.

Copper

Aside from the differences between what is known about the behaviors of copper and aluminum, it may be useful to review here some of the prevailing theories, and observations in the fatigue of copper. Cyclic hardening is generally observed, with a plateau in stress following the initial hardening, and failure eventually follows. The plateau or saturation region is observed for plastic shear strain amplitudes $10^{-4} < \gamma_p < 10^{-3}$. It has been observed,[32,33,34] however, that copper can achieve a prolonged secondary hardening stage if the material is fatigued under the proper conditions (large enough plastic strain and/or high-vacuum). The distinction between primary and secondary hardening becomes moot when $\varepsilon_p > 5x10^{-2}$ when there is not a saturation plateau.[32] It is generally believed that secondary hardening is due to slip on secondary slip systems (cross slip).[35] The cyclic hardening behavior has also been related to the dislocation structures (which tend to arrange themselves into minimum energy

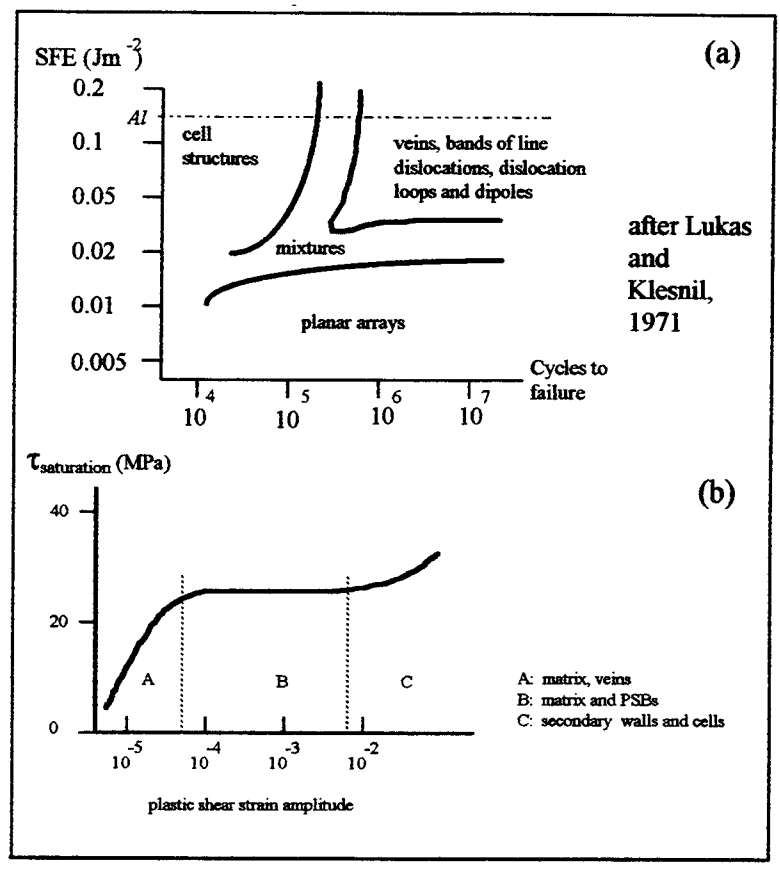

Figure 6. Dislocation structures in face centered cubic metals are found to occur based on (a) stacking fault energy, and (b) plastic strain amplitude (for copper).

configurations.[16,36,37]) [+] For example, in the plateau region, it has been noted that the volume fraction of PSBs varies linearly with accumulated plastic strain, and that slip is localized in the PSBs while straining in the plateau region.[39,40] [*] There has also been evidence presented which appears to show that the progressively higher-energy dislocation structures originate in the center of a specimen, then propagate outward.[42]

The dislocation structures in copper that are associated with the various "degrees of fatigue damage" have been characterized by various techniques. It is generally believed that a heterogeneous vein/channel substructure evolves from dislocation tangles and debris, where the veins are areas of dense dislocation (edge dipole) population. This substructure may eventually decompose into a ladder (or "wall") substructure.[41,42,43,44] Tabata et al [43] found that PSBs were not found in [111] oriented crystals of copper, but were found in [123] oriented crystals. They also found that ladders in the [123] specimens were easily sheared by dislocations in cross slip--but, those same ladders were effective obstacles to primary dislocations. In the [111] samples, the dislocation walls were effective obstacles to all mobile dislocations. Jin and Winter also investigated the directional dependence of cross-slip in copper (see [Jin and Winter[45], and Cheng and Laird[46]]). The ladder structure seems to show up only once the plateau region is reached, and is thought to carry the vast majority of the plastic strain. With the onset of saturation, localized straining is said/seen to occur in "persistent slip bands" which cannot be removed by polishing.[2] Also seen when saturation is started is the change in shape of the hysteresis loop: in copper the hysteresis loop tends to start out somewhat pointed, and changes shape to a more rectangular shape at the onset of saturation (for constant strain, or plastic strain amplitude controlled tests).[41] This is sometimes measured by a "loop factor" (V_h)

[+] Note: The driving force behind forming minimum energy dislocation structures is the reduction of strain energy of the material [Mughrabi[38]].

[*] For a discussion of PSB formation in copper see [Jin[41]; Ackermann[34]].

which is a ratio of loop area to that of a circumscribed rectangle, and can be used as an indication of the onset of strain localization.[35,41,47]

Aluminum

Recent work has also led to a better understanding of the fatigue processes in aluminum. The cyclic hardening behavior of single crystal aluminum, where there is an initial rapid hardening followed by either a plateau or a softening and then secondary hardening, has been observed by all investigators of fatigue in aluminum, including Vorren and Ryum[48,49], Dhers and Driver[50], Giese and Estrin[51], Alden and Backofen[5], Xia[52,53], and Alhamany et.al.[54] It has also been found that the degree of hardening is dependent on the orientation of the crystal.[49,52,55,43,56] Also typical, is a vein/channel dislocation substructure, followed by a cellular arrangement, and slip localized into bands after the initial hardening ends.[1,5] At 77K, Giese and Estrin[51] claim to have found a dislocation structure similar to the "ladder" structure observed in copper--this was not observed by Vorren and Ryum.[48] It has been noted that "macrobands" form in aluminum--possibly as an analog to the ladder structure in copper.[48] "Rumples" similar to Vorren and Ryum's macrobands (and "tweed" structure[56]) were observed in polycrystalline aluminum by King and Teer[57]. "Bands" were noted by Dhers and Driver[50], at room temperature in aluminum single crystals, but it was not clear if these were the same manifestation as that of the macrobands.

Localization of slip in slip "bands" has been noticed in single crystals for quite some time.[58] An interesting point made about the development of persistent slip bands in aluminum versus copper is the following from Vorren and Ryum[48]: in copper, the barriers to propagation of PSBs are relatively weak, so PSBs will tend to accommodate plasticity by propagation (and possibly multiplication); while, in aluminum, the barriers to

propagation of PSBs are relatively high (high SFE), so PSBs aren't as likely to propagate in aluminum, as they might be to nucleate. The multiple PSBs that nucleate near each other may form the macrobands seen by Vorren and Ryum (1987).

Hysteresis loops for aluminum do not change shape much during room temperature fatigue, but at 77K they are seen to become more rectangular at the onset of saturation.[48] As was also pointed out by Vorren and Ryum, the change in temperature from room temperature to 77K causes a change in the resolved shear stress of a factor of 10 in aluminum single crystals, but only a factor of 2 in copper single crystals--this does not seem to be consistent with a simple change in homologous temperature. This seems to imply a change or differences in hardening (or possibly, recovery) mechanisms.[48] The Bauschinger effect seems to have a "larger" effect at lower strain amplitudes (presumably due to strain being more completely reversible at small strains).[1]

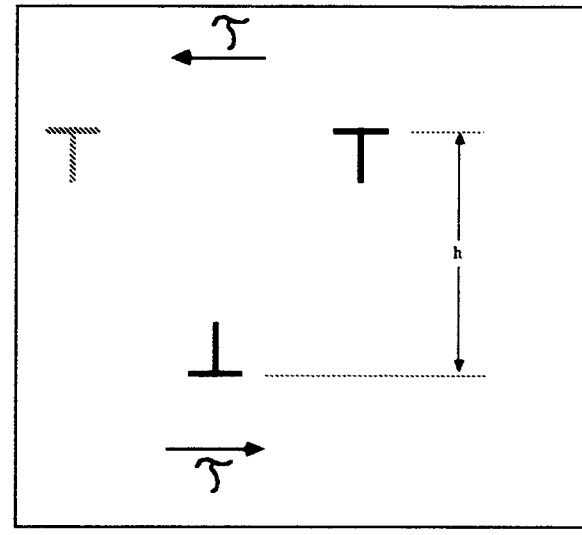

Figure 7. Schematic of an edge dislocation dipole loop "flipping" under an applied shear. The upper edge moves from the right to the left under the applied shear.

Plasticity

Three possible/popular explanations describing fatigue plasticity are (1) dipole flipping or flip-flop, (2) screw shuttling and (3) loop expansion.[59] In (1), plasticity may be accommodated by edge dipoles, under an applied shear stress, "flipping" their relative positions, from one equilibrium position at 45° to each other, to the opposite equilibrium

position, also at 45°; then upon application of the reversed shear stress, the dipole "flips" back to its original equilibrium orientation (see Figure 7).[59] With (2), plasticity may be accommodated by the shuttling of screws in one direction (possibly in the channels of a vein/channel substructure) under a positive shear stress, and then glide in the opposite direction upon application of a negative shear stress; shuttling of edge dislocations has also been observed.[59] + In (3), edges are seen to expand from the dense dipole bundles, into the channels. This bowing out can proceed until the loop reaches another vein and the edge component may annihilate (or be absorbed by the vein) with another edge, leaving behind two screws in the channel. While these three mechanisms sound completely different, they may work at the same time, and may even work together: a dislocation with edge components in the veins and screw character in a channel may (under applied shear) have the screw component shuttle and have the edge components flip-flop in concert--possibly, one mechanism being enhanced by the other. Screws dragging edges has been seen in aluminum by Yamamoto et al.[59] An edge may bow out from a vein and intersect the opposite vein/wall, thus annihilating the edge component (possibly) and leaving behind a screw(s) in the channel.[60] It is not clear which of these mechanisms dominates the plastic strain.

Hardening

Understanding of hardening mechanisms, be they cyclic or monotonic hardening, must come from understanding dislocation processes.[16] The items for explanation include monotonic hardening (stages I, II and III) both in tension and compression, and also in

---

+ It has been noticed by Lepinoux and Kubin[60] that the screws which shuttle in one direction, don't necessarily bow in the opposite direction immediately upon reversed loading. Also, [Mori and Fujita[61]] noticed reversed bowing and reversed dislocation motion on unloading in copper.

torsion; cyclic hardening during fatigue stressing (see Figure 5); cyclic softening of prestrained materials; rapid hardening in fatigue which often changes to a saturation in stress; saturation stress which can lead to secondary hardening; and last, but equally important is the Bauschinger effect, where it is observed that the yield stress on reversed loading is less than for forward loading. We will focus here on fatigue hardening and the Bauschinger effect. There are several tools that we have to try to explain these phenomena: edge dislocations, screw dislocations (and combinations of the two--possibly dislocation loops), point defects, "texture" of the material (or variation in properties due to orientation), and various other manifestations. The more commonly accepted explanations of the fatigue mechanisms in FCC metals have involved the motion or interaction of edge and or screw dislocations. Hardening has been attributed to dislocation pile-ups, increased debris, increased number of dislocations, internal stresses, and enhanced "ability" of obstacles to inhibit dislocation motion. One explanation of fatigue plasticity and hardening involves a combination of these. In this explanation, dislocations move in the forward sense to form some dislocation structure (e.g., cell walls); then on reversed straining, the same dislocations "dissolve" the newly formed cell wall and move in the opposite direction to form a new wall.[4] Said another way, the dislocation structures formed in tension are stable or resistant to tensile loads, but are not stable under compressive loads.[36,57,61,63,64] Yamamoto et al[59] have observed from in-situ experiments on aluminum, the formation and dissolution of cell walls as predicted by Hasegawa et al.[62] A loosening of the dislocation tangles has been observed in copper, as well as a loosening of dislocation tangles in the vein structure.[43] The hardening aspect comes in as the dislocations separation decreases (increasing the dislocation density) and raises the required shear stress to move dislocations.

The stresses generated in the dislocation substructure have also been used to try to explain some aspects of fatigue. It has been reasoned that there must be large "compatibility" stresses in the region adjacent to veins, walls or ladders where there is a

large disparity in dislocation density, from very high in the veins to very low in the channels. Some have argued that this causes a "long range internal stress" which tends to repel dislocations, decreasing the required stress for reversed straining--thus, a possible explanation for the Bauschinger effect.[36,38,39,63] It was found that the stress is relatively high in the vicinity of the walls and low in the channels. However, these long range internal stresses may only be evident for the larger plastic strain amplitudes, and possibly only in post primary hardening.[34] The experimental evidence used to support this idea of long range internal stresses has largely been generated by the following tool: the idea is to relate the radius of curvature of dislocation lines to the shear stress required to bow that dislocation.[38,39,60,65,66] However, some questions naturally arise when this method is used: 1) how is the radius of curvature affected by a *non-uniform* stress field (which is undoubtedly the case in real materials); 2) can you be sure that the dislocations you are analyzing aren't interacting with obstacles that you can't see?[60] 3) are the relevant dimensions such that the dislocations are not being acted on by surface effects? While these points are valid, the internal stress model has received wide acceptance. Interaction of dislocations with debris, both in the channels and in dislocation "structures" has also been used as partial explanations for hardening mechanisms.[16,67] It has been remarked that the high density of dislocation loops observed in high cycle fatigue is similar in appearance to that of quenched aluminum.[68]

A model for the formation of PSBs in copper has been proposed by [Tabata et al][43] which predicts that PSBs will form in the places where the first slip bands form. Specifically, in polycrystals, PSBs will form in crystals with single slip orientation at or near the surface. In the post "saturation" secondary hardening stage, the hardening is generally attributed to the activation of secondary slip systems where slip is much more difficult to initiate (but necessary, after the primary slip system(s) become too "hard" for plasticity).[53]

Direction of Work Performed

In order to ultimately understand metal fatigue in general, we cannot study just one metal (e.g., copper) and generalize to the others; we would not generalize the fatigue mechanisms of an FCC material, to a BCC material, nor should we generalize one FCC material to another. Consequently, if we are to understand fatigue in FCC metals, we must eventually study the comparison between the fairly well known behavior of copper, to the behavior of other FCC metals. While work on other single crystals (e.g., silver and nickel) may seem to support the work done on copper, the work done on aluminum does not appear to mirror that of copper in all respects. Being able to observe the dislocations during fatigue will also be important. For the first *in-situ* tests, we have chosen aluminum since it is a commercially important metal and because it is relatively electron transparent (i.e., thicker foils may be used for in-situ HVEM tests). Thus, the testing reported here will be performed on single crystals of aluminum. As ambient temperature is a relatively high homologous temperature for aluminum (compared to copper), single slip is not observed at ambient temperature. Thus, the mechanical testing was performed at 77K to induce single slip.

The in-situ tests will allow unique and direct insight into the mechanisms of cyclic deformation. Static TEM analysis will help determine the "range" of materials that the extensive copper conclusions are applicable. Inasmuch as we find that the results of aluminum crystals deformed in single-slip are comparable to copper, the in-situ tests results may be more general than to just aluminum.

EXPERIMENTAL PROCEDURE

Macroscopic Mechanical Testing

Mechanical testing of the aluminum single crystals was preceded by mechanical testing of commercial purity (99.7% pure) and high purity (99.999% pure) polycrystalline aluminum samples. These tests were useful to establish, and validate, the single crystal testing procedure. In addition, these mechanical tests were beneficial to the in-situ tests in that they allowed us to prescribe the beginning dislocation microstructure for the start of each set of in-situ experiments. The samples, testing apparatus, data acquisition and method of control, were in accordance with ASTM E606-92 (Standard Practice for Strain Controlled Fatigue Testing).[69]

Samples

The commercial purity specimens (99.7% aluminum) were machined from an ingot, (supplied by the Northwest Aluminum Company, The Dalles, OR), to a final shape (Figure 8) with gage diameter 15.3-mm, 50.8-mm gage length, 25.4-mm long grip sections, with grip section diameters of 17.6-mm and 19.2-mm (i.e., opposing ends of a given sample had different grip section diameters) with a fillet radius of 4.4-mm. Grip sections were smooth so as to fit in our collet type grips, as per ASTM E606-92.[®] Prior to testing, these samples were annealed at 550°C for five hours and then air cooled in order to bring the samples to a fully annealed condition, to obtain a specimen of strength as similar to the single crystal as possible.

[®] The grip design--Figure 10--is based on a similar set-up by [Lehmann et.al.],[70] used to test soft metals at low temperatures.

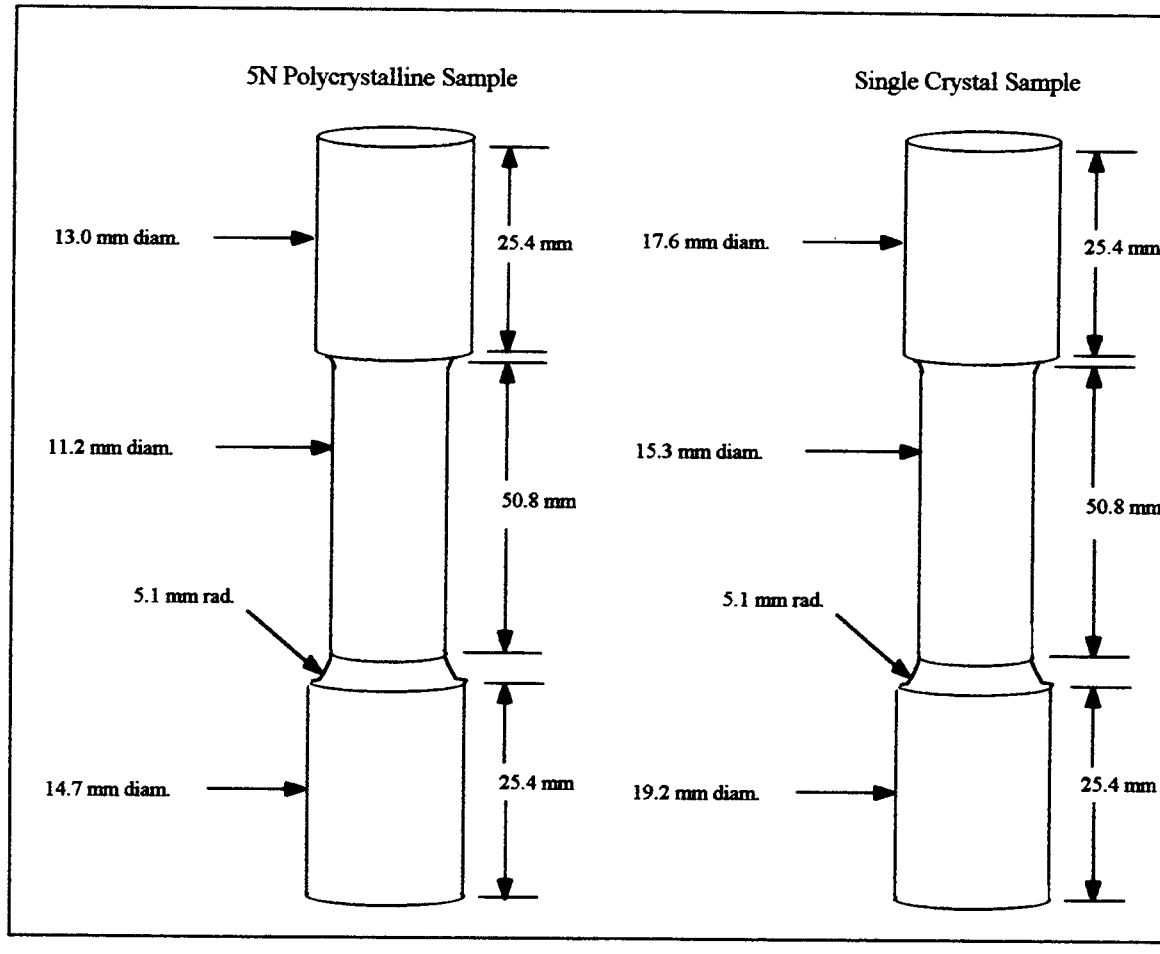

Figure 8. Schematic showing sample dimensions for macroscopic fatigue testing. (a) Configuration of 99.999% pure polycrystalline aluminum samples. (b) Configuration of commercial purity polycrystalline, and single crystal samples.

The high purity (99.999% pure) aluminum polycrystalline specimens were machined from a rod provided by The Metron Group, Milburn, New Jersey. These specimens had a final shape (Figure 8a) with gage diameter of 11.2-mm, 50.8-mm gage length, grip sections of 25.4-mm length and 13.0 and 14.7-mm in diameter (i.e., opposing ends of a given sample had different grip section diameters) with a fillet radius of 5.1-mm. The specimens were annealed at 325°C for two hours followed by air cooling.

The single crystals of aluminum were also purchased from the Metron Group, Milburn, New Jersey. The crystals were of high purity (99.999% pure), and were oriented for single slip. A <111>, and <110> type directions were aligned at 45° (and coplanar) to the long axis of the sample (i.e., maximum Schmid factor of 0.5) (see Figure 9). The dimensions of the crystal were 101.6-mm long by 19.2-mm in diameter. The crystals were machined by turning on a Hardinge Brothers lathe with silicon carbide cutting tools at about 1600 rpm, with a tool feed rate of 0.5-0.8 mm/sec. Each pass removed 0.025-mm , with the final 10 passes removing 0.013-mm each. The single crystals were not heat treated after machining.

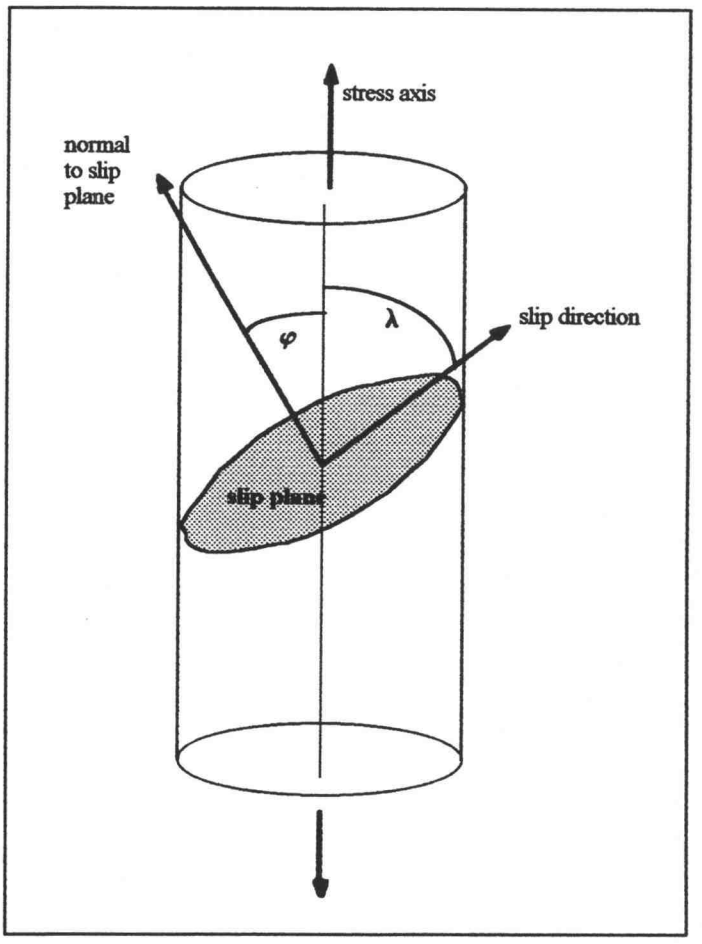

Figure 9. Schematic of single crystal orientation and slip geometry. For the single crystals that were tested, δ and φ were ≅ 45°, so that the Schmid factor was maximum. The slip direction is a <110> and the normal to the slip plane is a <111>.

Apparatus

Preliminary constant strain amplitude fatigue tests at ambient temperature were controlled using an extensometer. However, strain gages were used in accordance with

ASTM E251-92[71] for dynamic strain measurement on all tests reported here. The strain gages were Micro Measurements type "WK-13-250BG-350" which are suitable for low temperature (77K) testing, fatigue straining, have integral leads, and are self-temperature compensated for aluminum 2024-T4. Two gages, diametrically opposed, were bonded to each specimen, so as to minimize any strain signal due to bending. Cyano-acrylate adhesive was used to bond the gages to the specimens tested at ambient temperature, while Micro Measurements M-Bond 610 (cured at 135°C for four hours and furnace cooled, as per Micro Measurements instructions) was used for low temperature (77K) tests. Two "control" gages of the same type and adhesive were bonded to a commercial purity aluminum specimen, in a Wheatstone bridge with the test specimen and test specimen gages. This was done to facilitate strain control of the test, as the gages were linked to the control apparatus via an Instron unterminated extensometer cable with self-identifying resistors, which could interpret the signal from a Wheatstone bridge. Loads for all tests were measured using a bi-axial Instron load cell model 6467-107 having 89 kN (20 kip) thrust capacity and values are accurate to within ±0.5% of the measured value.

The specimens were fixed at each end in a precision aligned Reed-Prentice lathe collet. (Substantial effort was taken to minimize bending in the samples, although it has been shown in similar testing on aluminum single crystals at room temperature, that the alignment of the grips with respect to each other, do not influence the formation of deformation bands. In other words, the alignment of the grips does not cause strain localization.[72]) The grips were made from 304 stainless steel with 6061-T6 aluminum tightening rods (see Figure 10a) and were machined by Commercial Welding of Lewisburg, Oregon. This design caused tightening of the grip onto the specimen with decreasing temperature. The diameter of the grip was reduced by about 1% (0.2-mm) while the sample only decreased about 0.4% (0.08-mm) as the temperature changed from 293K to 77K. A double walled, vacuum filled dewar was mounted to the actuator of the test apparatus so that both grips, and specimen, could be immersed in liquid nitrogen for

the low temperature tests (see Figure 10b). It has been shown that a liquid nitrogen environment does not alter the fatigue behavior of aluminum.[37]

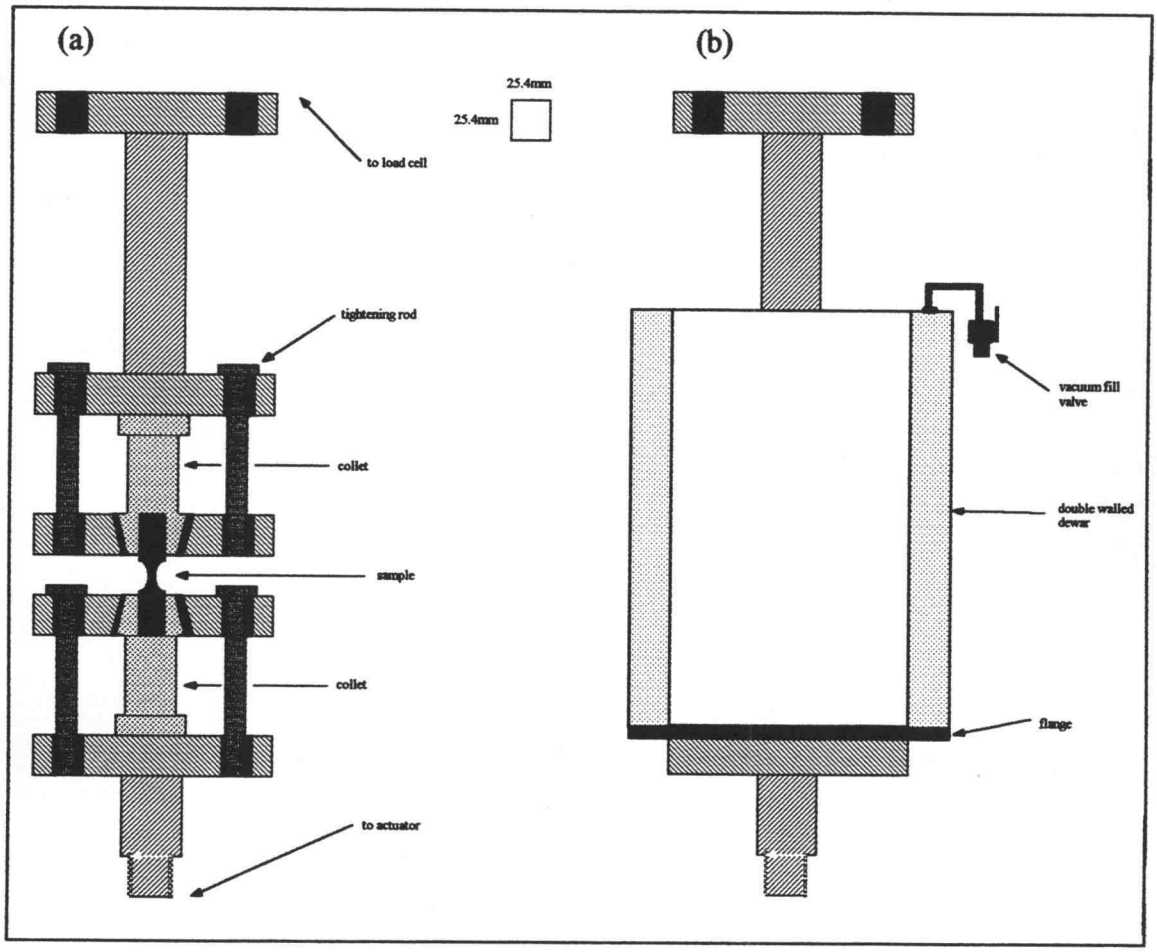

Figure 10. Line drawing (cross-section) of the low temperature grips (a), and vacuum walled dewar (b). Note: Sample, collets, and tightening rods are not to scale.

Testing was performed using an Instron 8521 digitally controlled servo-hydraulic bi-axial testing system. The machine was controlled by an Apple™ Macintosh SE/30 using a GPIB interface and LabVIEW 2®. Data acquisition was primarily performed using a Macintosh SE/30 with LabVIEW 2® software, (concurrent with controlling the fatigue testing). A back-up set of data was recorded on another Macintosh SE. Load and strain data were output from the Instron co-axial outputs, converted to an analog signal

through a Fluke® Hydra data acquisition unit, and then recorded by the (back-up) Macintosh. The load cell temperature was also monitored by the Macintosh SE via the Fluke®. This was performed to determine if, at any time during the test, the load cell temperature had a significant effect on the load output. Hysteresis loops were visually monitored on an oscilloscope connected to other Instron co-ax outputs.

The load cell was electronically calibrated (using standard Instron procedure) prior to each test. This electronic calibration was checked once prior to the first test, by application of a fixed 200 kg load to the load cell. The strain gages were electronically calibrated prior to each test. This calibration was revalidated prior to each fatigue test and included the following general steps: Gages identical to those to be used in the test were mounted to a well characterized steel sample (modulus, yield stress and dimensions were known), and then loaded to produce strain (static) in tension, and then compression; five data points were used in each "direction". Strain values were compared to predicted values, and hysteresis of the load reading was monitored.

Method of Control

As was mentioned above, the fatigue process was controlled by an Apple™ Macintosh SE/30 with a GPIB interface and LabVIEW 2®. This allowed the computer to control any mechanical features of the Instron, as well as perform data acquisition. As the purpose of these tests was to produce fatigued samples with a reproducible dislocation substructure, the tests were not load (or stress) controlled, but were strain controlled--as is consistent with current practice.

Plastic strain controlled tests were used to deform the specimens (for a comparison of the different types of mechanical fatigue tests (e.g., push-pull, torsion, bending), see [Cheng and Laird][46]). The Instron was controlled, from the Macintosh, using strain

control, i.e., the feedback loop for controlling sample deformation was using strain.[♦] The Macintosh (Mac) started the fatigue cycling in compression at a constant, specified strain rate. The Mac determined the apparent elastic modulus of the sample, by averaging the measured modulus using 15 data points, and rejecting any individual point (modulus) that was not reasonable (21 GPa < Modulus < 119 GPa). The program then determined when the set plastic strain amplitude had been accumulated for the half-cycle. This was accomplished by estimating the (anelastic) strain on unloading. The elastic strain (calculated using the measured modulus) was subtracted from the total strain to determine the plastic strain. This was acceptably close to the actual plastic strain if the plastic strain amplitude was greater than the elastic strain amplitude[74], as for the present tests where the stress amplitude is less than 140 MPa.[♠] Once the predicted strain was within a preset tolerance (strain tolerance = 3.5×10^{-5}) of the set plastic strain, the specimen was unloaded at an equal, but opposite, strain rate. This gave a triangle wave form in strain vs. time (which was monitored on the Mac.SE). The strain tolerance was adjusted to improve/maximize the performance of the test in two ways; first, by increasing the tolerance value, forward straining was stopped a fraction of a second *prior* to the time when the plastic strain endpoint (one-half of the plastic strain range) was reached, preventing overstraining; and, second, by decreasing the tolerance value, forward straining was allowed to continue somewhat *past* the plastic strain endpoint, such that this "extra" strain could account for anelastic recovery. The controller was calibrated to account for anelastic recovery on unloading.[⊛] These two effects (increasing and decreasing the plastic strain tolerance) were optimized to yield the best overall strain control. The subsequent half-cycles proceeded just as the first, except that the modulus was not recalculated--the

---

[♦] See [Wilson and Robinson][73] for a similar method for plastic strain control.

[♠] If this were not so, I could not reasonably approximate the plastic strain on unloading in this way, since anelasticity would be a much larger component of the total strain[75].

[⊛] For a discussion of anelastic recovery in high purity aluminum at room temperature see [Nir, Hart and Li][76].

value from the first half-cycle was used for all subsequent cycles. The "center" of the hysteresis loop was recorded immediately prior to the first cycle, and was fixed (strain = 0), resulting in each following loop being forced to be centered about that fixed point (similar to [Wilson and Robinson][73]).

The stress in each test was always found to be greater in the compressive half-cycle than in the tensile (generally, on the order of 1 MPa), as has been noted by others.[39,73,75,77]

Test Execution

The step-by-step details of the mechanical testing procedure are presented in outline form in the Appendix.

In-Situ Testing

Sample Preparation

The fatigued crystal was kept in liquid nitrogen until TEM sample preparation commenced. The crystal was placed in room temperature air (20°C), and allowed to warm until it could be safely handled by unprotected fingers. The total time that a specimen spent at room temperature prior to in-situ testing in the HVEM was between four and six hours. Sample preparation was divided into two major parts. The first part, was orienting the crystal. It was critical that the TEM foil could eventually be precisely oriented so that forward and reverse slip would be obtained on the primary slip plane with maximum Schmid factors. Second, the crystal (with known orientation) was sliced, and mechanically and electro-chemically thinned to produce an electron transparent foil, which

could be accommodated in the in-situ reversed deformation HVEM stage. These two procedures are subsequently discussed.

A single crystal aluminum sample was pre-oriented in such a manner as to be able to image a dislocation with $\mathbf{b} = [01\bar{1}]$ on a (111) primary slip plane. A slice was cut from each single crystal, then prepared for electron diffraction. The orientation of the crystal was then determined from the electron diffracted spot pattern recorded from the TEM. This was facilitated by using a double tilt TEM stage.

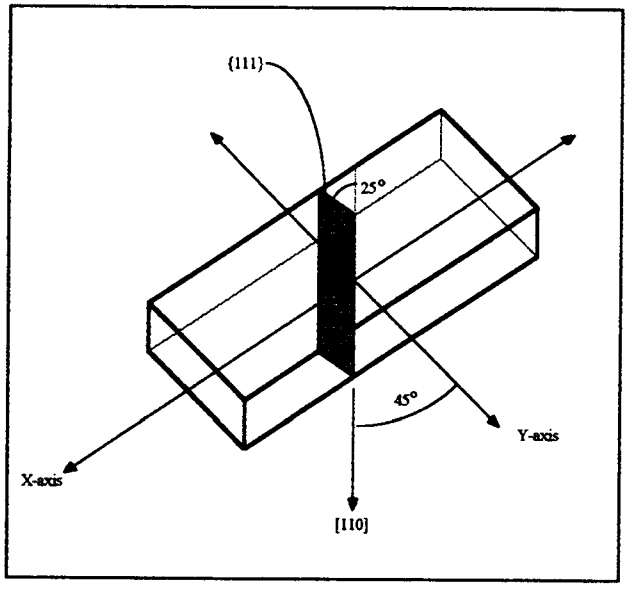

Figure 11. Slip plane geometry with respect to in-situ foil.

The foils could be extracted once the orientation of the crystal was determined. Foils were cut so that the primary slip plane was inclined approximately 25° to the foil normal. A <110> direction was contained in the plane of the foil and at the same time was oriented at 45° to both the X and Y tensile axes, as shown in Figure 11. The in-situ specimens were required to contain this prescribed crystal geometry in order to maximize the + and - Schmid factors for this specific slip system while having an adequate inclination of the (111) plane to yield sufficient contrast when imaging in the TEM. Also, the samples had no perforations (holes), yet were thin enough to be transparent to the electron beam and have good dislocation imaging ability. The shape and geometry of the in-situ fatigue specimens are detailed in Figure 12. The estimated maximum thickness for good imaging conditions is approximately 2-6 microns at 1.5 MeV. The basic steps for the production of the in-situ specimens was a combination of slicing, lapping, and electropolishing. First, a rectangular block measuring (12.7 mm × 11.4 mm × 6.4 mm)

was cut, with a low speed diamond saw, from the single crystal. The sloped sides of the specimens were then made by cutting at an angle of 8°.

Next, two slices were made along the specimen's long axis, parallel to the length of the specimen; one from the "top" to a length of 2.5 mm, and the other from the bottom to a length of 6.4 mm. The purpose of the slots was to create a tensile gage section in region P of Figure 12. This was the electron transparent region after the final electropolishing step. The clamping holes were then made at the locations shown in Figure 12. These were made using a drill press with a positioning control table (accurate to within +/- 0.03 mm). The larger set of holes on each side of the electropolished region served to create another gauge section in region P and perpendicular to the gage section between the slots. 0.8-mm slices through the thickness of this block were made using a Buehler low speed diamond saw (0.305mm × 101.6mm diamond tipped blade) after the holes and slots were machined. Each slice was then mounted to a gravity feed lapping device with Duco™ cement. Then, each slice was wet lapped (using kerosene) equally on both sides using 600 grit silicon carbide paper to a final

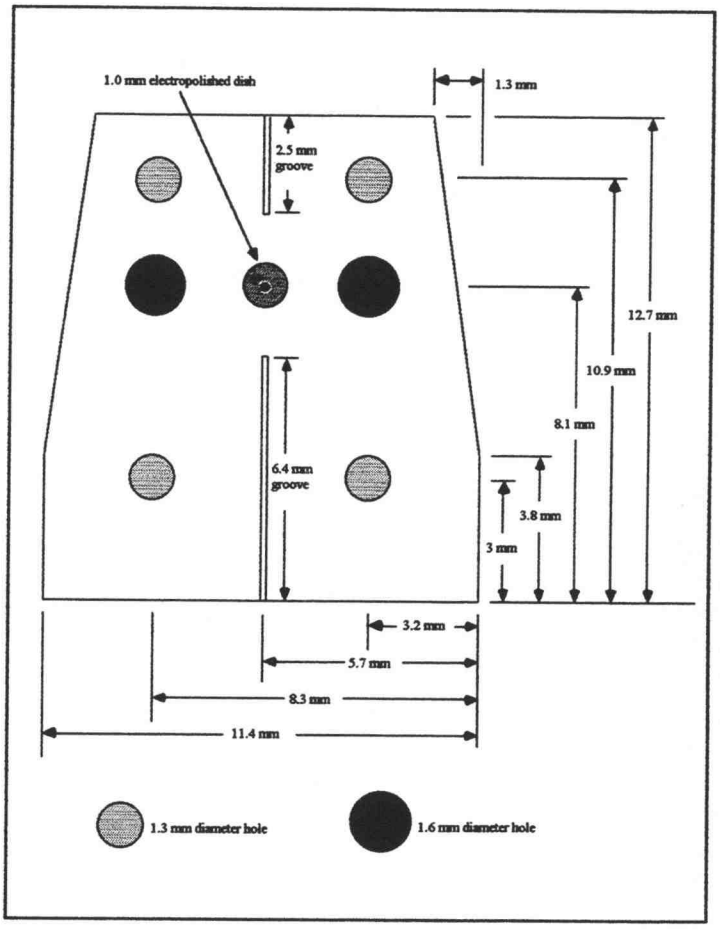

Figure 12. Dimensions of the HVEM in-situ foil which fits in the X-Y deformation stage.

thickness of 0.3 to 0.4 mm. The final specimen thickness was a trade-off between potential damage, foil stability and electron transparency of the foil: lapping to thinner dimensions could lead to mechanical damage in the central portions of the specimen, while making the sample more electron transparent, and increasing the likelihood of buckling during testing. Thicker specimens allowed greater mechanical stability during in-situ testing, but sacrificed image quality due to absorption or scattering of more electrons during viewing.

A special electropolishing holder was designed and built for the Fischione™ electropolisher. The new holder was made mostly from Delrin, and used a platinum wire to apply the bias to the foil to be polished. The center hole of the holder was non-standard, with a small opening of just 1.0 mm. O-rings were used to isolate the desired electropolish region such that other portions of the sample would not be electro-polished surreptitiously. The specimens were clamped into the holder with region "P" at the 1.0 mm diameter electropolishing holder opening. The electropolishing solution consisted of 5 v/o perchloric acid, 20 v/o butoxyethanol, and 75 v/o methanol and was applied to the sample in two streams, one on each side of the foil. The electropolishing parameters were -25°C, 30-35 volts, and 45-50 mA (as measured by a mercury thermometer and an external analog volt and am-meter respectively).

It was necessary to first polish a reference sample in order to accurately determine the rate of material removal. The reference sample was polished to perforation (as detected by a laser/photodiode couple) using known voltage, current, initial etchant concentration, and jet speed. Once the sample had been perforated, its initial thickness (measured in the non-etched region with a micrometer to ±0.002mm) was divided by the time required to perforate, to give the polishing rate in microns per second.

A specimen was then electropolished for a time equal to the predicted time to perforation minus approximately 10-20 sec. This should result in a final specimen thickness at region P, slightly greater than that of a typical transparent specimen for

aluminum in a HVEM operating at 1.5 MeV (approximately 2-6 microns). The microscope was the 1.5 MeV Kratos High Voltage Electron Microscope (HVEM) located at the National Center for Electron Microscopy at Lawrence Berkeley Laboratory, Berkeley, California. The samples were then examined in the HVEM, and repolished for short periods (2-10 sec.) if not yet transparent. These steps were continued until a non-perforated electron transparent region was evident.

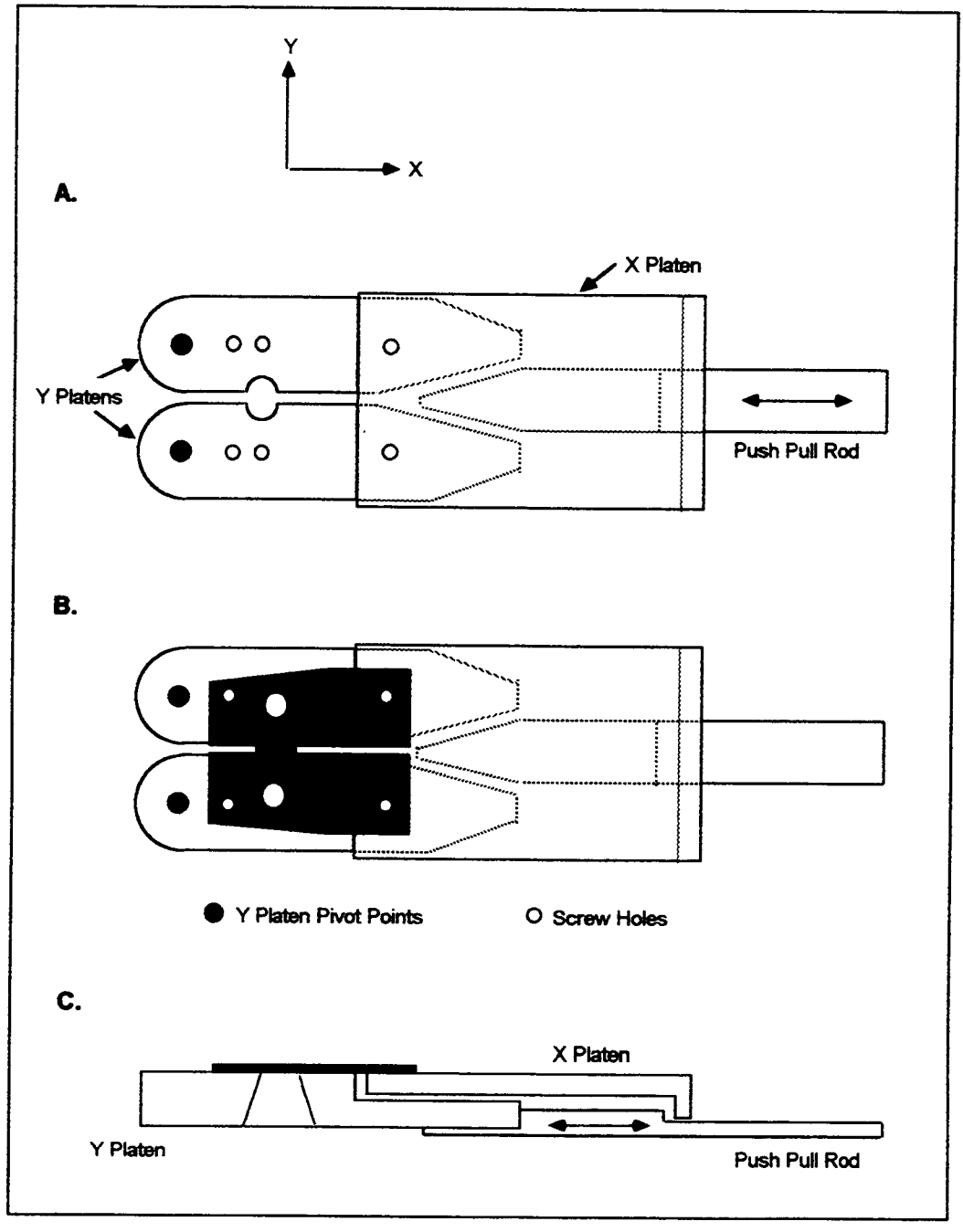

Figure 13. Schematic of the in-situ straining stage. (a) Top view. (b) Top view with simulated specimen (foil). (c) Side view.

In-Situ HVEM Fatigue Procedure

The reversed deformation specimen stage for use in-situ in the Kratos was built by M.L. Tech, Stockton, CA. A schematic of the basic parts of the in-situ fatigue stage is shown in Figure 13a. Prior to placing the specimen onto the platens, an adhesive (Duco™ cement) was used for additional fixturing support. The specimen was then placed on top of the X and Y loading platens such that the two holes of the specimen align with the holes on the platens (see Figure 13b). The specimen gripping was then achieved by inserting the screws into their corresponding holes. Threaded screws (0-80) were inserted in the holes on both sides of the electropolished region. Care was taken to not tighten the screws too much, as this could deform the specimen.

The stage (with the mounted single crystal foil) was then inserted into the HVEM. In order to attain good diffraction (bright field) imaging conditions, the stage was typically tilted approximately 14° to a $[11\bar{1}]$ diffracting vector, with $\mathbf{g}\cdot\mathbf{b} = -2$ for $\mathbf{b} = [0\bar{1}1]$. This tilt further increases the projection of the primary (111) on the photographic plane (i.e., increases the projection of dislocations).

Once imaging was obtained of static (still) dislocations in the foil, deformation could proceed. The X and Y platens of the stage moved independent of each other, and their motion was along orthogonal X and Y axes (refer to Figure 13). This orthogonal motion allowed for the reversal of the stress state by alternately tensile stressing in mutually perpendicular directions. The X and Y platens were actuated by a push-pull rod. When the push-pull rod was moved forward, it wedged between the Y platens and moved them apart (see Figure 13a). This applied tension in the specimen along the Y axis (perpendicular to the axis of the stage). When the push-pull rod motion was reversed, the Y axis was unloaded. As the push-pull rod was further reversed, it contacted the X platen (see Figure 13c). This began tensile loading on the specimen along the X axis and reversal of the stress state (change in sign of the Schmid factor).

There was, typically, some translation of the specimen during the loading of the platens, and it was necessary to translate the specimen accordingly so as to keep the same area in the viewing screen. A small amount of bending in the specimen on initial loading could cause imaging conditions to change, and small adjustments of the specimen tilt were often necessary. Loading was continued in a given direction, until dislocation motion was visible. Unloading was achieved by reversing the direction of the push-pull rod.

The image was processed using a Westinghouse video camera with 1000 lines of resolution, coupled with a Vidicon image intensifier using standard co-axial cables. In-situ deformation was recorded using a VHS video tape (on standard play mode for best resolution) on a four head Mitsubishi U30-VHS video tape recorder.

Radiation damage was a concern when performing HVEM experiments on aluminum. It's been shown that in 99.999% aluminum, under 1 MeV and up to 10 dpa, there is radiation damage present, and there is little detectable void formation.[78] Another concern is the thickness of the foil. As the foil thickness decreases (especially below 2 microns), the analogy to bulk material becomes precarious,[79,80] and the surface area to volume ratio is such that surface effects (e.g. image forces) increase, complicating our ability to relate the experiments to bulk behavior.[24] For this reason, our in-situ specimens were left as thick as possible (2-6 microns). Some research has shown that relatively thick samples of high purity aluminum retain the "bulk" dislocation substructure.[44] However, we believed, based on earlier experiments, that 2-6 micron thick foils had a significant "surface" effect, and that repeated cyclic deformation in the thin foil would not produce the same microstructure as macro specimens. Hence, in-situ deformation of thin foils was continued in-sequence from our cyclically deformed macro crystals.

Several other researchers have attempted different methods of in-situ TEM fatigue with varying degrees of success.[34,42,43,44,59,60,61,64,65,81,82,83] In addition, one group has performed in-situ fatigue experiments in an SEM using bulk samples (not thin foils)[84]; two others have performed reversed deformation in-situ on titanium crystals.[65,85]

RESULTS

Macroscopic Mechanical Testing

Polycrystalline Samples

Constant plastic strain amplitude fatigue tests were performed at ambient temperature on polycrystalline aluminum alloy (AA 1100) to evaluate the mechanical testing apparatus. Several of the hysteresis loops are presented in the Appendix. The early tests had several undesirable aspects manifested in the hysteresis loops. First, the loops moved left or right (in strain) during the course of fatigue, while maintaining a constant plastic strain amplitude (but not centered about zero strain). This problem was solved by forcing the loops to be centered about zero strain. Specifically, the center of all loops was selected prior to the first cycle, and each subsequent cycle measured strain relative to that original center. Second, testing with an extensometer (recall that the controlling parameter for the fatigue test is strain) produced wide variation and random spread in strain measurements. Third, testing with strain gages (i.e., strain gages producing the strain feedback signal) resulted in very smooth hysteresis loops, with corresponding smooth cyclic hardening curves. Fourth, the loop shape could be idealized by adjusting the strain tolerance value (see Experimental Procedure, Method of Control). Primary and back-up data collection methods were checked and found to mirror each other, as well as match predicted values.

Mechanical tests were also performed on high purity polycrystalline aluminum (99.999% pure). These tests proved useful to further refine the mechanical response of the testing system. Prior to unloading in any given half-cycle, a small delay was evidenced (see Appendix) between when the desired strain was attained, and when the sample was unloaded. In other words, the sample was not unloaded at the exact instant that the desired strain was achieved--it continued to load for a fraction of a second after the desired strain had been reached. Also, the "zero stress" values used for determining the strain on unloading were found to not correspond to zero load. Said another way, the

sample was not truly at zero load when the program thought that it should be at zero load. As was mentioned in the procedure, this problem was remedied by optimizing the strain tolerance value, which counteracted the delay in mechanical response.

At room temperature, the high purity polycrystalline samples exhibited a primary hardening stage followed by a plateau in cyclic stress. This appeared to be *the* saturation stress in each case tested, but may not be the *true* saturation stress, as the tests only accumulated plastic strains of 0.32 for the cases of 0.001 and 0.0015 plastic strain range, and cumulative plastic strains of 0.42 and 0.52 in the cases of 0.002 and 0.0025 plastic strain range respectively. However, for the cumulative plastic strains achieved at room temperature, there was no hardening or softening once the observed saturation stress had been reached. It should be noted that the compressive stress was greater in magnitude than the tensile stress for all strain amplitudes tested (this has been observed by other investigators[63,75]). The amount that compressive stress exceeded tensile stress was not observed to be a constant from test to test, and had a maximum magnitude of about 2% of the maximum stress.

The apparent saturation stress vs. plastic strain amplitude for the high purity polycrystals is plotted in Figure 14. There appears to be a linear relationship between saturation stress and log(plastic strain range) with a slope of 2.0 GPa for the strain amplitudes tested. This compares well to values of 2.5 and 2.0 GPa

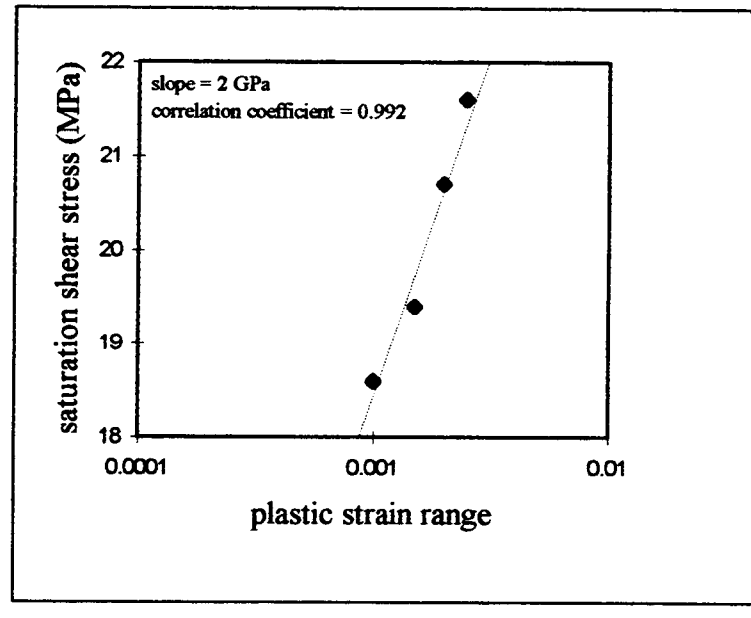

Figure 14. Saturation shear stress vs. plastic strain range for 99.999% pure aluminum polycrystalline samples tested at room temperature.

reported by two other investigators.[86,87] The correlation coefficient for a least squares fit to the data is 0.992. The corresponding hysteresis loops, and cyclic hardening curves are presented in the Appendix.

Low temperature tests (77K) on 99.999% pure polycrystalline aluminum were not deformed to saturation. This was done partly because the samples were found to slip in the grips when stresses of about 90 MPa were reached. Saturation was not reached prior to 90 MPa at 77K for the plastic strain amplitudes tested, and a strain rate of 2×10^{-4} s^{-1}. The low temperature tests on high purity polycrystalline aluminum evinced well defined cyclic hardening curves, and hysteresis loops (see Appendix). As these compared very well with other research, it appeared that our mechanical apparatus and procedures are reliable.[63,75] Cyclic compressive stresses exceeded cyclic tensile stresses by less than 1%.

Single Crystal Samples

Four single crystals were cyclically deformed at 77K. The first single crystal tested suffered two misfortunes in the laboratory. During its testing, it was inadvertently preloaded (due to tightening of the grips) to about 400 N. The preloading appeared to "predispose" the microstructure to that of deformation in compression. The cyclic stress strain curve shows that the stress in compression was significantly higher (about 3 MPa) than in tension. Next, following a successful low temperature fatigue test at $\varepsilon_p=1.2\times10^{-3}$ and a shear strain rate of 2×10^{-4} s^{-1} the sample would not release from the grips. After an application of approximately 12 kN in tension, the sample released from the grips. At this point, the sample no longer had a circular cross-section: its cross section was roughly elliptical with a major axis of 15.5 mm and a minor axis of 12.2 mm at its most eccentric section. The gage length of the specimen was elongated to 41.8 mm from 34.7 mm. The crystal was not used for in-situ testing with this history. The crystal was retested at 77K with the same plastic strain amplitude and strain rate to a cumulative plastic strain of 5

(including the 2.5 from the first test). For this "retest," the stresses in each compressive cycle were greater than those in tension, but by less than 0.4% in each half cycle.

Subsequent single crystal tests proceeded without any mishaps. The cyclic hardening curves behaved as expected, with a rapid hardening which slowed to a lesser hardening rate. Each test was stopped prior to any softening or saturation of the stress. The cyclic hardening curves, and selected hysteresis loops are illustrated in Figures 15 and 16 respectively. The crystals were all continuing to harden when mechanical testing was completed. The axial stress was typically 42 MPa after a cumulative plastic shear strain of 2.5, which is similar to the aluminum single crystal results of Vorren and Ryum[48] for 77K and a plastic strain amplitude of $\varepsilon_p = 1.2\times10^{-3}$. According to the data of Vorren and Ryum,[48] our crystals have achieved a stress of about half that necessary for saturation. By deforming to a "presaturated" state, we ensure a microstructure that is absent of PSBs. We expect to have a vein (dipole bundle)/channel microstructure for the conditions tested. However, one crystal was deformed to 0.48 cumulative plastic strain (100 cycles), and had "lost" the dislocation substructure imparted by the prefatigue by the time it was viewed in the HVEM: the vein/channel substructure was absent, or had not formed.

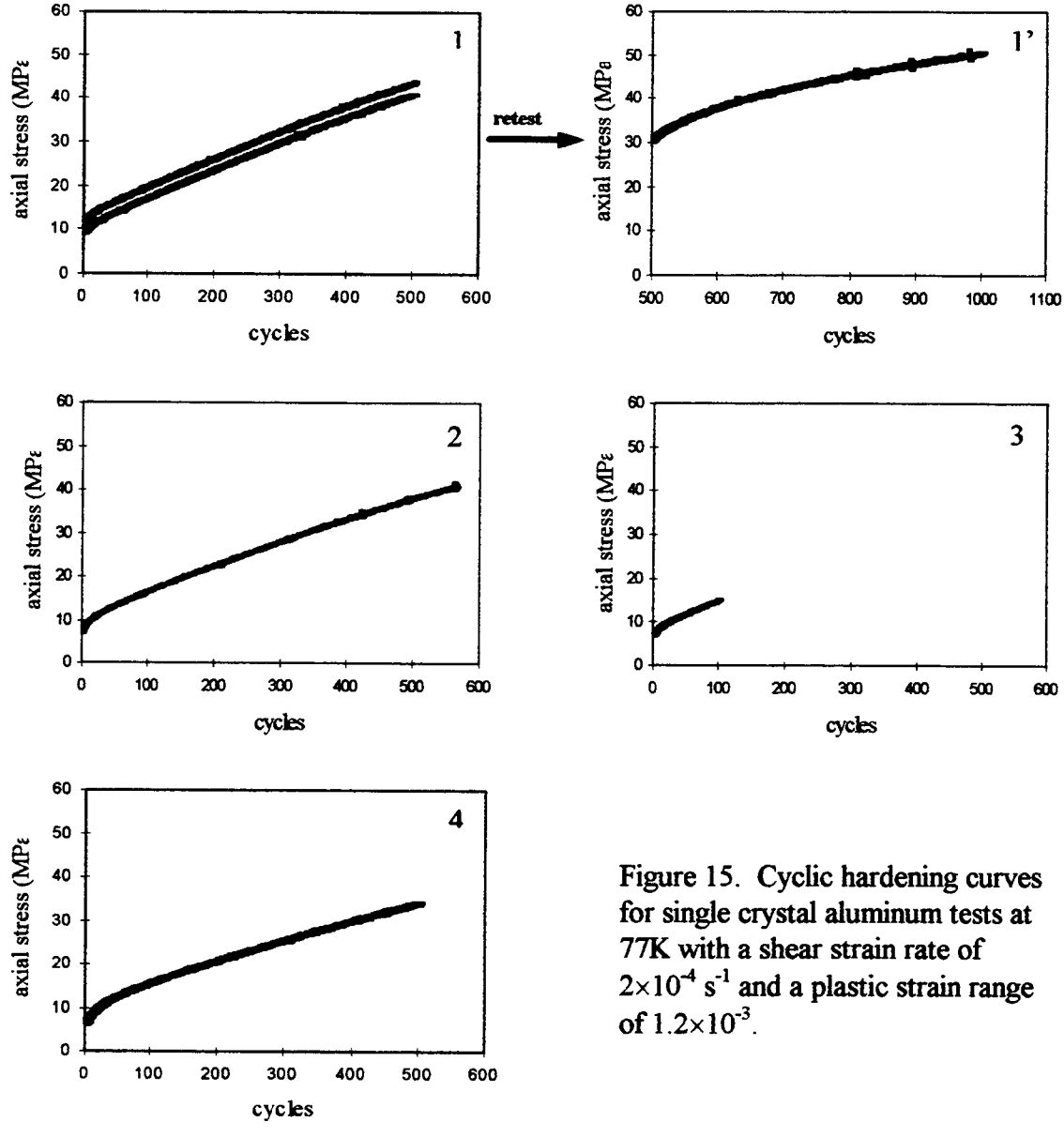

Figure 15. Cyclic hardening curves for single crystal aluminum tests at 77K with a shear strain rate of 2×10^{-4} s^{-1} and a plastic strain range of 1.2×10^{-3}.

The shape of our hysteresis loops did not change from rectangular to more pointed elongated loops, since we did not reach saturation (i.e., did not form PSBs). No slip lines were evident on the surface of any of the fatigued single crystals.

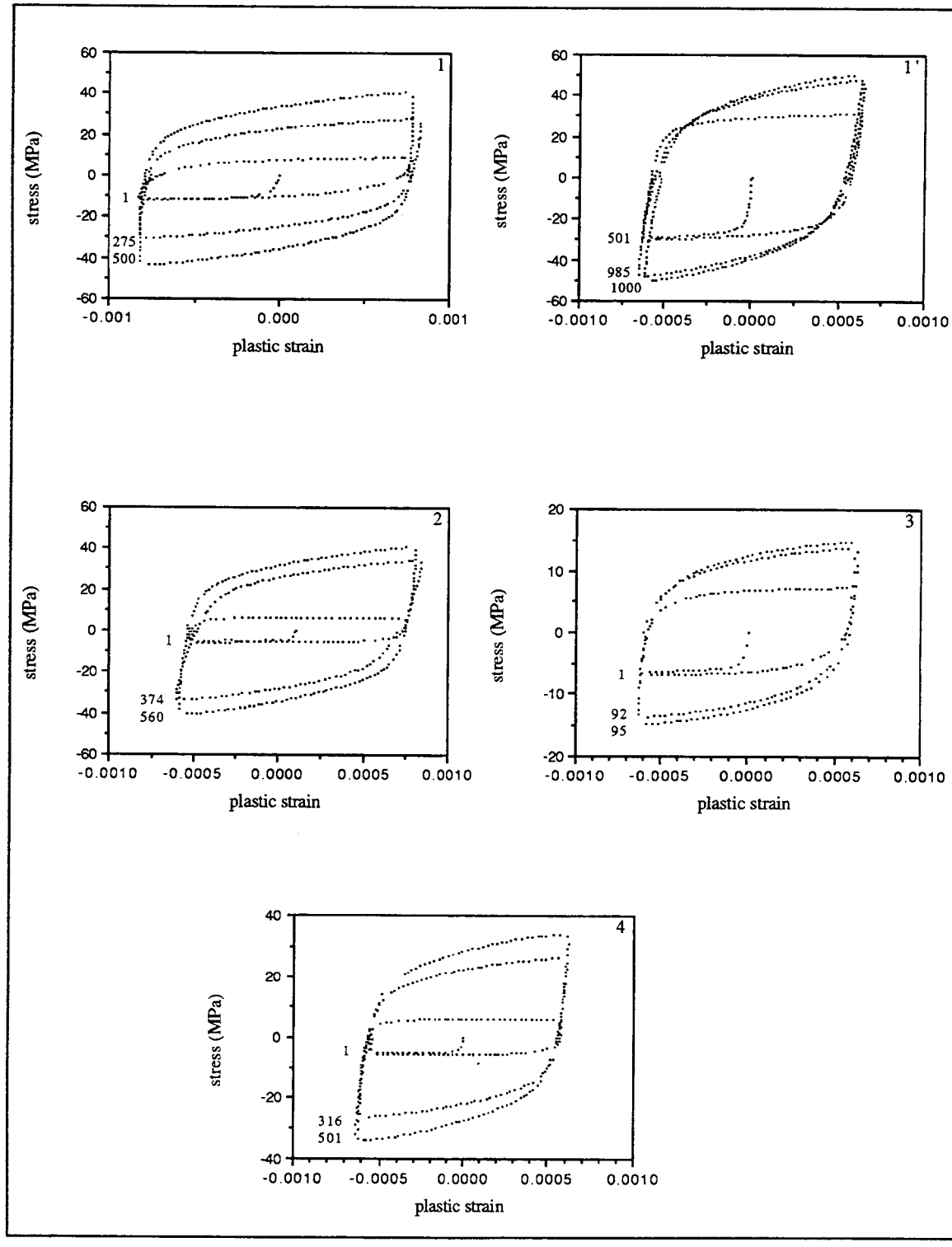

Figure 16. Selected hysteresis loops from the aluminum single crystals tested at 77K with a strain rate of 2×10^{-4} s^{-1} and a plastic strain range of 1.2×10^{-3}.

In-Situ HVEM Fatigue Results

The dislocation microstructure observed by conventional (200 kV) TEM is illustrated in Figure 17 in a simulated 3-D montage. The top face is the primary slip plane (111). Invisibility conditions are not completely satisfied by $\mathbf{g}\cdot\mathbf{b}=0$ since there is still residual contrast. This is why the $(\bar{2}11)$ plane of the illustrated cube still shows primary dislocation contrast. The remaining cube face, the $(01\bar{1})$ is perpendicular to the primary Burgers vector. The microstructural features are very consistent with the trends observed in copper at room temperature. A classic vein substructure is observed, and is also illustrated in Figure 18.

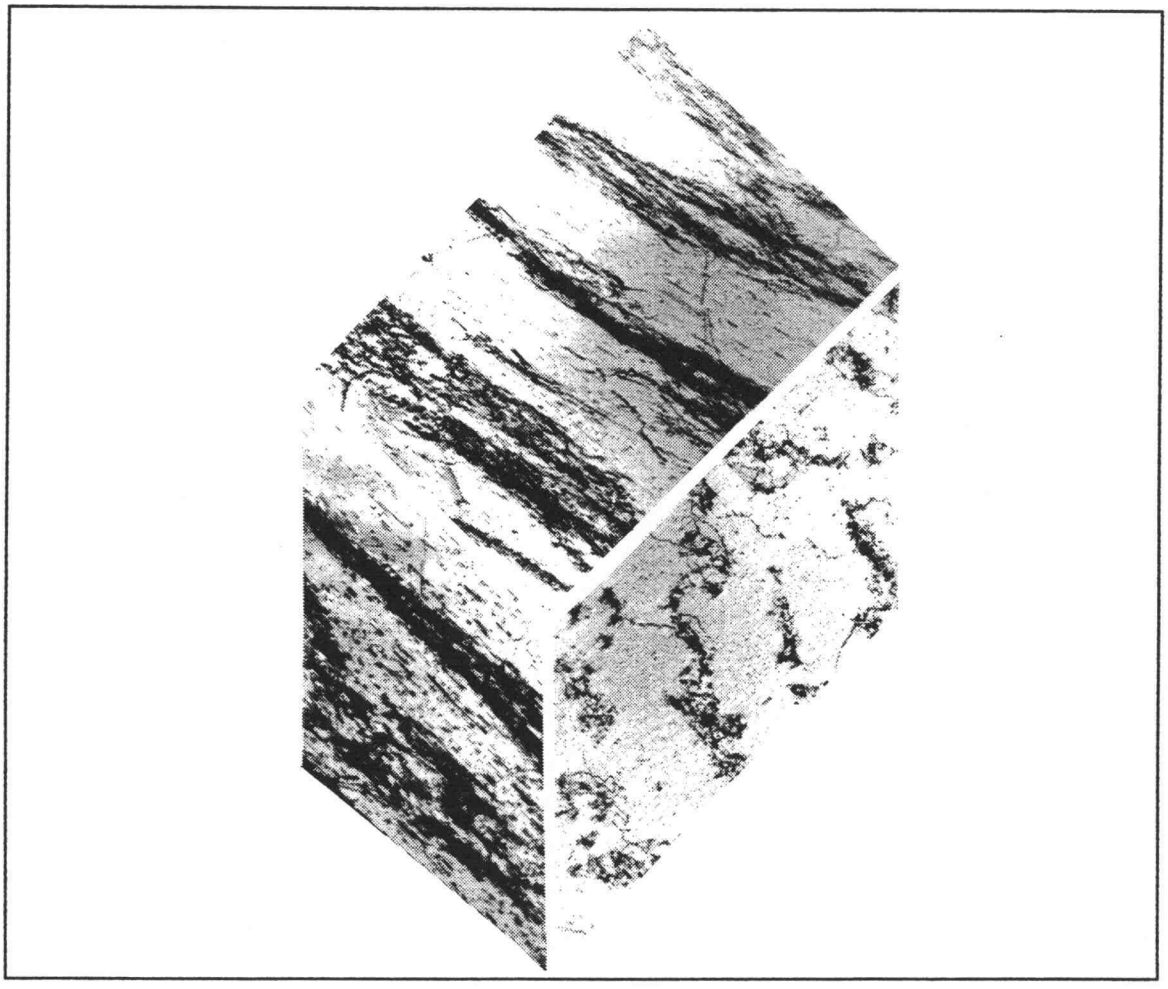

Figure 17. TEM montage of the dislocation substructure in fatigued single cyrstal aluminum showing three mutually perpendicular faces.

Figure 18. TEM image of the classic vein and channel structure from an aluminum single crystal deformed at 77K.

Invisibility experiments reveal that nearly all (over 99%) of the observed dislocations are of a single burgers vector, the $[01\bar{1}]$. The vein spacing is about one micron (vein spacing of 0.55 microns was observed by Vorren and Ryum[48] after 6000 cycles and a plastic strain amplitude of 5.4×10^{-3}), and the volume fraction occupied by the veins is about 25%. The dislocation density in the veins is about 5.1×10^{9} cm^{-2} while the density in the channels is only about 10^{9} cm^{-2}. These appear higher than observed by Woods,[88] but lower than Antonopoulos et al[89] and similar to Feltner[67] (for tension-tension fatigue of polycrystalline aluminum at 77K). At first, there appear to be two types of defects within the channels: dipoles, just as in the veins, but perhaps of somewhat shorter dimensions; there also appear to be dot-like features that others have observed.[22,48,68,78,79] Some attributed these to vacancy loops while others to tiny dipoles.[89] Our work using weak beam techniques and careful stage tilting tends to agree with the latter investigators. We were always able to resolve dipoles from the channel debris. Figure 19 shows the veins and channels with special tilting to maximize the projected dipole separations. Curiously, we find that the average height, h, of dipoles (distance perpendicular to the burgers vector) is typically 8.2-nm, while the lateral separation distance is typically 17-nm, almost twice h. We do not have an explanation for this deviation from expected equality.

It is of some concern that this substructure may be somewhat recovered from the as-deformed crystal, especially since the in-situ sample preparation is performed at ambient temperature (i.e., higher than the temperature at which the pre-fatigue was performed[90]). No recovery was noted after 24 hours at ambient temperature (Feltner[67] noticed no significant change in dislocation microstructure after four days). In the extreme case, we find substantial recovery of the dislocation substructure in foils exposed to ambient temperature for four weeks. It is expected that some rearrangements of dislocations occur on warming to room temperature, but the veins have been found to be generally resistant to handling.[90] Wilsdorf and Schmitz[79] have shown that long, smooth dislocations are formed when the TEM foil is deformed inadvertently during sample preparation. We observed none of these types of dislocations.

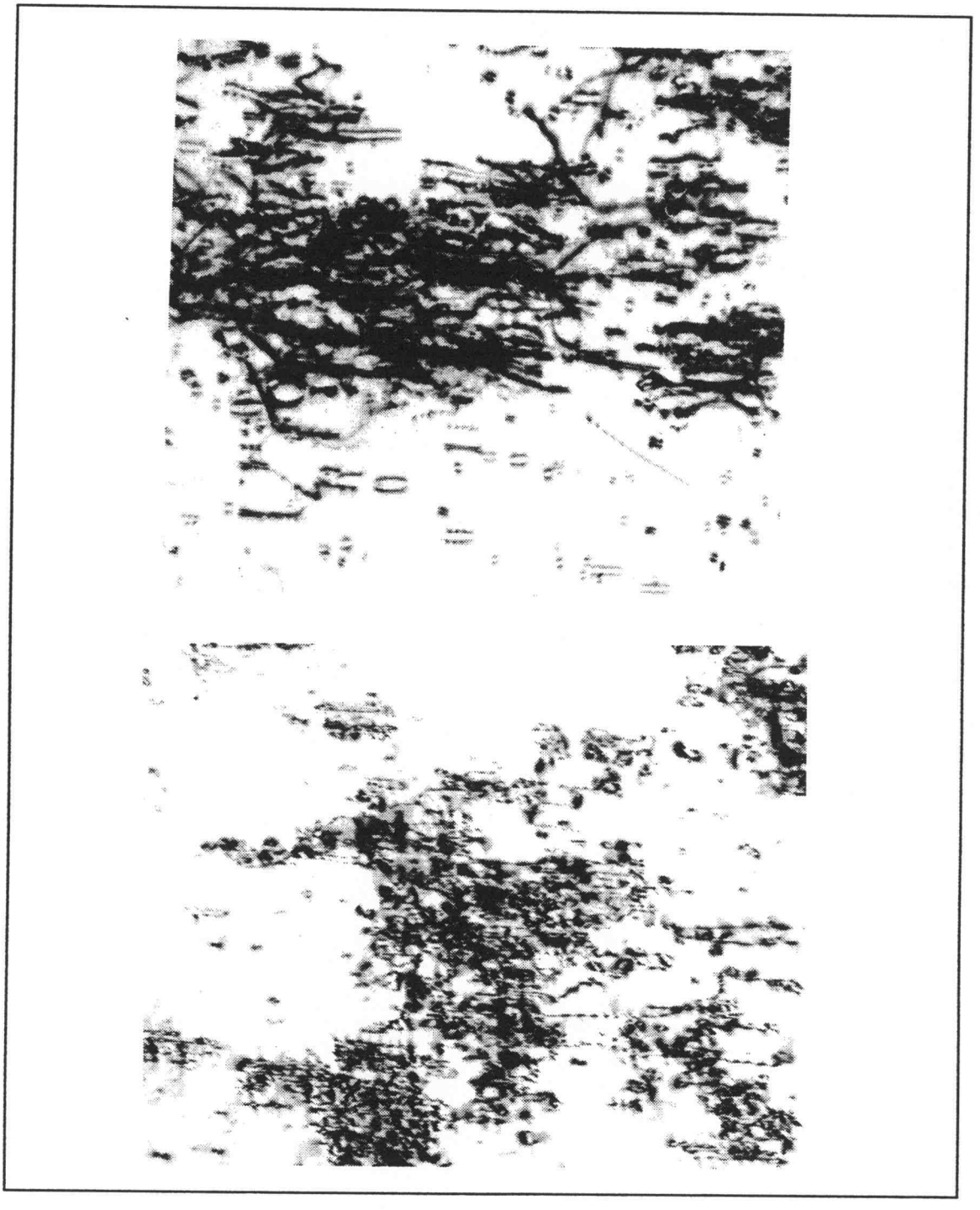

Figure 19. TEM foil imaged with special tilting required to view maximum dipole separation distance.

In-situ experiments were also performed. The platens of the in-situ stage were very slowly engaged so as to prevent loading to a stress higher than the final stress level during testing of the macrocrystal. It was hoped that this would help to avoid (at least initially) strain "bursts" or "avalanches." Care was taken to determine the source of initial plasticity in the in-situ specimens. Our early tests show that screw dislocations move quite easily along channels, as others have observed, and which are widely believed to be responsible for a substantial portion of plastic strain during cyclic deformation. They easily reverse their direction of motion with X-Y stress reversal. Figure 20 illustrates an in-situ experiment in which dislocation reversal was observed. Loops were observed to bow out from the veins. The stresses required to activate these loops may be higher than that necessary to activate the shuttling of screws in the channels. We often observed dislocation traces (dislocations between the metal film and the oxide layer) of several channel widths. These findings appear to be somewhat different than those in-situ observations by Yamamoto et al.[42] and Tabata et al.[43] We did not observe significant evidence of dislocation activity during unloading or in the unloaded state. This is consistent with our earlier preliminary in-situ reverse deformation experiments.[4] Such activity would be evidence for internal backstresses.

The events during reversal appear identical in nature to those in the forward sense. We do occasionally note, on reversal of the platens, and with a relatively large amount of prior monotonic deformation, some dislocation activity, but what we have been able to show is consistent with unbuckling the thin foil. We were unable to cause dipole flipping. In fact, we attempted to activate the edges of dipoles both within the channel and at the perimeter of the dipole bundle (vein). Only once was there even the possibility that one edge was activated and "left" the viewing area. Hence we do not find dipole flipping to be relatively easy as compared to screw shuttling.

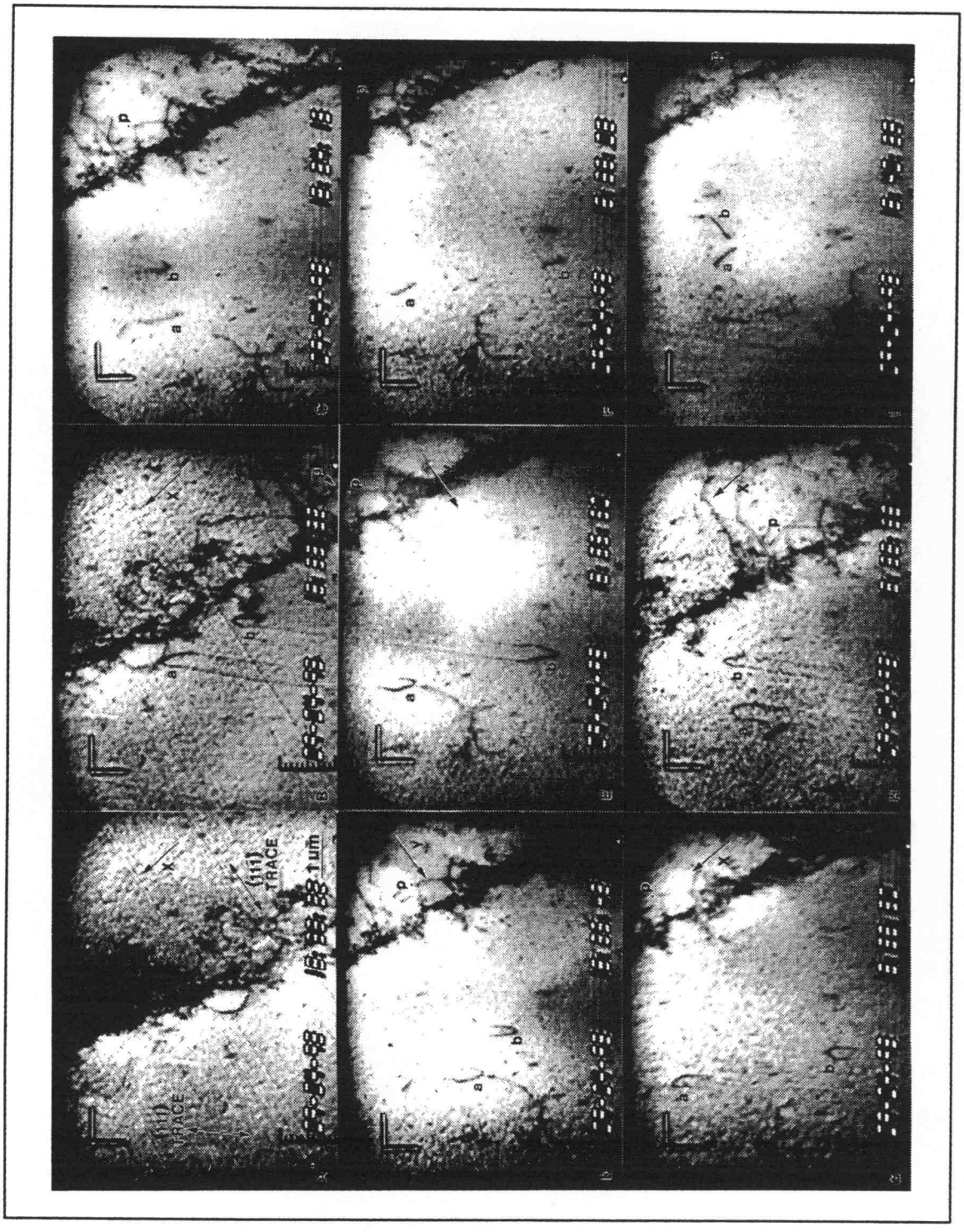

Figure 20. Series of in-situ HVEM micrographs depicting a stress reversal. Frame (A) is the unloaded state. Frame (B) is loading in the forward sense. Frame (C) is the unloaded state. Frames (D) and (E) are loading in the reverse sense. Frame (F) is the unloaded state. Frames (G) and (H) are loading in the forward sense. Frame (I) is the unloaded state. Note the reversal of dislocation segments "a" and "b".

BIBLIOGRAPHY

1. K. U. Snowden, *Acta Metall.*, (1963) 11, pp. 675-684.

2. N. Thompson, C. K. Coogan, and J. G. Rider, *J. Inst. Met.*, (1955/6) 84, pp. 73-80.

3. R. L.Woolley, *Phil. Mag.*, (1953) 353, pp. 597-618.

4. M. E. Kassner, M. A. Wall and A. W. Sleeswyk, *Scripta Metall.*, (1991) 25, pp. 1701-1706.

5. T. H. Alden and W. A. Backofen, *Acta Metall.*, (1961) 9, pp. 352-366.

6. T. S. Sriram, C. M. Ke and Y. W. Chung, *Acta Metall.*, (1993) 41, pp. 2515-2521.

7. J. Krejci and P. Lukas, *Phys. Stat. Sol. (a)*, (1971) 8, pp. 299-307.

8. D. M. Fegredo and G. B. Greenough, *J. Inst. Met.*, (1958/59) 87, pp. 1-9.

9. J. M. Roberts and N. Brown, *Trans. AIME.*, (1960) 218, pp. 454-463.

10. T. Erber, S. A. Guralnick and S. C. Michels, *Annals of Physics*, (1993) 224, pp.157-192.

11. Z. S. Basinski and S. J. Basinski, *Prog. Mat. Sci.*, (1992) 36, pp. 89-148.

12. H. Mughrabi, Dislocations and Properties of Real Materials, Conference Proceedings, The Institute of Metals, London, (1985), pp. 244-262.

13. H. Mughrabi, Strength of Metals and Alloys, H. J. McQueen, J. P. Baillon, J. I. Dickson, J. J. Jones and M. G. Akben eds., Pergamon Press, Oxford, (1986) pp. 1917-1942.

14. C. Laird, "The Application of Dislocation Concepts in Fatigue", Ch. 26 in Dislocations in Solids, F. R. N. Nabarro ed., North-Holland Publishing Company, 1983.

15. P. Neumann, Physical Metallurgy, 3rd edition, R. W. Cahn and P. Haasen, eds., Elsevier Science Publishers BV, 1983, Ch. 24, pp.1553-1594.

16. D. Kuhlmann-Wilsdorf and C. Laird, *Mat. Sci. Eng.*, (1977) 27 pp. 137-156.

17. J. C. Grosskreutz, *Phys. Stat. Sol. (b)*, (1971) 47 pp. 11-31.

18. A. R. Rosenfield and B. L. Averbach, *Acta Metall.*, (1962) 10, pp. 71-74.

19. D. Hull and D. J. Bacon, Introduction to Dislocations, 3rd ed., International Series on Materials Science and Technology, Vol. 37 (1984), Pergamon Press, pg. 96.

20. C. E. Feltner and C. Laird, *Trans. AIME*, (1968) 242, pp. 1253-1257.

21. P. Charsley, U. Bangert and L. J. Appleby, *Mat. Sci. Eng.*, (1989) A113, pp. 231-236.

22. P. Charsley and L. J. Harris, *Scripta Metall.*, (1987) 21, pp. 341-344.

23. P. Lukas and M. Klesnil, *Mat. Sci. Eng.*, (1973) 11, pp. 345-356.

24. M. Judelewicz, *Scripta Metall.*, (1993) 29, pp. 1463-1466.

25. M. E. Kassner, J. Pollard, E. Evangelista and E. Cerri, *Acta Metall.*, (1994) 42, pp. 3223-3230.

26. F. Haessner and J. Schmidt, *Acta Metall.*, (1993) 41, pp. 1739-1749.

27. J. Kwiecinski and J. W. Wyrzykowski, *Acta Metall.*, (1993) 41, pp. 3089-3095.

28. T. Hasegawa and U. F. Kocks, *Acta Metall.*, (1979) 27, pp. 1705-1716.

29. R. O. Scattergood and T. Hasegawa, *Scripta Metall.*, (1979) 13, pp. 723-727.

30. G. Van Drunen and S. Saimoto, *Acta Metall.*, (1971) 19, pp. 213-221.

31. Z. S. Basinski and S. J. Basinski, Strength of Metals and Alloys, Proc. ICSMA8, Vol. 1, (1988), Pergamon Press, pp. 13-24.

32. R. Wang and H. Mughrabi, *Mat. Sci. Eng.*, (1984) 63, pp. 147-163.

33. A. Abel, *Mat. Sci. Eng.*, (1978) 36, pp. 117-124.

34. F. Ackermann, L. P. Kubin, J. Lepinoux and H. Mughrabi, *Acta Metall.*, (1984) 32, pp. 715-725.

35. J. Polak, J. Helesic and K. Obrtlik, *Met. Mater.*, (1991) 29 (2), pp. 68-75.

36. T. Hasegawa, T. Yakou and U. F. Kocks, *Mat. Sci. Eng.*, (1986) 81, pp. 189-199.

37. P. Lukas and L. Kunz, *Mat. Sci. Eng. A.*, (1988) A103, pp. 233-239.

38. H. Mughrabi, *Acta Metall.*, (1983) 31, pp. 1367-1379.

39. H. Mughrabi, Continuum Models of Discrete Systems 4, O. Brulin and R. K. T. Hsieh eds., North-Holland Publishing Company, (1981) pp. 241-257.

40. H. Mughrabi, *Mat. Sci. Eng.*, (1978) 33, pp. 207-223.

41. N. Y. Jin, *Acta Metall.*, (1989) 37, pp. 2055-2066.

42. A. Yamamoto and T. Imura, Dislocation Modelling of Physical Systems: An Acta-Scripta Metallurgica Conference, Gainsville, FL, Pergamon Press (1980) pp. 74-79.

43. T. Tabata, H. Fujita, M. Hiraoka, and K. Onishi, *Phil. Mag.*, (1983) 47, pp. 841-857.

44. T. Tabata, S. Yamanaka, and H. Fujita, *Acta Metall.*, (1978) 26, pp. 405-411.

45. N. Y. Jin and A. T. Winter, *Basic Questions in Fatigue: Volume 1, ASTM STP 924*, J. T. Fong and R. J. Fields, Eds., American Society for Testing and Materials, Philadelphia, 1988, pp. 17-25.

46. A. S. Cheng and C. Laird, *Mat. Sci. Eng.*, (1981) 51, pp. 55-60.

47. J. Polak, J. Helesic and K. Obrtlik, *Mat. Sci. Eng. A*, (1988) 101, pp. 7-12.

48. O. Vorren and N. Ryum, *Acta Metall.* (1987) 35, pp. 855-866.

49. O. Vorren and N. Ryum, *Acta Metall.* (1988) 36, pp. 1443-1453.

50. J. Dhers, and J. Driver, Basic Mechanisms in Fatigue of Metals, eds. P. Lukas and J. Polak, Academia (1988), ISBN 0-444-98926-9, pp. 33-40.

51. A. Giese and Y. Estrin, *Scripta Metall.*, (1993) 28, pp. 803-807.

52. Y. B. Xia, *Scripta Metall.*, (1993) 29, pp. 999-1003.

53. Y. B. Xia, Z. G. Wang and R. H. Wang, *Phys. Stat. Sol (a)*, (1990) 120, pp. 125-132.

54. A. Alhamany, J. Chicois, R. Fougeres and A. Hamel, *J. Phys. III*, (1992) 2, pp. 1491-1508.

55. E. Roberts and R. W. K. Honeycombe, *J. Inst. Metals*, (1962/63) 91, pp. 134-141.

56. M. Videm and N. Ryum, Advances in Fatigue Science and Technology, C. Moura Branco and L. Guerera Rosa (eds.), (1989), pp. 765-772.

57. A. E. King and D. G. Teer, *Met. Sci. J.*, (1969) 3, pp. 121-136.

58. H. J. Gough, S. J. Wright and D. Hanson, *J. Inst. Metals*, (1926) 36, pp. 173-190.

59. A. Yamamoto, C. Morita, T. Tono, S. Saimoto, H. Saka and T. Imura, *Proc. Fifth Int. Conf. on High Voltage Electron Microscopy*, Kyoto, (1977) pp. 395-398.

60. J. Lepinoux and L. P. Kubin, *Phil. Mag. A.*, (1985) 51, pp. 675-696.

61. H. Mori and H. Fujita, *J. Phys. Soc. Japan*, (1975) 38, pp. 1349-1356.

62. T. Hasegawa, T. Yakou and S. Karashima, *Mat. Sci. Eng.*, (1975) 20, pp. 267-276.

63. R. C. Daniel and G. T. Horne, *Met. Trans.*, (1971) 2, pp. 1161-1172.

64. H. Mori and H. Fujita, *J. Phys. Soc. Japan*, (1975) 38, pp. 1342-1348.

65. S. Farenc, D. Caillard and A. Couret, *Acta Metall.*, (1990) 41, pp. 2701-2709.

66. H. Biermann, T. Ungar, T. Phannenmuller, G. Hoffmann, A. Borbeley and H. Mughrabi, *Acta Metall.*, (1993) 41, pp. 2743-2753.

67. C. E. Feltner, *Acta Metall.*, (1963) 11, pp. 817-828.

68. R. L. Segall and P. G. Partridge, *Phil. Mag.*, (1959) 4, pp. 912-919.

69. Annual Book of ASTM Standards, ASTM, Philadelphia, (1993), E606-92, pp. 522-536.

70. P. Lehmann, G. S. Yuan, and K. T. Hartwig, *Cryogenics*, (1985) 25, pp. 164-165.

71. Annual Book of ASTM Standards, ASTM, Philadelphia, (1992), E251-92, pp. 402-420.

72. F. Inoko, M. Kurimoto and T. Nagamoto, *J. Jap. Inst. Met.*, (1989) 53, pp. 281-289.

73. C. J. Wilson and A. Robinson, *J. Inst. Metals*, (1962/63) 91, pp. 129-132.

74. J. Polak and M. Hajek, *Int. J. Fatigue*, (1991) 13, pp. 216-222.

75. D. S. Kemsley and M. S. Paterson, *Acta Metall*, (1960) 8, pp. 453-467.

76. N. Nir, E. W. Hart, and C. Li, *Scripta Metall.*, (1976) 10, pp. 189-194.

77. S. N. Buckley and K. M. Entwistle, *Acta Metall.*, (1956) 4, pp. 352-361.

78. W. J. Yang, R. A. Dodd and G. L. Kulcinski, *J. Nuc. Mat.*, (1977) 64, pp. 157-166.

79. H. G. F. Wilsdorf and J. Schmitz, *J. Appl. Phys.*, (1962) 33, pp. 1750-1754.

80. A. B. Mitchell and D. G. Teer, *Phil. Mag.*, (1969) 19, pp. 609-612.

81. L. E. Murr, *Mat. Sci. Eng.*, (1981) 51, pp. 71-79.

82. A. Yamamoto, C. Morita, T. Tono, M. Nonoyama, H. Saka, K. Noda and T. Imura, *Proc. Fifth Int. Conf on High Voltage Electron Microscopy*, Kyoto, (1977) pp. 133-136.

83. T. Imura, Ishikawa, Y. Sakitani, T. Tono, C. Morita, H. Saka, K. Noda, A. Yamamoto and S. Saimoto, *Eighth Int. Cong. Elec. Micr.*, Canberra, (1974) 1, pp. 168-169.

84. J. Talesman, P. Kantzos and D. Brewer, "In Situ Fatigue Loading Stage Inside Scanning Electron Microscope," National Aeronautics and Space Administration, Fatigue and Fracture Branch, Cleveland, OH. Lewis Research Center, report date: May 1988, pp.(3)161-(3)172.

85. Z. Jieping, G. Haicheng, Z. Huiju and C. Laird, *Scripta Metall.*, (1989) 23, pp. 553-556.

86. A. Giese, A. Styczynski, and Y. Estrin, *Mat. Sci. Eng.*, (1990) A124, pp. L11-L13.

87. Y. Estrin, A. Giese, H. Mecking, and A. Styczynski, Strength of Metals and Alloys, Proc. ICSMA 9, Haifa, Israel, Pergamon Press (1991), Vol. 2, pp. 977-984.

88. P. J. Woods, *Phil. Mag.*, (1973) 28, pp. 155-191.

89. J. G. Antonopoulos and A. T. Winter, *Phil. Mag.*, (1976) 33, pp. 87-95.

90. U. Bangert and P. Charsley, *Mat. Sci. Eng.*, (1990) A128, pp. 39-44.

APPENDICES

APPENDIX A

Al 1100 hysteresis.

Note the nonconcentric hysteresis loops due to testing with an extensometer.

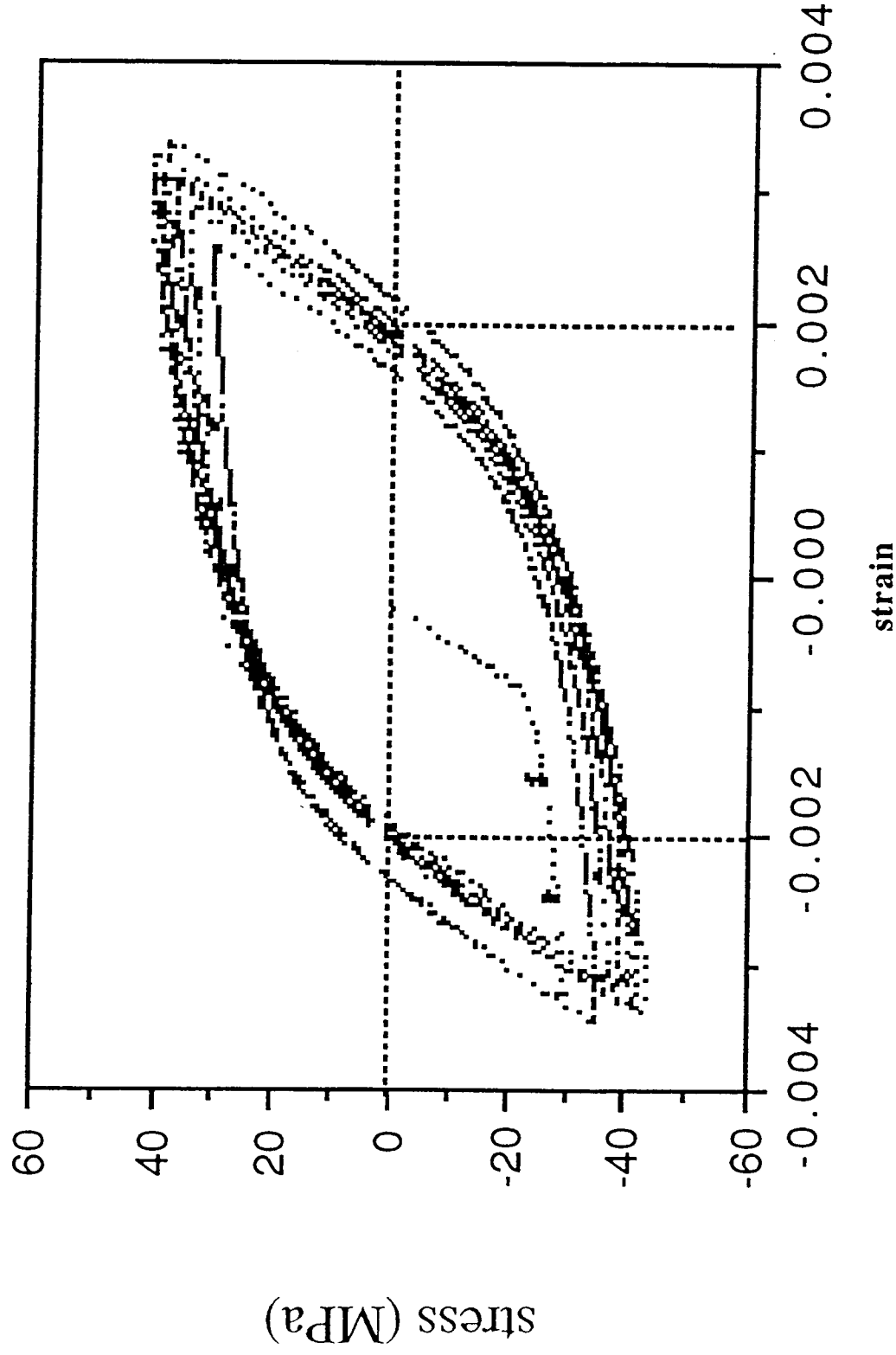

Al 1100 polycrystal tested at ambient temperature using an extensometer as the input device. Seven and one-half cycles are shown. The plastic strain range is 2×10^{-3} and the strain rate is 1×10^{-4} 1/s.

APPENDIX A

Al 1100 hysteresis.

Note the shift of the hysteresis loops from right to left from cycle number 1 to cycle number 175. This was eliminated in the "corrector" version of the LabVIEW program.

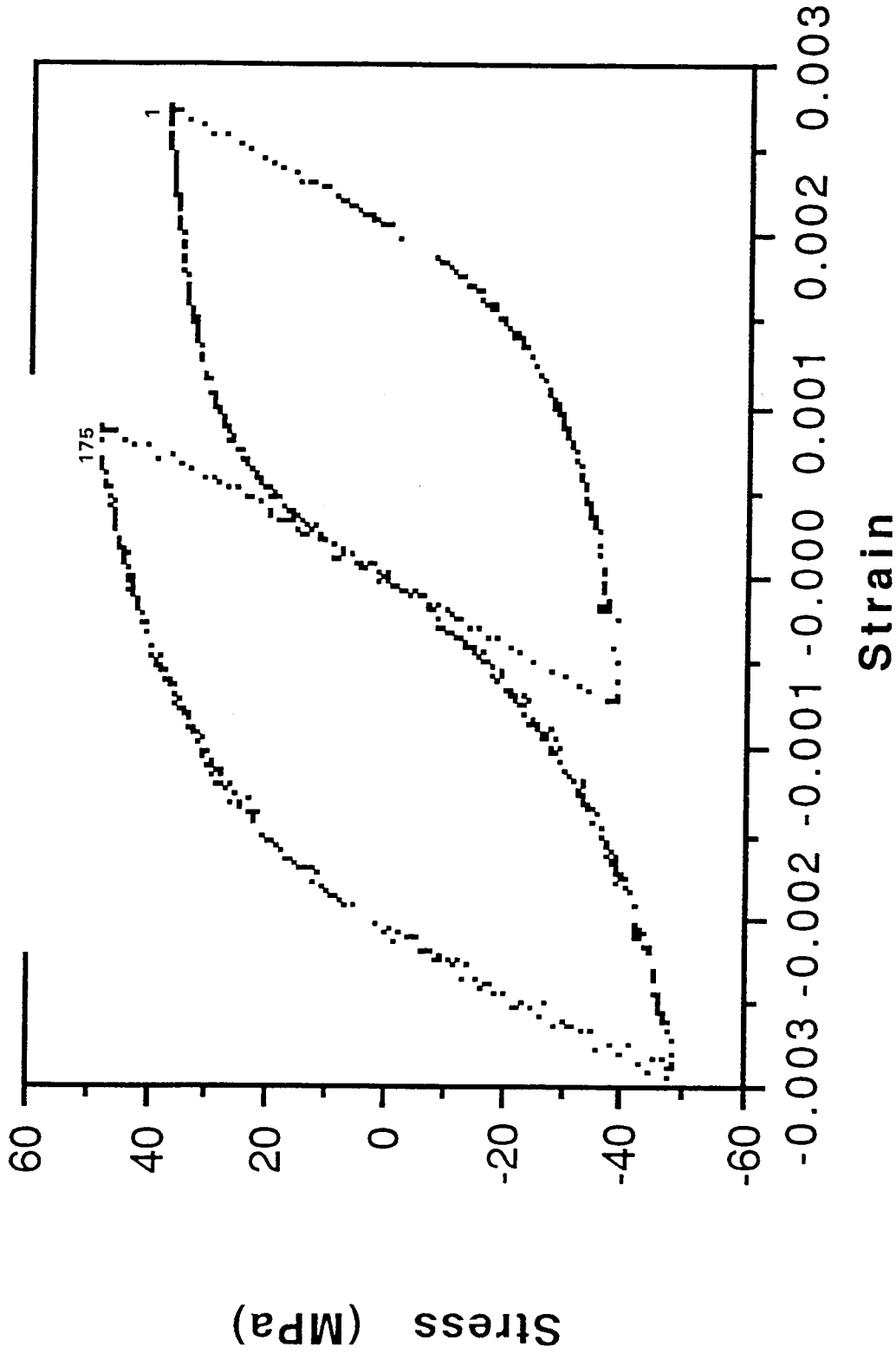

Al 1100 polycrystal tested at ambient temperature. Cycles number one and 175 are shown. The plastic strain range is 2×10^{-3} and the strain rate is 1×10^{-4} 1/s.

APPENDIX B

Loop adjustments using the "strain tolerance" value.

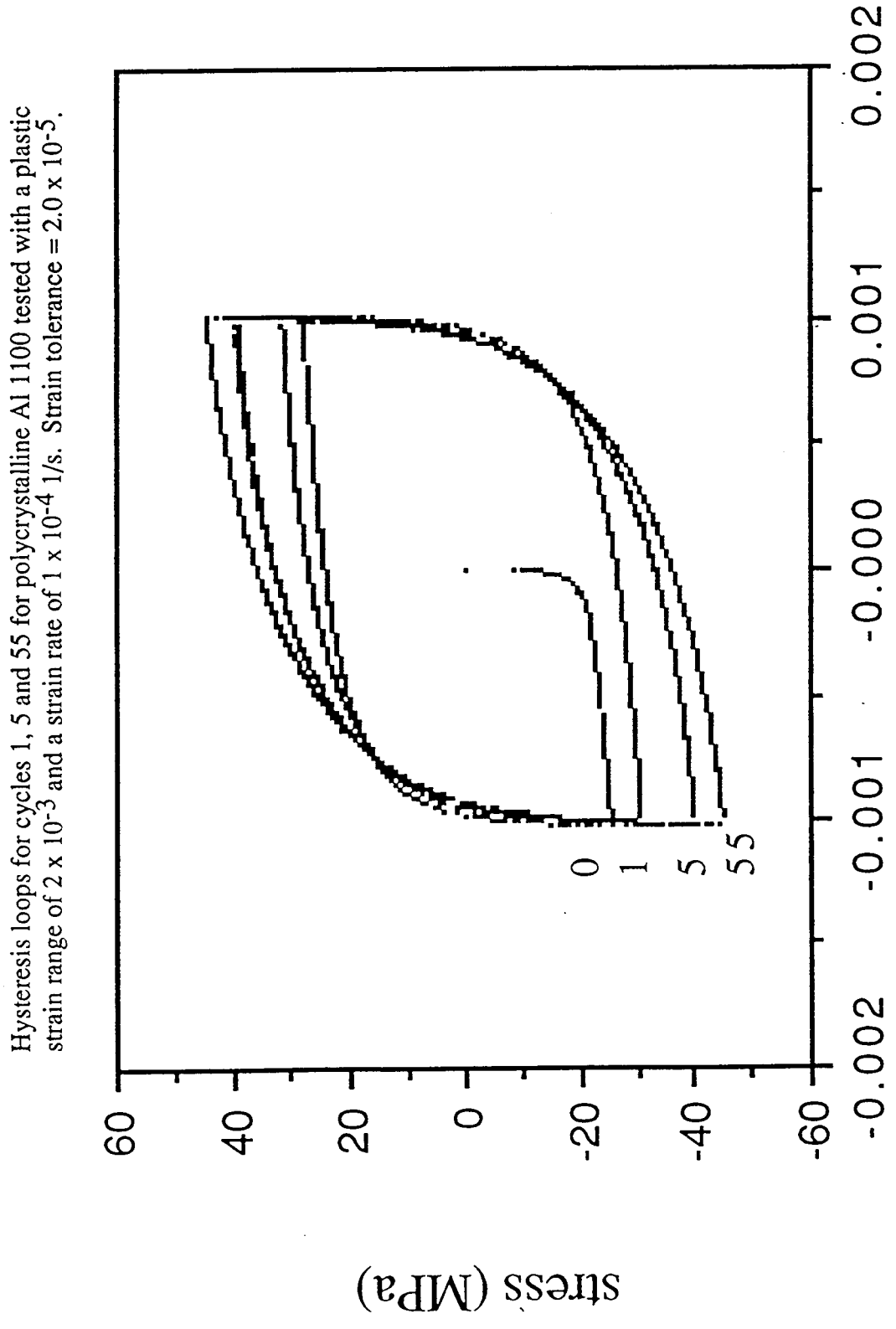

Hysteresis loops for cycles 1, 5 and 55 for polycrystalline Al 1100 tested with a plastic strain range of 2×10^{-3} and a strain rate of 1×10^{-4} 1/s. Strain tolerance = 2.0×10^{-5}.

Hysteresis loops for cycles 1, 2, 11 and 63 for polycrystalline Al 1100 tested with a plastic strain range of 2×10^{-3} and a strain rate of 1×10^{-4} 1/s. Strain tolerance $= 3.5 \times 10^{-5}$.

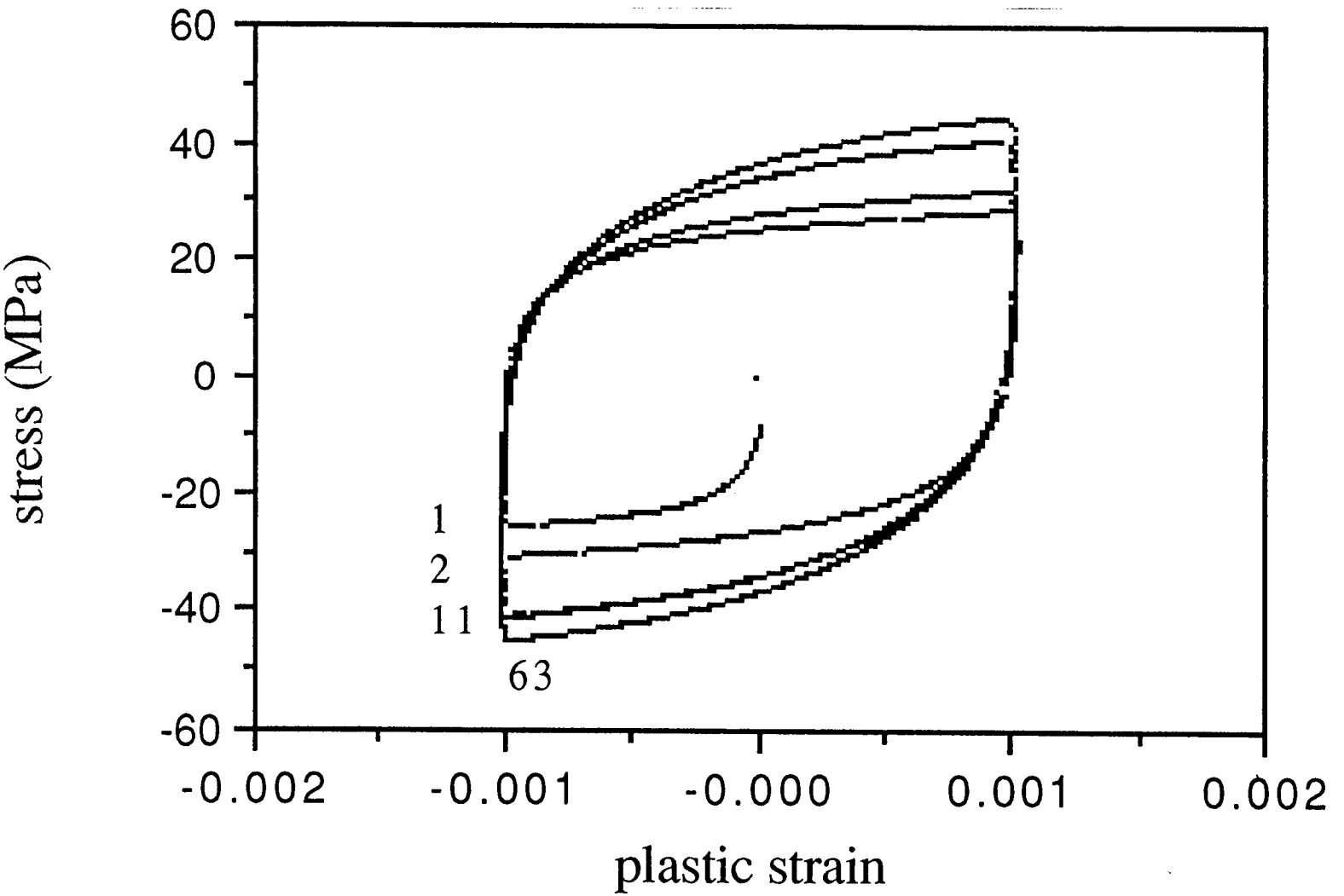

APPENDIX B

Loop adjustments using the "strain tolerance" value.

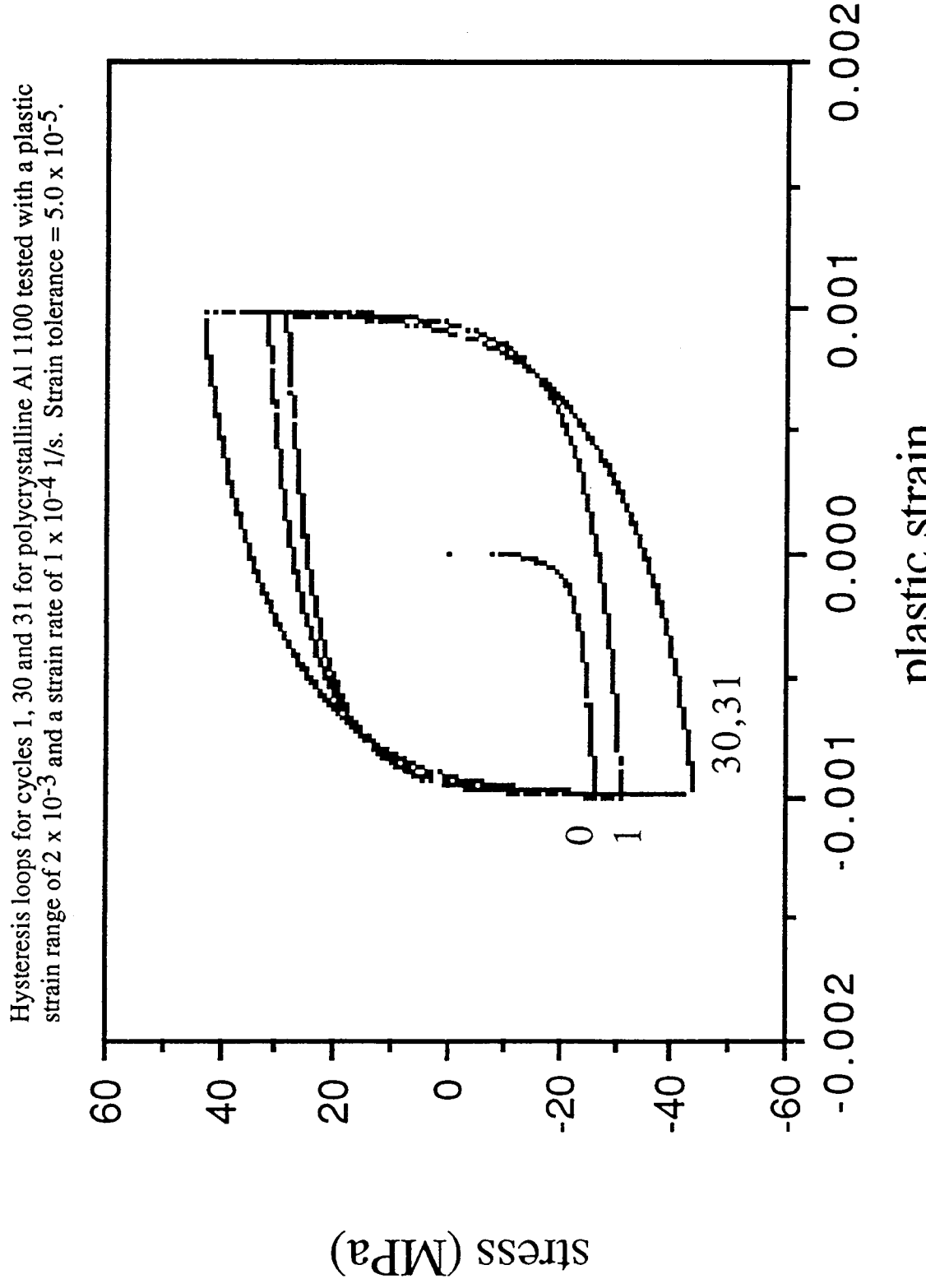

APPENDIX C

Cyclic hardening curves for 99.999% pure aluminum polycrystals. These are the data which constitute the saturation stress vs. strain plot in the body of the thesis.

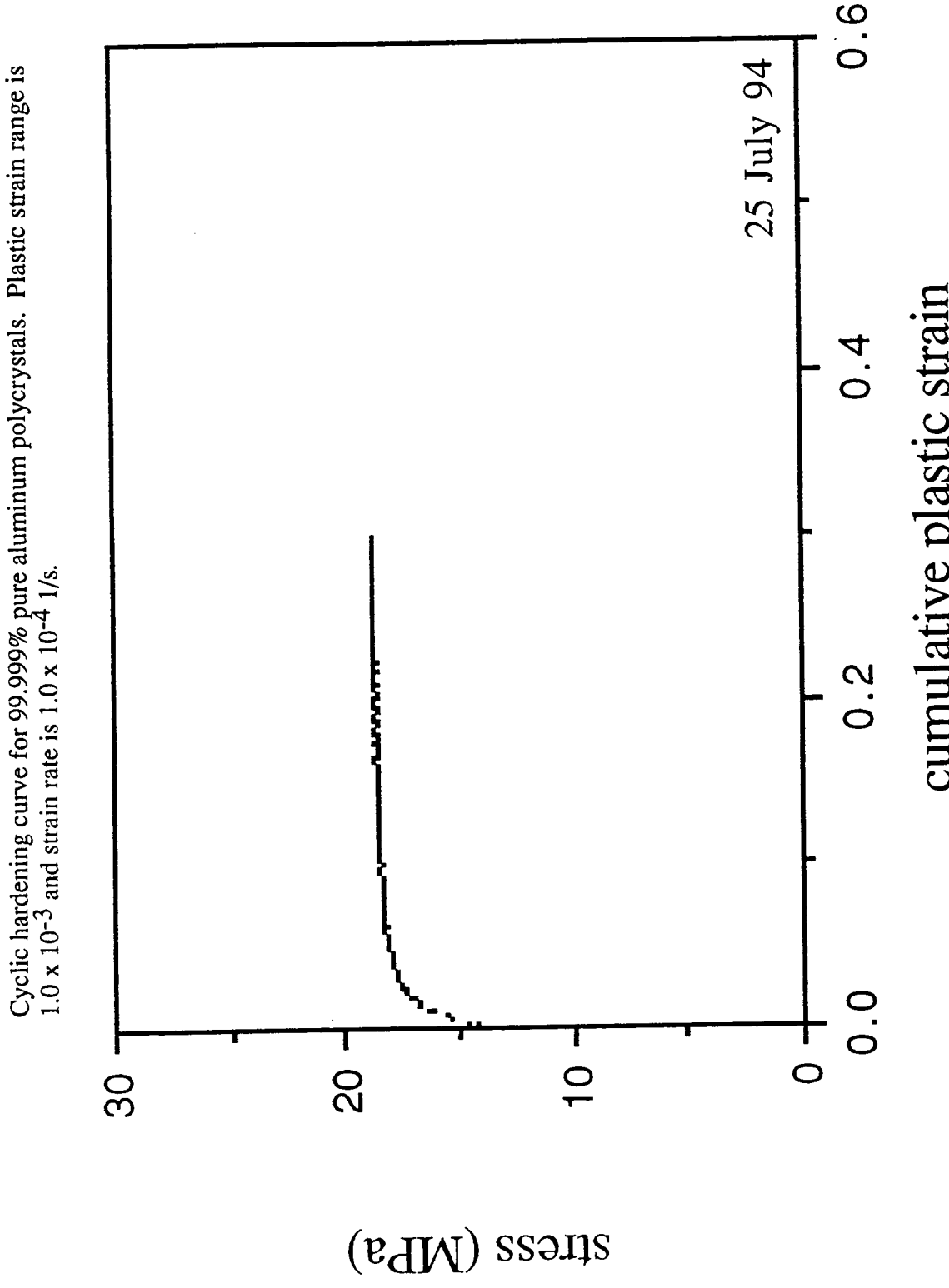

APPENDIX C

Cyclic hardening curves for 99.999% pure aluminum polycrystals. These are the data which constitute the saturation stress vs. strain plot in the body of the thesis.

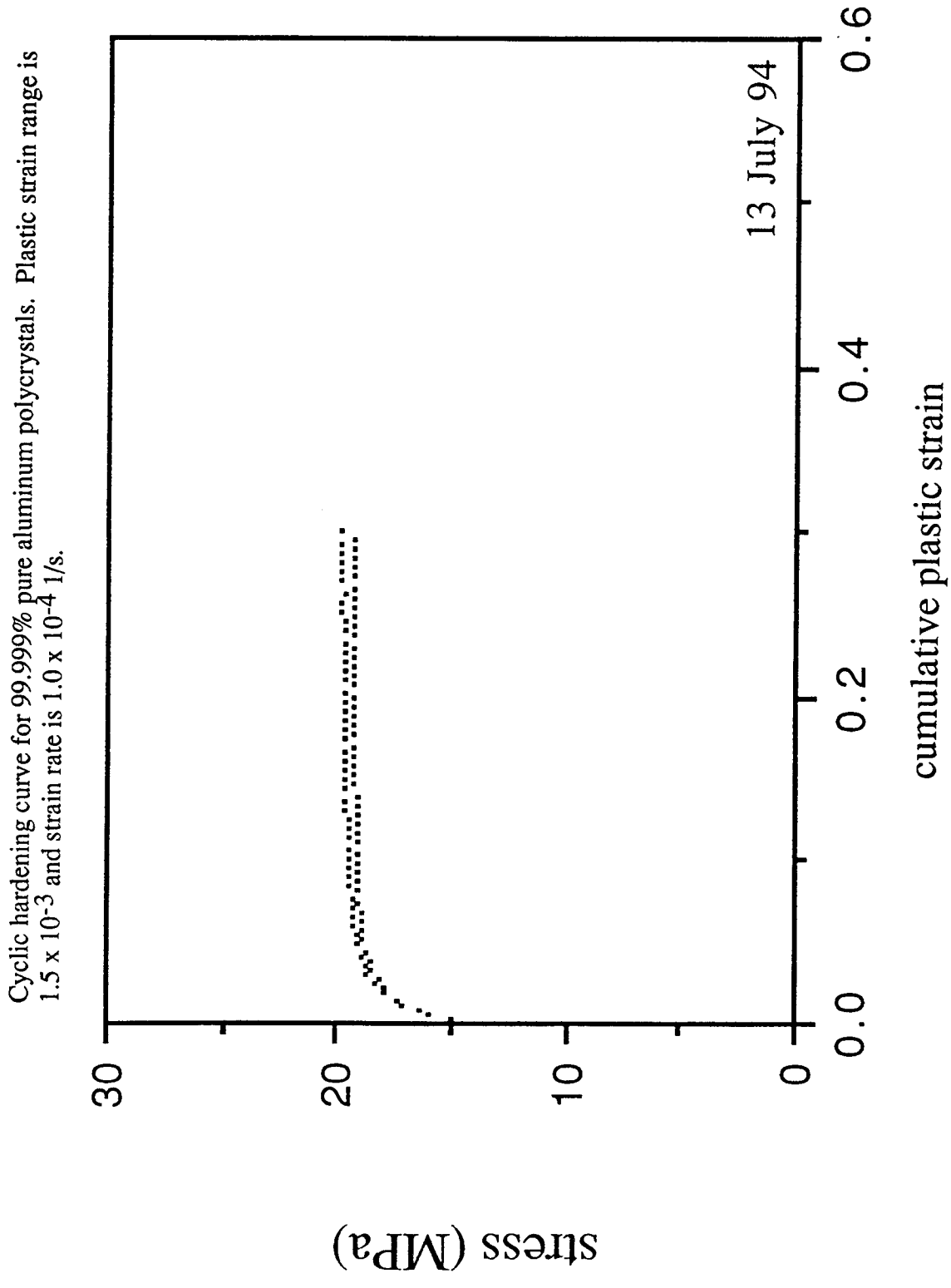

APPENDIX C

Cyclic hardening curves for 99.999% pure aluminum polycrystals. These are the data which constitute the saturation stress vs. strain plot in the body of the thesis.

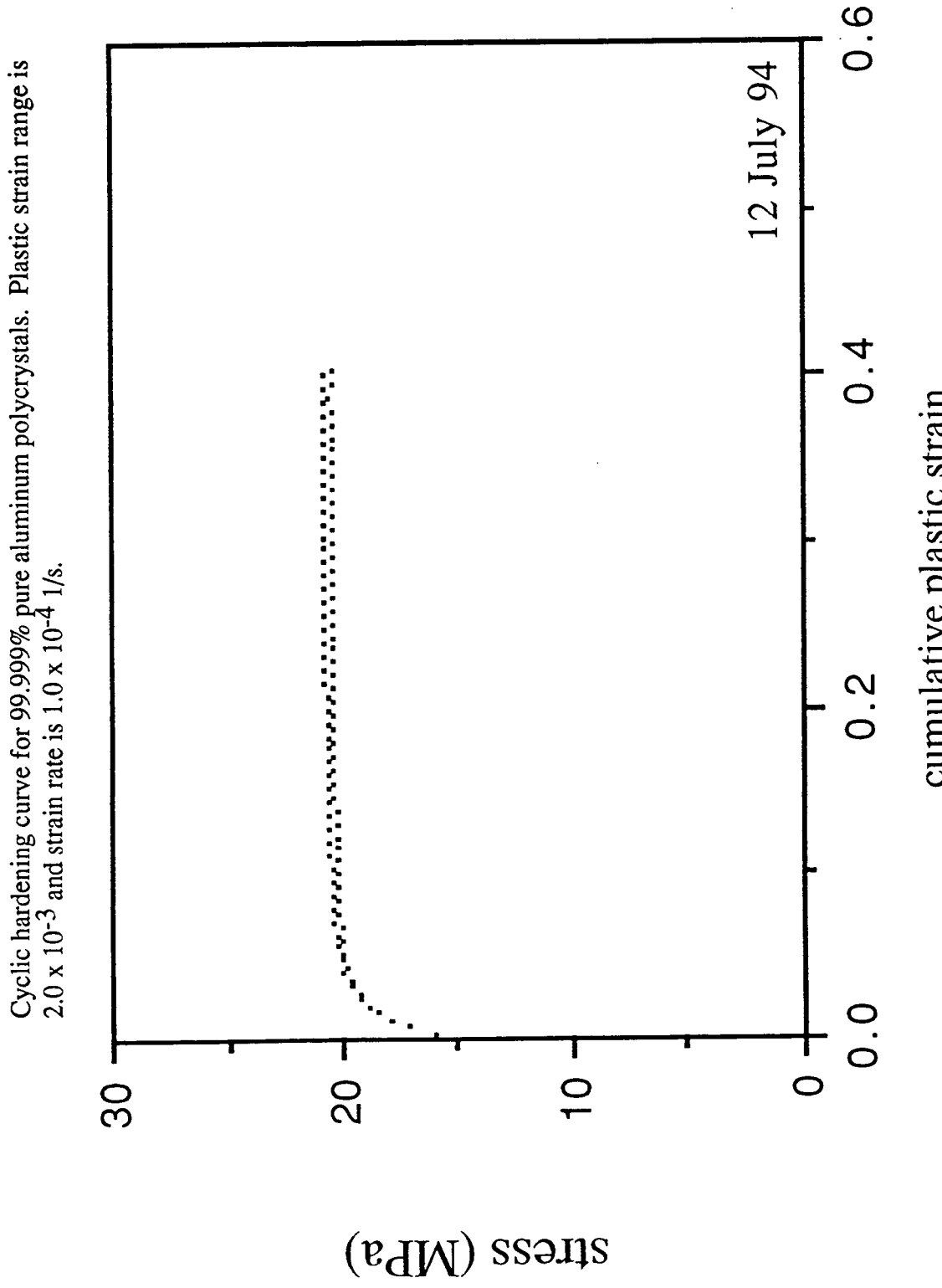

APPENDIX C

Cyclic hardening curves for 99.999% pure aluminum polycrystals. These are the data which constitute the saturation stress vs. strain plot in the body of the thesis.

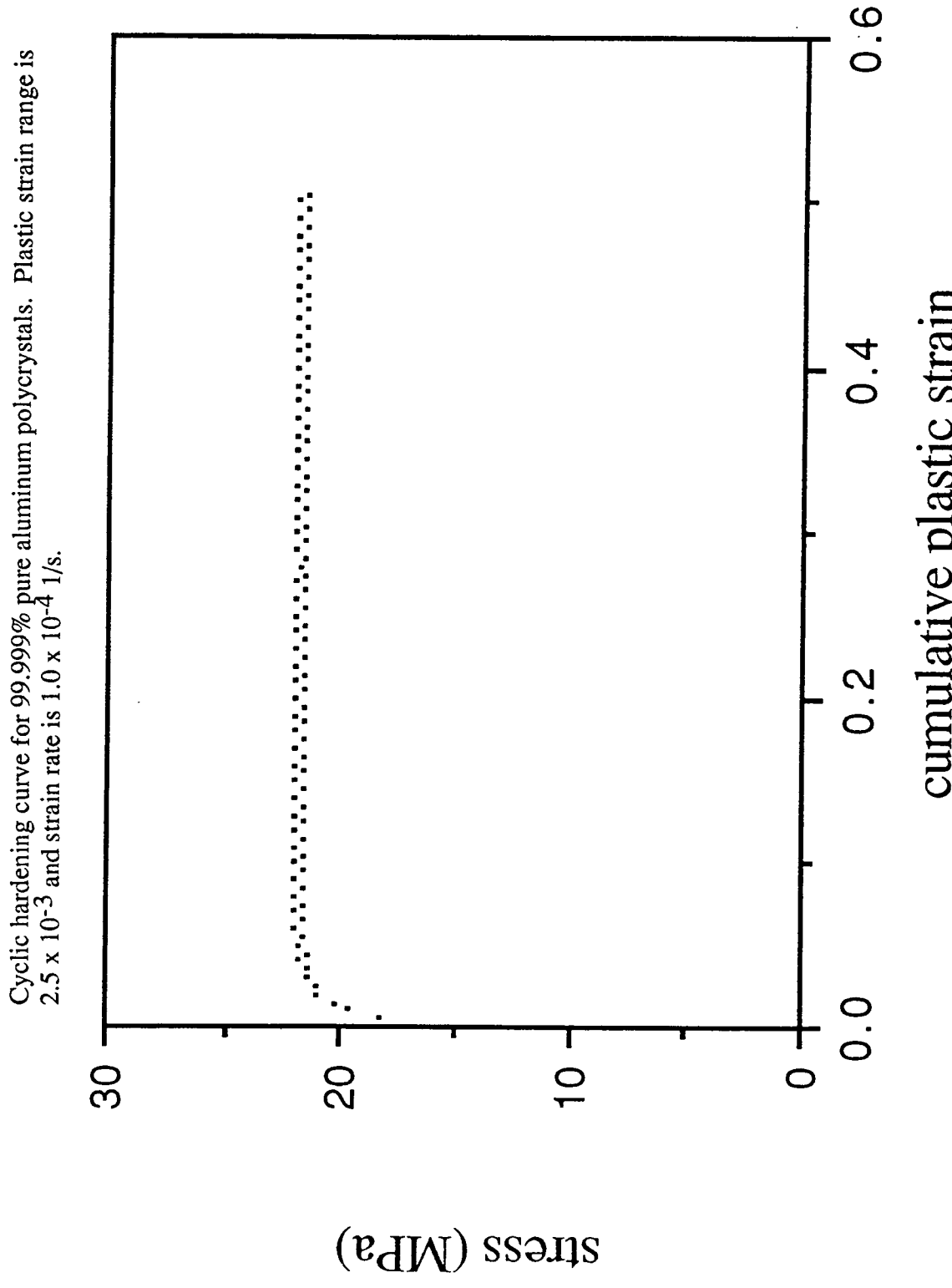

APPENDIX C

Hysteresis loops for 99.999% pure aluminum polycrystals. These are the data which constitute the saturation stress vs. strain plot in the body of the thesis.

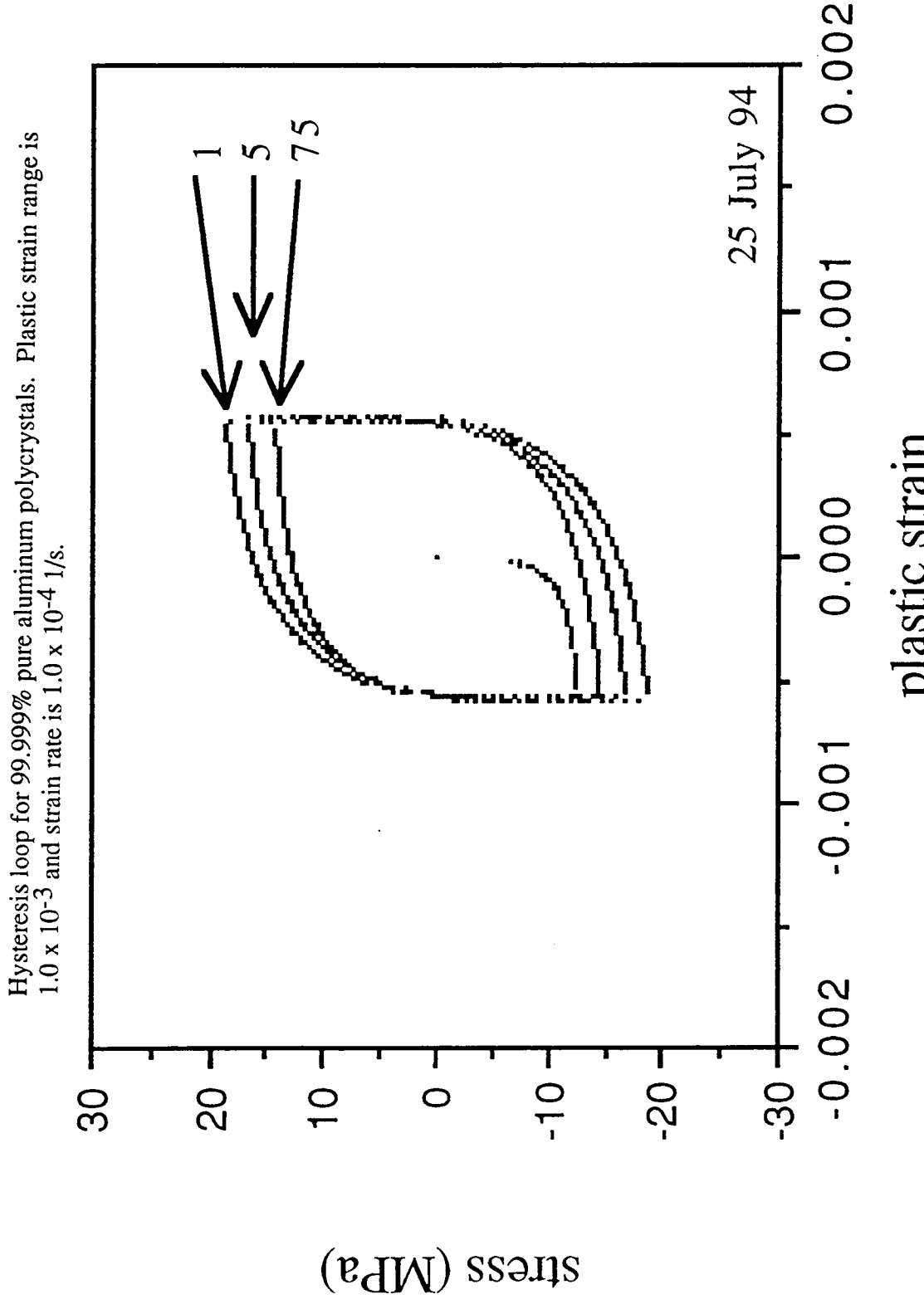

APPENDIX C

Hysteresis loops for 99.999% pure aluminum polycrystals. These are the data which constitute the saturation stress vs. strain plot in the body of the thesis.

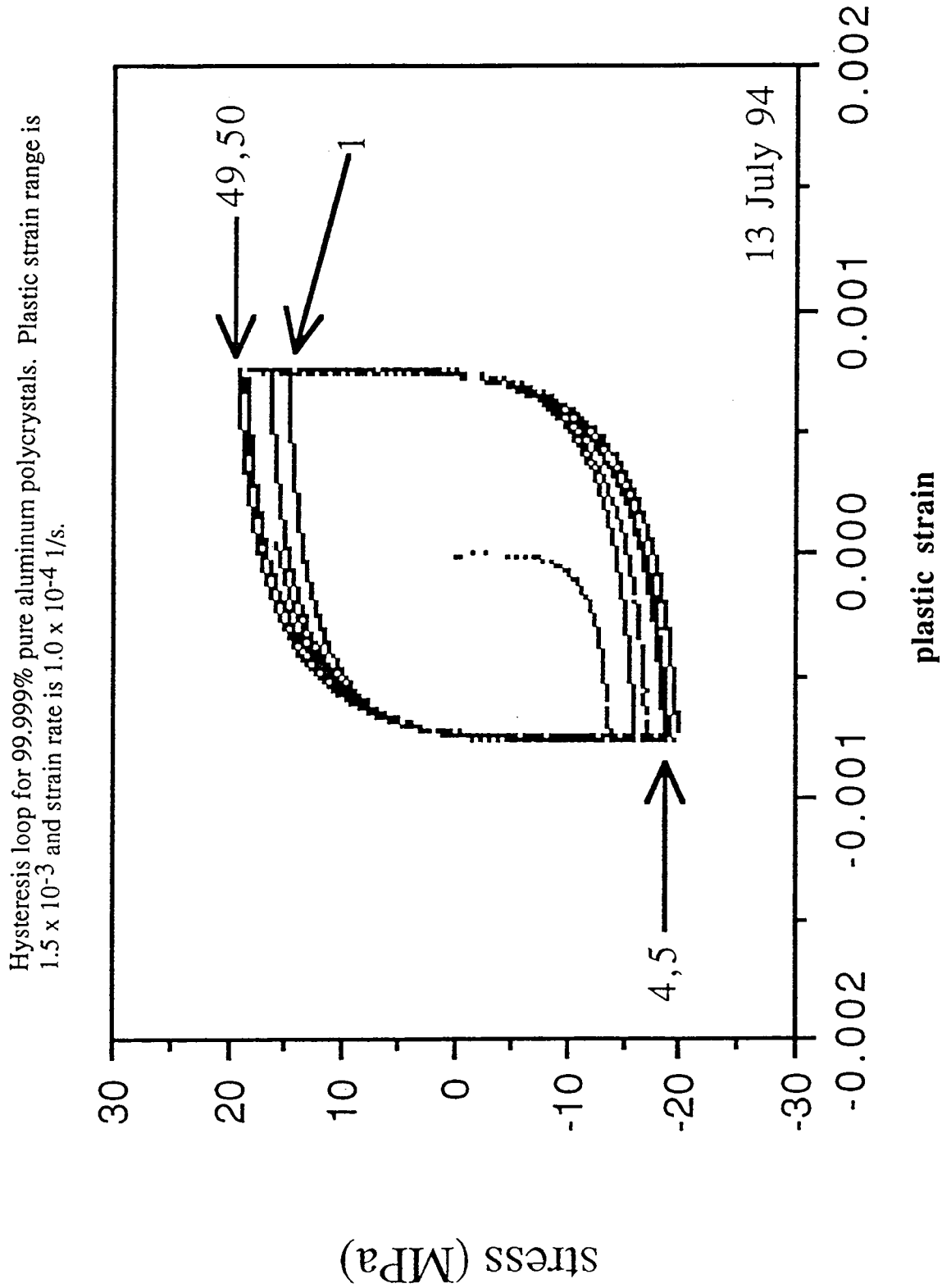

APPENDIX C

Hysteresis loops for 99.999% pure aluminum polycrystals. These are the data which constitute the saturation stress vs. strain plot in the body of the thesis.

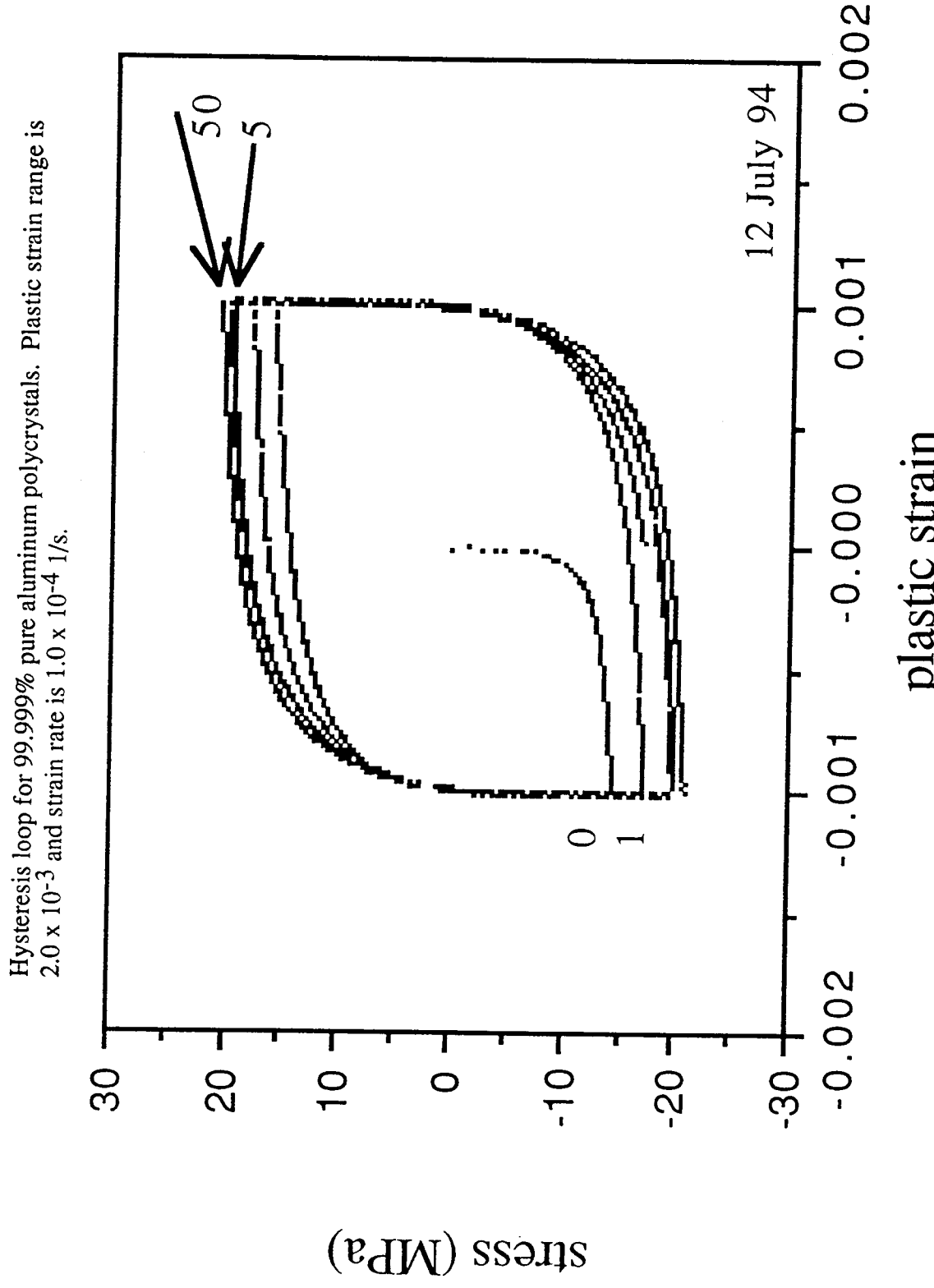

APPENDIX C

Hysteresis loops for 99.999% pure aluminum polycrystals. These are the data which constitute the saturation stress vs. strain plot in the body of the thesis.

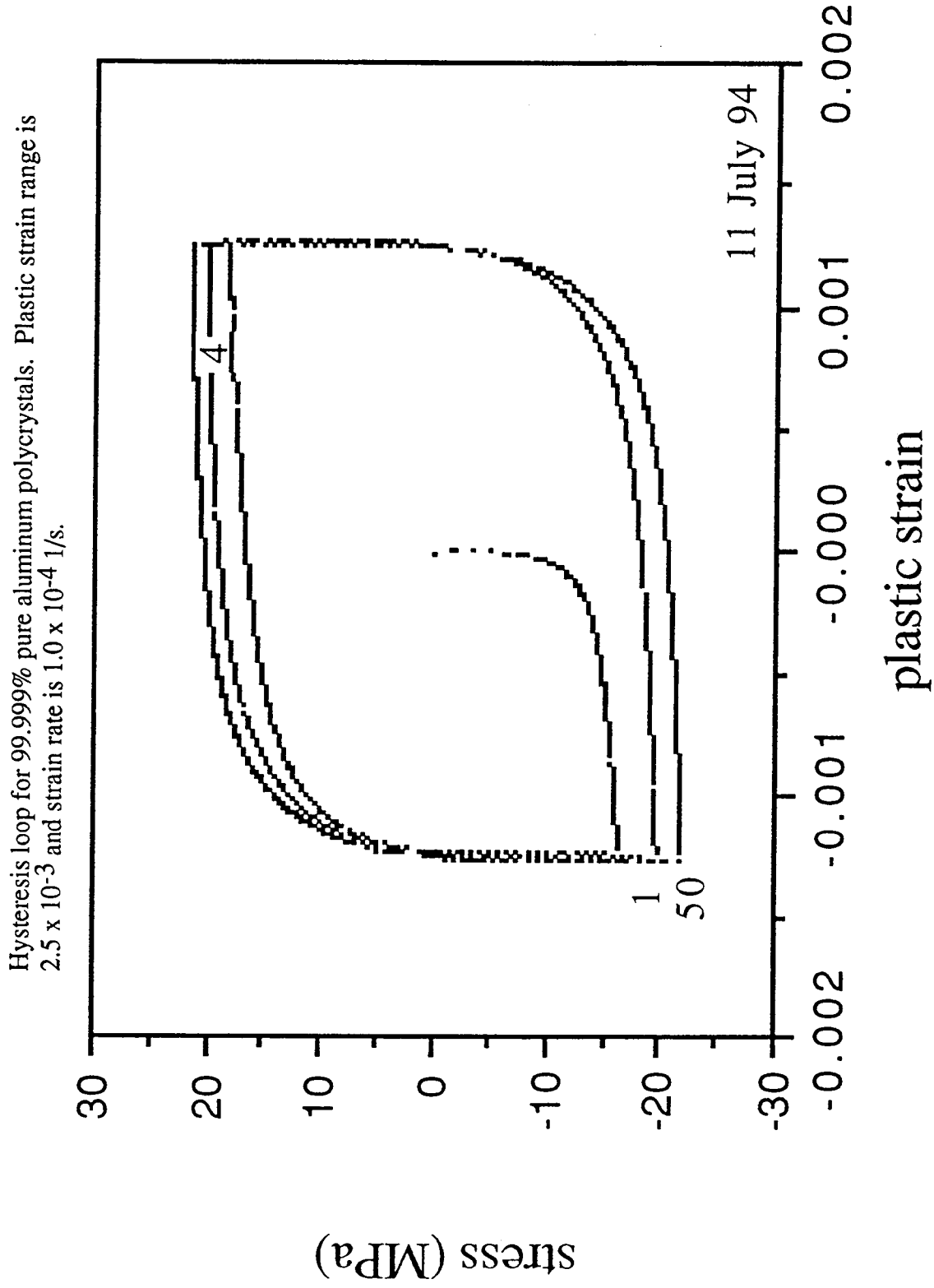

APPENDIX D

Hysteresis loop for 99.999% pure aluminum polycrystal tested at 77K.

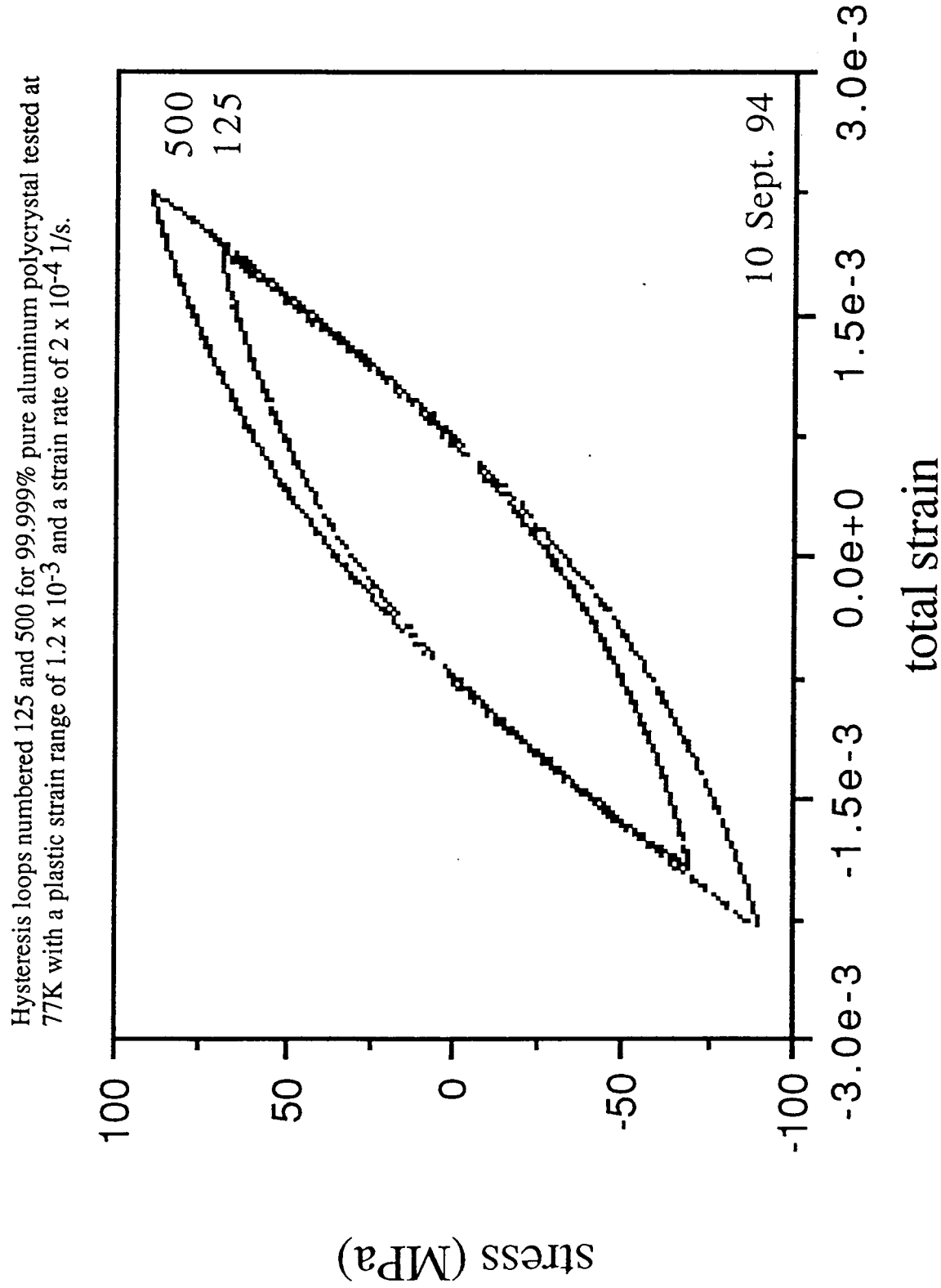

APPENDIX D

Cyclic hardening curve for 99.999% pure aluminum polycrystal tested at 77K.

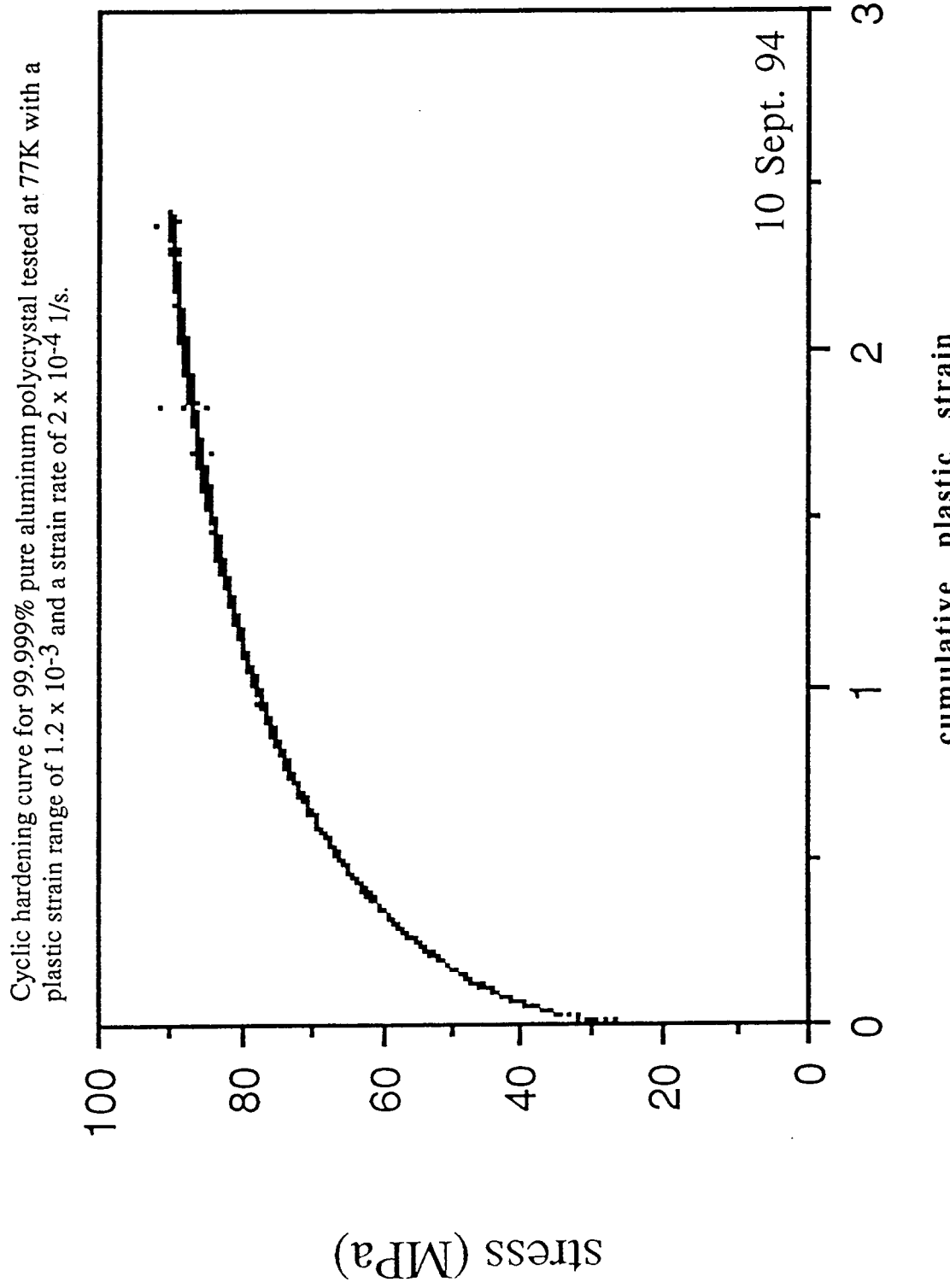

APPENDIX D

Hysteresis loop for 99.999% pure aluminum polycrystal tested at 77K.

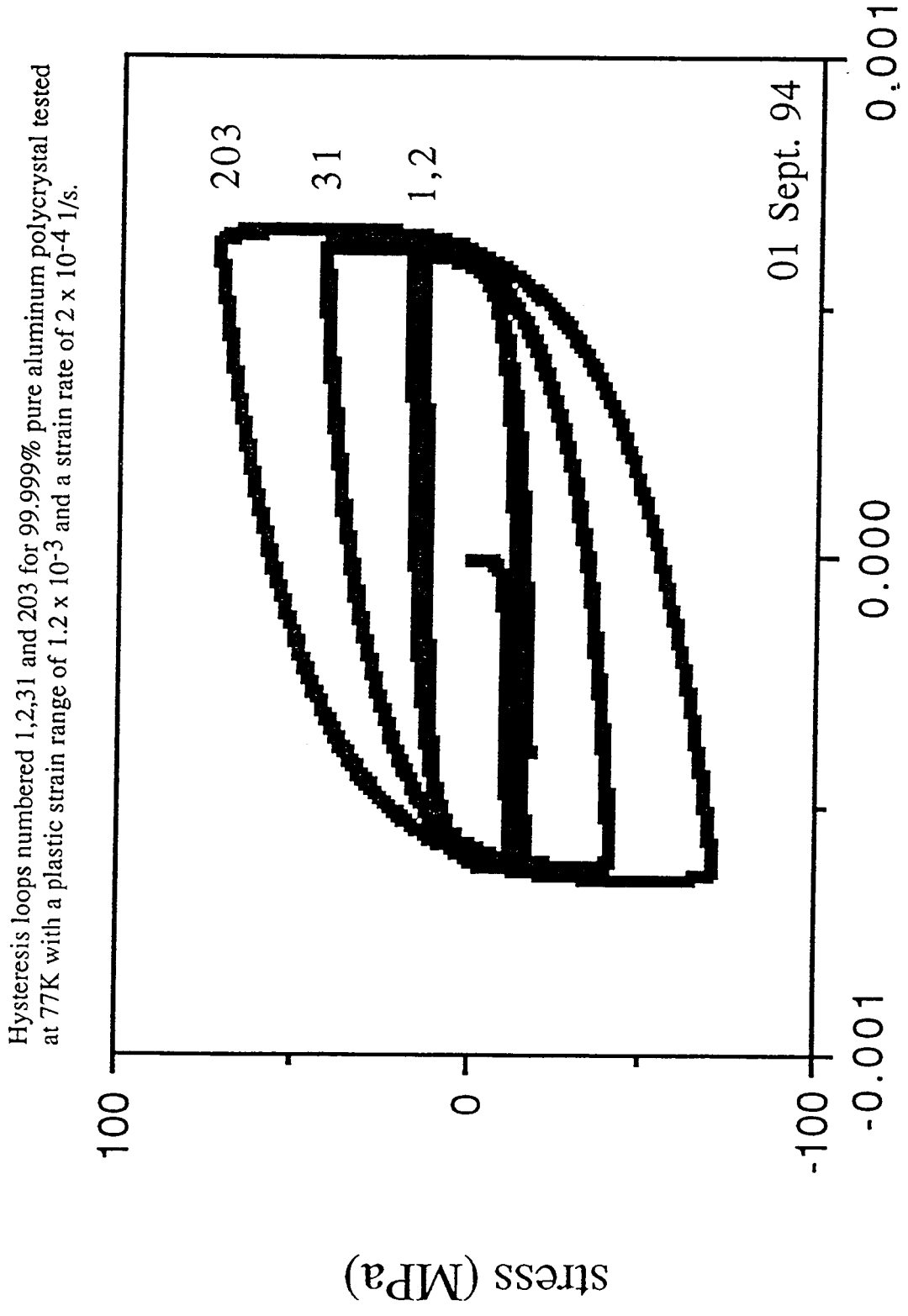

APPENDIX D

Cyclic hardening curve for 99.999% pure aluminum polycrystal tested at 77K.

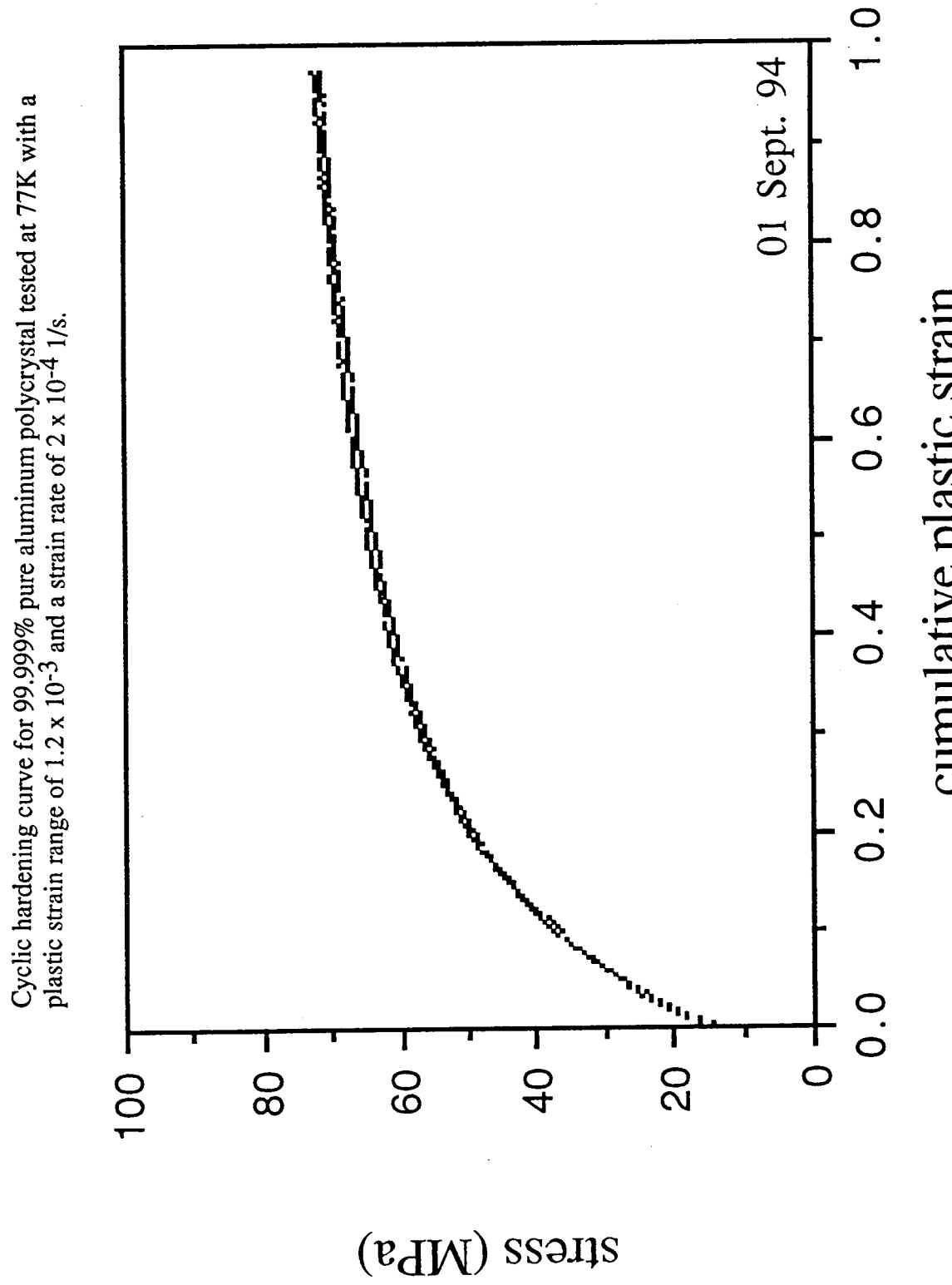

APPENDIX E

Standard Operating Procedure for Fatigue Testing with Instron 8521 and LabView

Pre-test

1. Heat treat sample if necessary.

    a) Al 1100: 550°C for 5 hours then air cool.
    b) 99.999% Al polycrystal: 325°C for 2 hours then air cool.

2. Measure sample dimensions.

    a) Record 3 diameter measurements with calipers +/- 0.001 in.
    b) Record gage length.

3. Bond strain gages to sample if needed.

    a) Room temperature: use super glue adhesive.
    b) 77 Kelvin: use M-bond 610 cured at 135°C for 4 hours and furnace cooled.
    c) Super glue gage leads.

4. Calibrate strain and load channels.

    a) Use electronic auto calibrate from Instron front panel.
    b) Check amount of space available on data acquisition.
        i) Need 10 Megabytes free on main Mac.
        ii) Need 30 Kilobytes free on back-up Mac.
    c) Load mdrcorrector26 on main Mac. and fatigue data acq. 2 on back-up Mac.
    d) Make sure strain multiplier (e.g., 92.24) is OK (main Mac. diagram: Upper 0,2; 4,2; 6,2, Lower 0,2; 4,2; 6,2; 8,2).

5. Mount sample in grips with zero load.

    i) Pull vacuum on dewar.
    ii) Put sample with dummy and wires through dewar.
    iii) Raise and affix dewar with support wire.
    iv) Mount lower flange--seal bottom only.
    a) Tighten lower grip to finger tight to prevent misalignment of sample (i.e., as loose as possible).
    b) Raise actuator to -1.000 in. and lower crosshead to insert sample into upper grip.
    c) Lower dewar onto flange **without** sealant.

    d) Completely tighten upper grip **CAREFUL**: if load increases something is wrong (torque 'till torque on Instron reads 150 in-lb).

e) Raise and affix dewar with support wire.
f) Completely tighten lower grip.
    1) Slowly tighten lower grip until load peaks at 8 lbs.
    2) Transfer to load control and finish tightening lower grip.
    3) Do not overtighten lower grip, esp. if using wrench.
g) Mount dewar, using high vacuum grease for sealant.
h) Affix thermocouple bead to load cell using rubber band.
i) Mount liquid nitrogen shield.
j) Fill dewar with liquid nitrogen.

6. Wait until sample temperature is at desired level (about 15 minutes).

    a) Monitor load cell temperature using Fluke Hydra.

7. Set data interval on back-up Macintosh.

    a) Try to record cycles 1, 4, 6, 9, 25, 50, 150.
    b) 50 data points per cycle is usually adequate (diagram).
    c) If recording cycles manually, toggle the "record" button to be white.

8. Change sample area in controlling program to area during test.

    a) For low temperature tests, area at test temp. must be calculated including coeff. of thermal expansion.
    b) Change areas in: upper,4,5; lower,4,4; lower,6,5.

9. Set modulus check parameters.

    a) For 77K, or small sample at room temp., with 0.0001 1/s, use delay = 0.4 seconds and 12 iterations.
    b) For room temp. with large sample, use delay = 1.5 seconds and 15 iterations.
    c) For 77K, with 0.0002 1/s, use delay = 150 ms and 12 iterations.

10. Set plastic strain amplitude for first and subsequent cycles.

    a) Values are axial strain--NOT shear strain.
    b) First cycle strain = 1/2 total strain.

11. Set strain rate for first and subsequent cycles.

12. Verify that data acquisition lines are connected properly.

    a) Main Macintosh GPIB connected to Instron linear axis.
    b) Back-up Mac. is on separate electrical circuit.
    c) Back-up Mac. GPIB connected to Fluke Hydra.
    d) Instron linear outputs connected to:
        1) "A"--Oscilloscope strain display.
        2) "B"--Oscilloscope load display.
        3) "X"--Fluke Hydra channel 1 (load).
        4) "Y"--Fluke Hydra channel 2 (strain).
    e) Thermocouple connected to Fluke Hydra channel 7 and load cell.

Test

13. Start Instron control program (DO NOT PUSH "READY" BUTTON).

    i) Mark on computer screen where "Stop Loop" toggle switch is.

    a) Make sure Instron is in Load Control.

    b) Flip toggle switch to "run loop."

    c) Switch slider to "run test."

    d) Ensure LabView is in "unlocked" state.

    e) Press "go arrow".

    f) Press "remote" button on Instron front panel.

    g) Enter names for data files (place into Fatigue Data folder) on main Mac.

    h) Top off liq. Nitrogen.

    i) Record time.

14. Start data acquisition on back-up Mac.: press "go arrow."

15. Push "ready" button on main Mac.

16. Record load at end of first 10 cycles on paper. Record modulus.

17. Periodically refill liquid nitrogen dewar such that liquid is always visible from above dewar.

18. Stop test via "stop loop" toggle switch on main Mac. 1/2 cycle before endpoint is reached.

19. Wait until waveform generator has stopped: "END".

20. Stop data acquisition.

21. Put Instron in "Load Control":

    a) Press "function" on Instron front panel.

    b) Press the "active" button if displayed.

    c) Press "load" button.

    d) Press "goto" then enter zero "0".

Post-test

22. Print front panel from both Macintoshes.

23. Remove sample:

a) Loosen top grip nuts until "finger tight."
b) Put Instron in "Position Control" (position immediate).
c) **CAREFUL**: Upper/small grip may not release. Lower actuator 1" to remove sample from upper grip with Instron key panel.

c*) If upper grip does not release, completely loosen nuts (try to leave at least one Al threaded rod attached to plate) until plate falls away from grip.

d) Raise the crosshead:

i) **CAREFUL**: steel support wire must not catch dewar valve.

1) Loosen "clamp" valve on Instron frame.
2) Loosen "raise" valve on Instron frame.
3) Allow crosshead to move within six inches of the top of its travel.
4) Tighten "raise" valve.
5) Tighten "clamp" valve.

6*) Loosen upper collet from above by opening with needle nose pliers, or by inserting a screw driver.
7*) Pull upper collet out by hand or pliers.
8*) Remove plate by Al threaded rod (insert rod if necessary).

e) Loosen bottom grip nuts with socket and ratchet.
f) Pull sample up by the strain gage wires, or pliers.
g) Clip strain gage wires with edge cutters.
h) Immerse sample in liquid nitrogen for transport.

24. Analyze data:

a) Delete data files MDRSTRAIN1,2,3,4.

b) Load "read cyclic" Labview program.

1) Press go arrow.
2) Select file corresponding to load maximums data file.
3) Select number of data points equal to number of logged data points.
4) Flip toggle switch.

c) Load "read fatigue" Labview program.

1) Change name of file to MDRSTRAIN2.
2) Select first data point as "0", then last as "300" to record first 300 data points.
3) Press go arrow.

4) Select file corresponding to "ascii" data file.
5) Flip toggle switch.
6) Repeat with MDRSTRAIN3,4 for middle and end sets of 300 data points by changing (1) and (2).

d) Plot with spreadsheet.

1) MDRSTRAIN1 is cyclic hardening data.

i) Load values are actual (first or last value may be garbage).
ii) Number of cycles data needs to be made positive (i.e., add 2*{total # of cycles} to all #s) and divided by 2.
iii) Stress is obtained by using crossectional area at test temperature (see 8.a.) 0.006895 MPa/psi.
iv) Cumulative plastic strain is 4*cycles*plastic strain amplitude.
v) Plot Cumulative plastic strain vs. Stress (MPa).

2) MDRSTRAIN4 (if 4 is the last set) is the file with all of the hysteresis data.

i) Select one "loop" of data from each 300 data points.
ii) Modify strain values by "x2" then divide by the multiplier used above in 4.d. to get the actual strain values. Don't forget to center the strain at zero.
iii) Stress is obtained by using crossectional area at test temperature (see 8.a.) 0.006895 MPa/psi.
iv) Subtract elastic strain from (ii) to get plastic strain. Use the measured modulus from front panel (see 16).
v) Plot Plastic strain vs. Stress (MPa).

APPENDIX F

LabVIEW2 Program

The following ten pages are the graphical depiction of the LabVIEW2 program entitled "mdr gages26corrector". The "mdr" is the author's initials; the "gages" refers to the input device for control being strain gages; the "26" refers to the number of complete versions that the program has been through in its development; and the "corrector" refers to the fact that the program "corrects" the natural response of the testing system to move hysteresis loops left or right in strain, and also the corrector describes the program's ability to account for the delay between the time when a command is given and when it is realized at the sample.

This program does basically two things. First, it controls an Instron 8521 Bi-Axial Servo-hydraulic Testing Machine. Second, it performs data acquisition.

The program operates on an Apple Macintosh, and communicates with the Instron through a GPIB interface.

The first five pages of the program listing plots the general structure of the program. It is actually a three-dimensional program, with two dimensions being plotted from left to right (first five pages) and top to bottom of each page. The third dimension is represented in the subsequent five pages. These subsequent pages represent "nested" loop type structures that would be "below" the structures on the first five pages. These nested loops are denoted by a lowercase Greek letter at the bottom of their respective location in the first five pages, and at the top of the corresponding nested loop in the subsequent pages. These nested loops are ordered from top-to-bottom, and left-to-right.

These complications come from the way in which the program was developed. Since the equipment that the program is controlling is very expensive, the program must be very robust, and must do all that is possible to protect the equipment. Consequently, there are many parts of the program that check on the machinery, and may stop the test at any point. As an additional precaution, this program was written using "data dependence" as a programming convention. In other words, the execution of step "e" depends on the successful execution and redundant checking of the success of step "d". This adds to the size and complexity of the program, but should make it safer to samples, machinery, and operator.

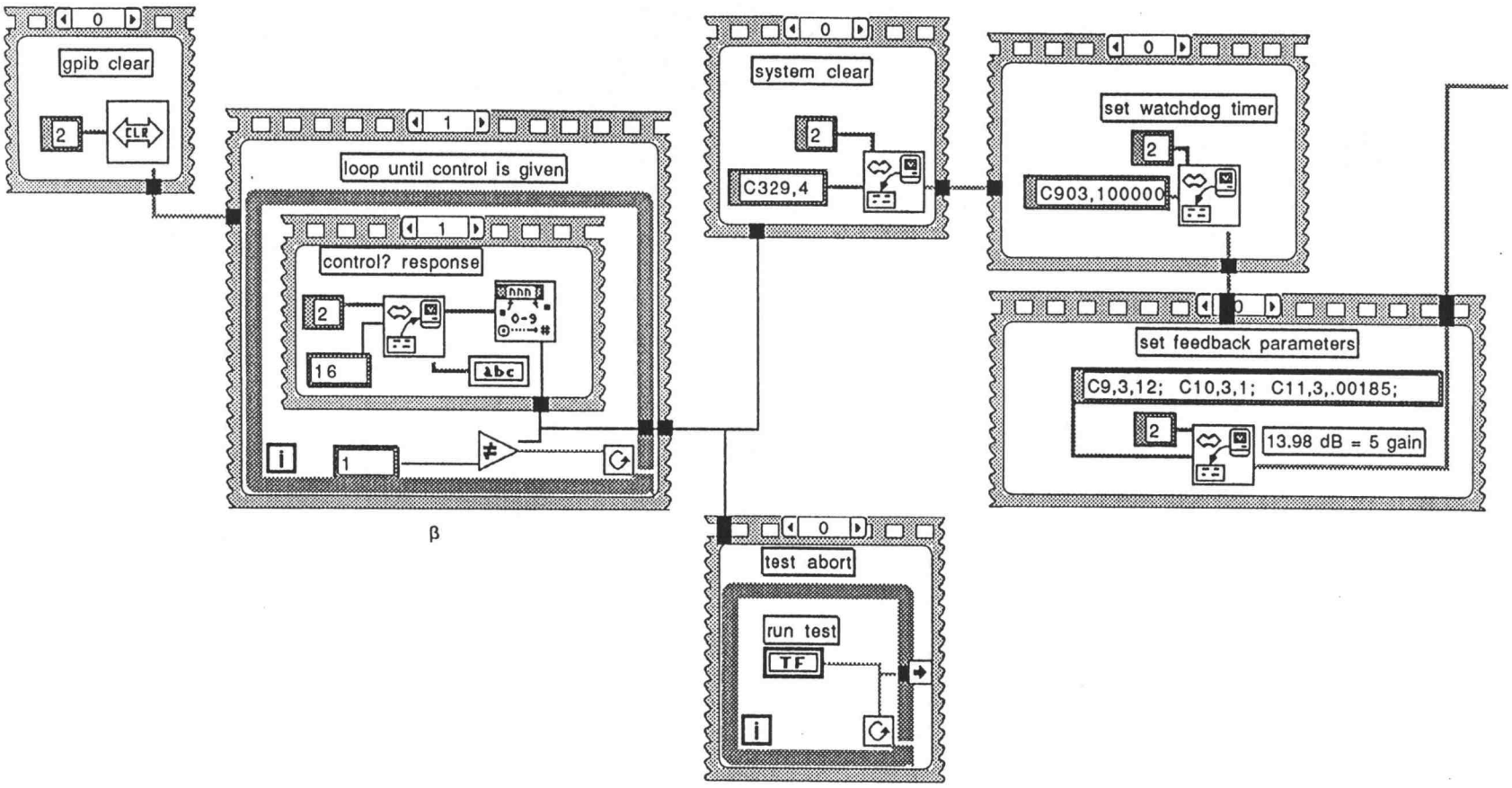
0
gpib clear
2
CLR
1
loop until control is given
1
control? response
2
16
abc
0-9
i
1
β
0
system clear
2
C329,4
0
set watchdog timer
2
C903,100000
0
set feedback parameters
C9,3,12; C10,3,1; C11,3,.00185;
2
13.98 dB = 5 gain
0
test abort
run test
TF
i
δ

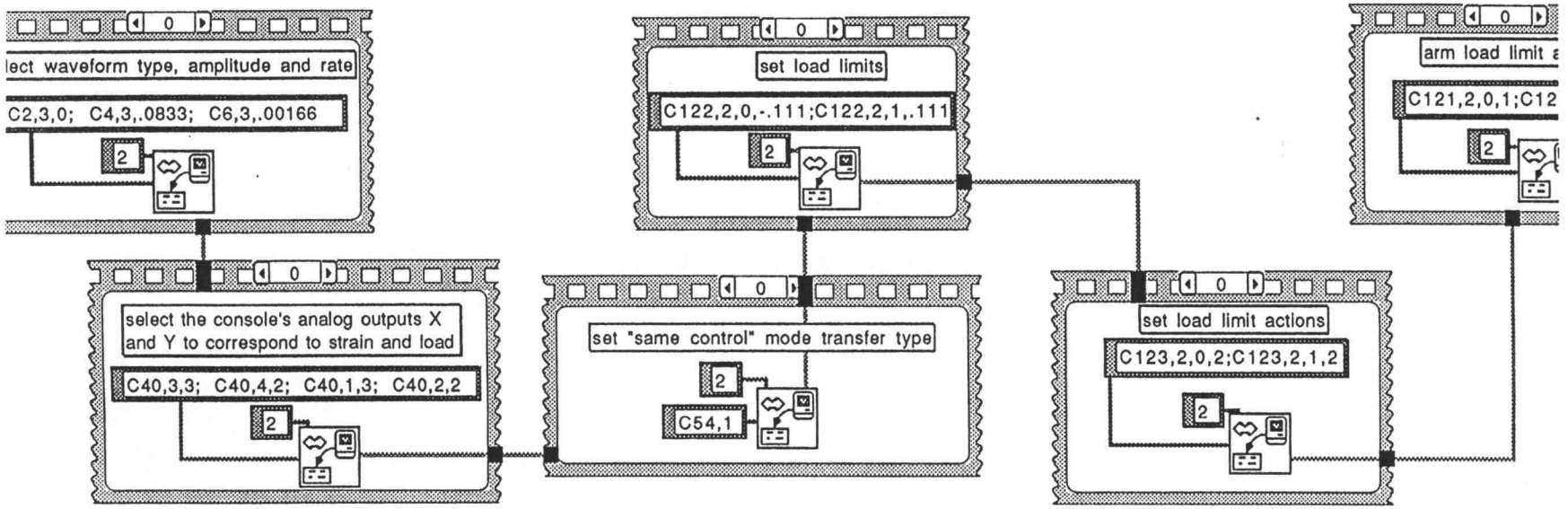
lect waveform type, amplitude and rate
C2,3,0; C4,3,.0833; C6,3,.00166
2
select the console's analog outputs X
and Y to correspond to strain and load
C40,3,3; C40,4,2; C40,1,3; C40,2,2
2
set "same control" mode transfer type
2
C54,1
set load limits
C122,2,0,-.111;C122,2,1,.111
2
set load limit actions
C123,2,0,2;C123,2,1,2
2
arm load limit a
C121,2,0,1;C12
2

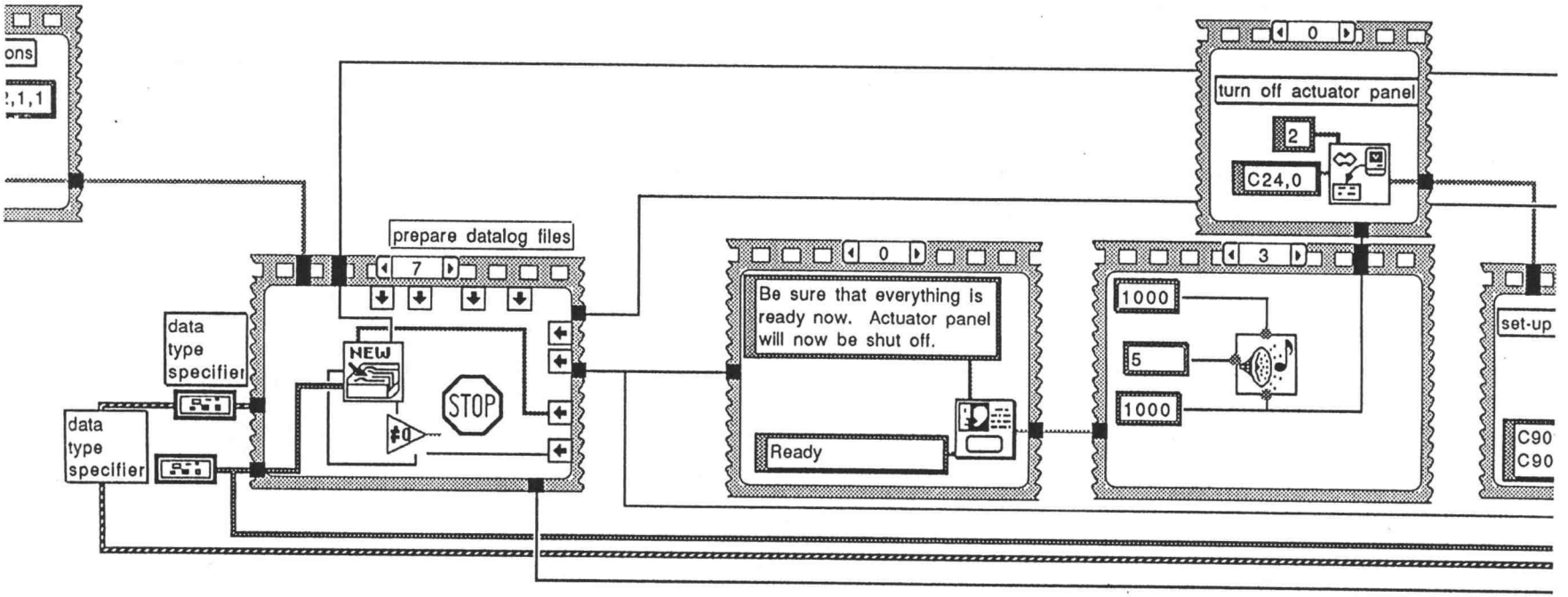
ons
:,1,1
prepare datalog files
7
data
type
specifier
data
type
specifier
NEW
STOP
#0
0
Be sure that everything is
ready now. Actuator panel
will now be shut off.
Ready
0
turn off actuator panel
2
C24,0
3
1000
5
1000
set-up
C90
C90

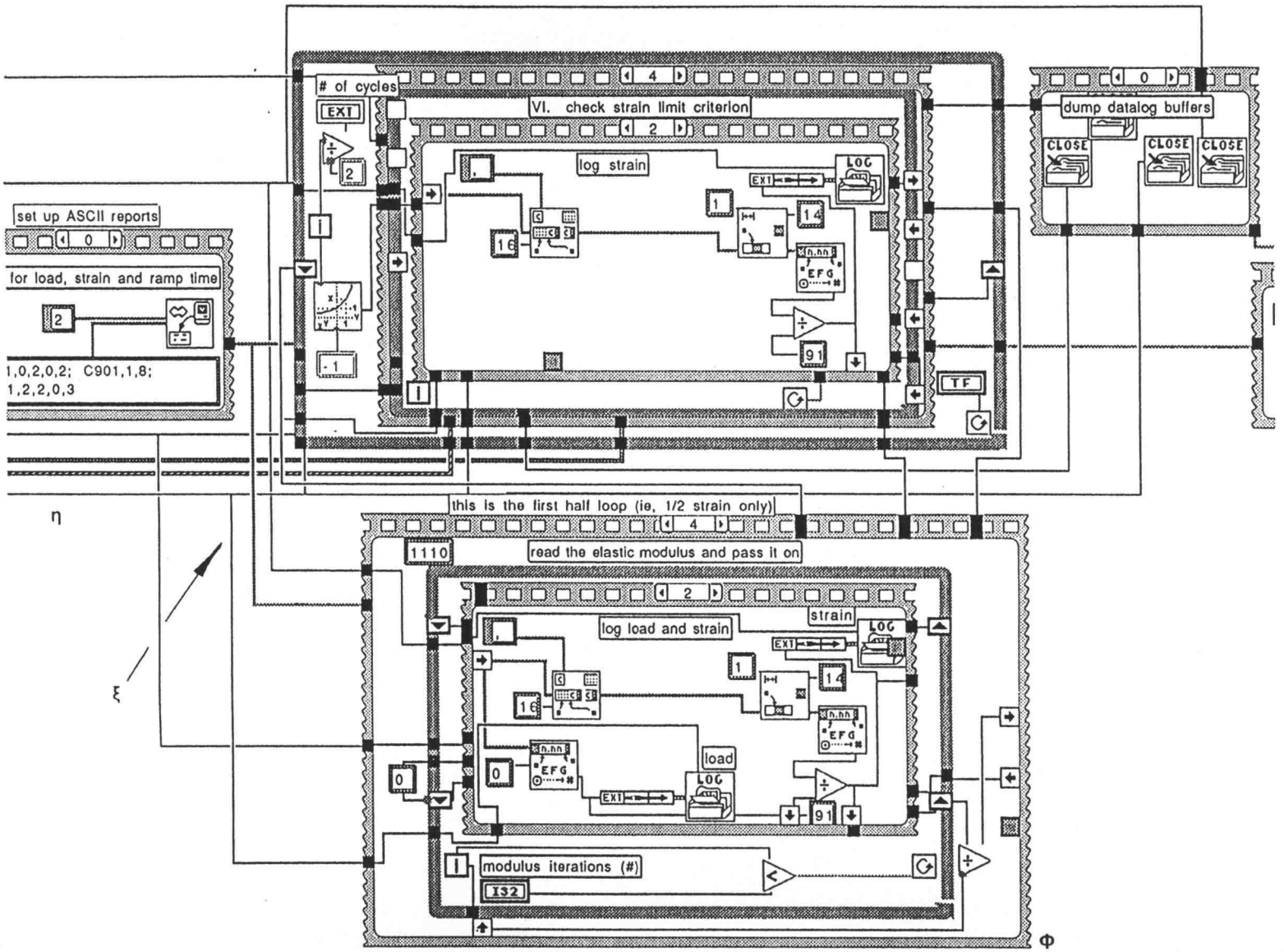
set up ASCII reports
for load, strain and ramp time
1,0,2,0,2; C901,1,8;
1,2,2,0,3
# of cycles
EXT
VI. check strain limit criterion
log strain
dump datalog buffers
CLOSE
CLOSE
CLOSE
TF
this is the first half loop (ie, 1/2 strain only)
1110
read the elastic modulus and pass it on
log load and strain
strain
load
modulus iterations (#)
I32
η
ξ
Φ

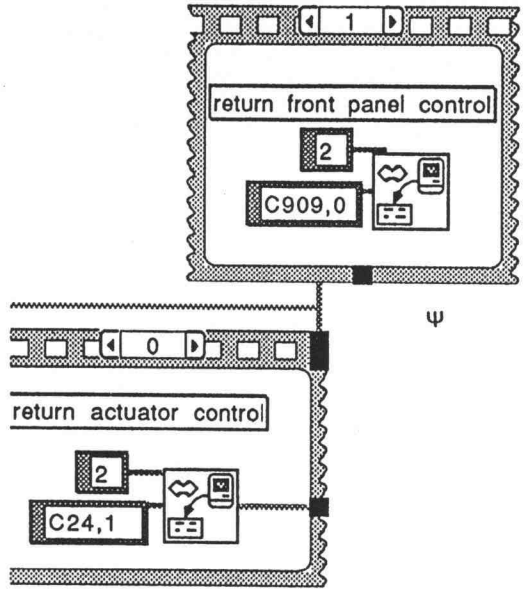
1
return front panel control
2
C909,0
Ψ
0
return actuator control
2
C24,1

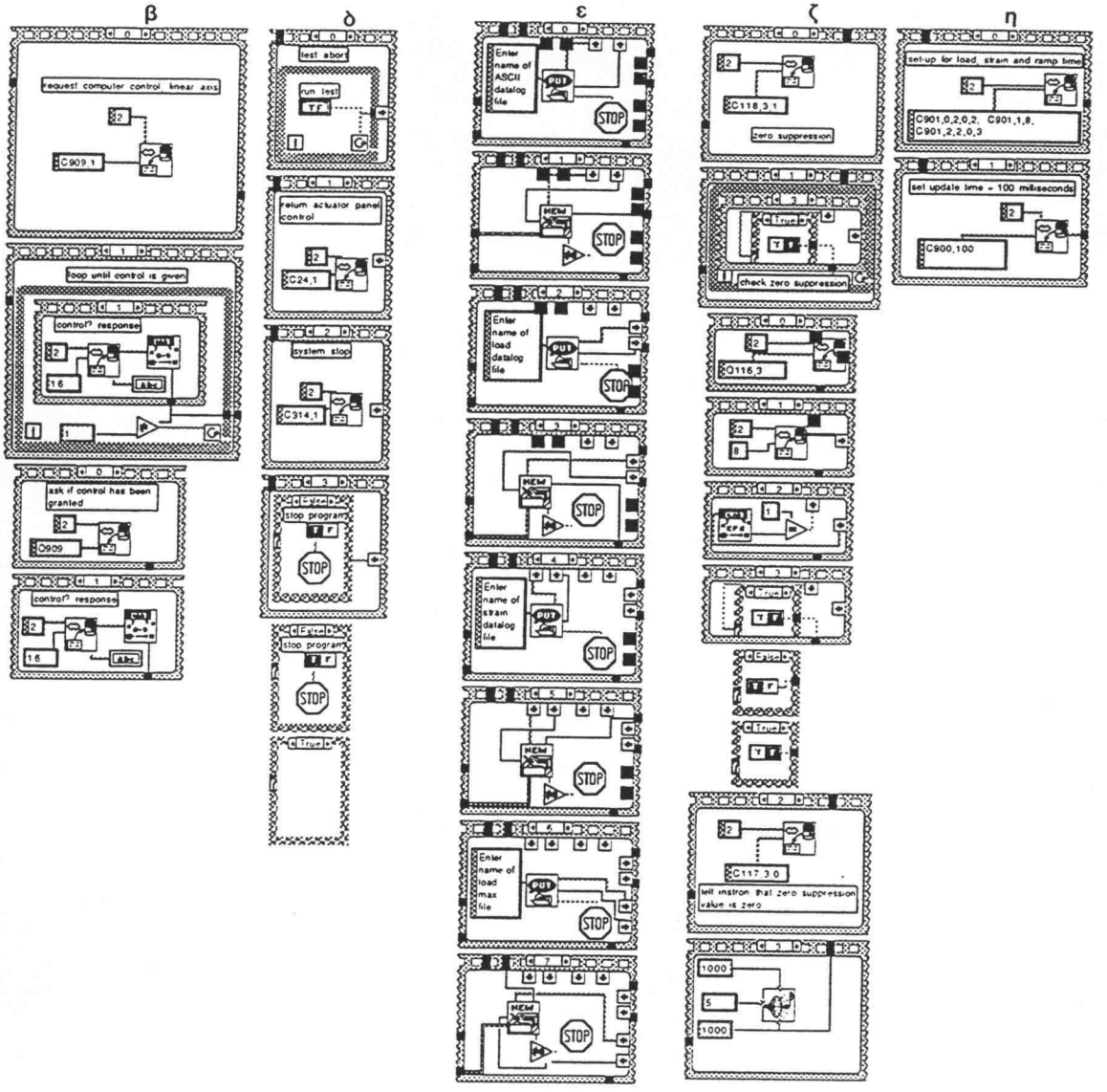
β
request computer control linear axis
C909,1
loop until control is given
control? response
ask if control has been granted
O909
control? response
δ
test abort
run test
return actuator panel control
C24,1
system stop
C314,1
stop program
STOP
stop program
STOP
ε
Enter name of ASCII datalog file
PUT
STOP
MEM
STOP
Enter name of load datalog file
PUT
STOP
MEM
STOP
Enter name of strain datalog file
PUT
STOP
MEM
STOP
Enter name of load max file
PUT
STOP
MEM
STOP
ζ
C118,3,1
zero suppression
check zero suppression
O116,3
C117,3,0
tell instron that zero suppression value is zero
1000
5
1000
η
set-up for load, strain and ramp time
C901,0,2,0,2; C901,1,8; C901,2,2,0,3
set update time = 100 milliseconds
C900,100

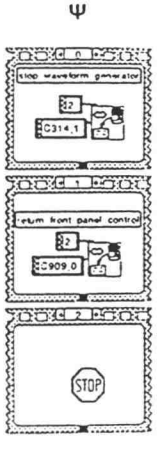
Ψ
stop waveform generator
C314,1
return front panel control
C909,0
STOP

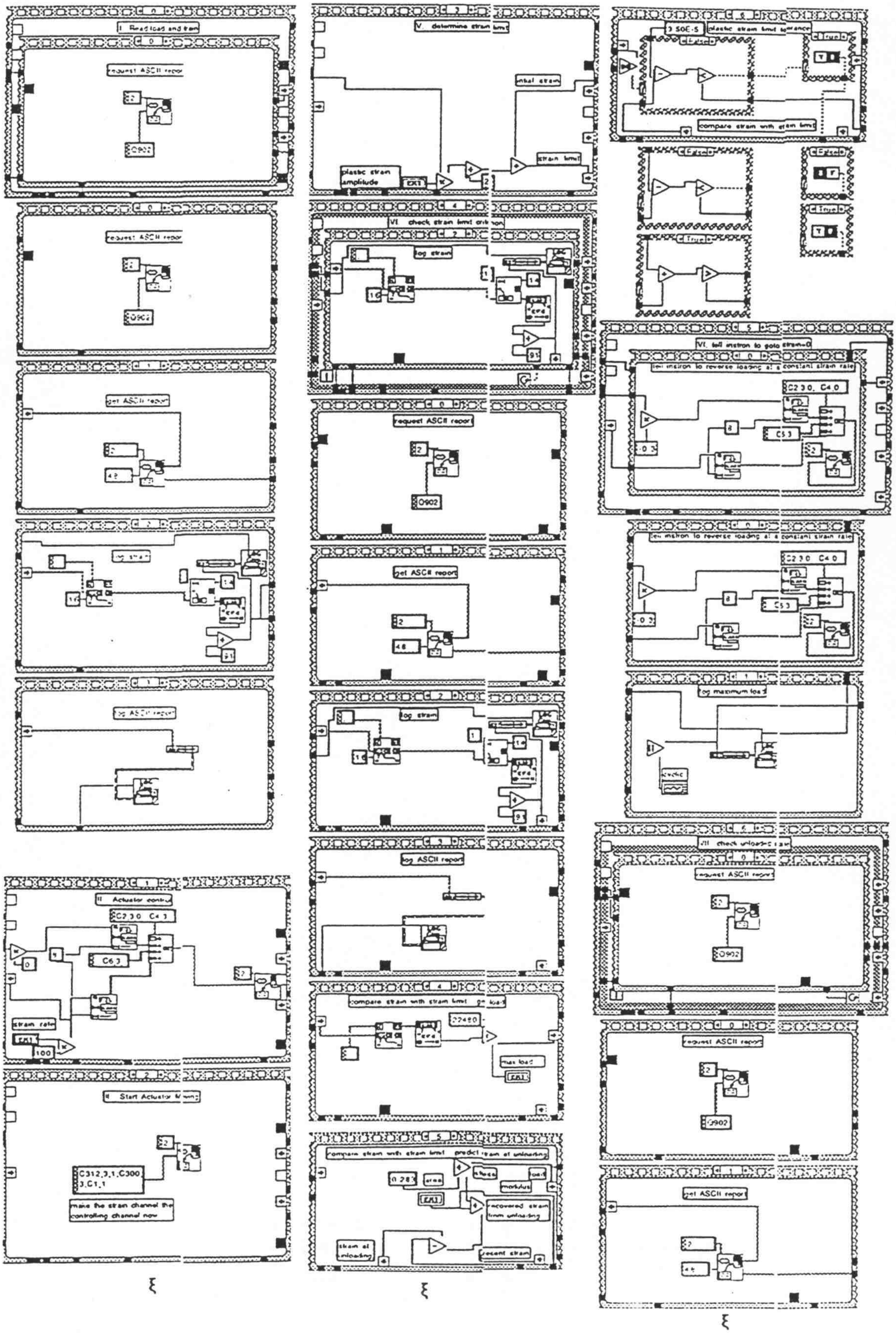

request ASCII report
get ASCII report
log strain
log ASCII report
II. Actuator control
strain rate
III. Start Actuator Moving
make the strain channel the controlling channel now
V. determine strain limit
plastic strain amplitude
strain limit
VI. check strain limit criterion
compare strain with strain limit
max load
recovered strain from unloading
strain at unloading
plastic strain limit tolerance
tell instron to reverse loading at a constant strain rate
log maximum load

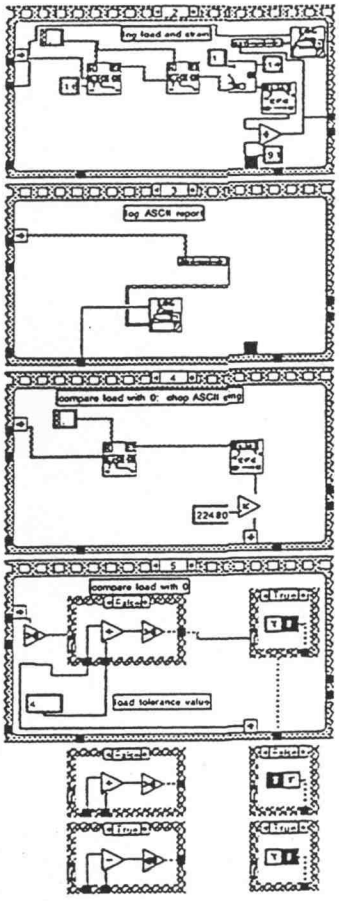
log load and store
log ASCII report
compare load with 0: chop ASCII
22480
compare load with 0
Load tolerance value
True
False

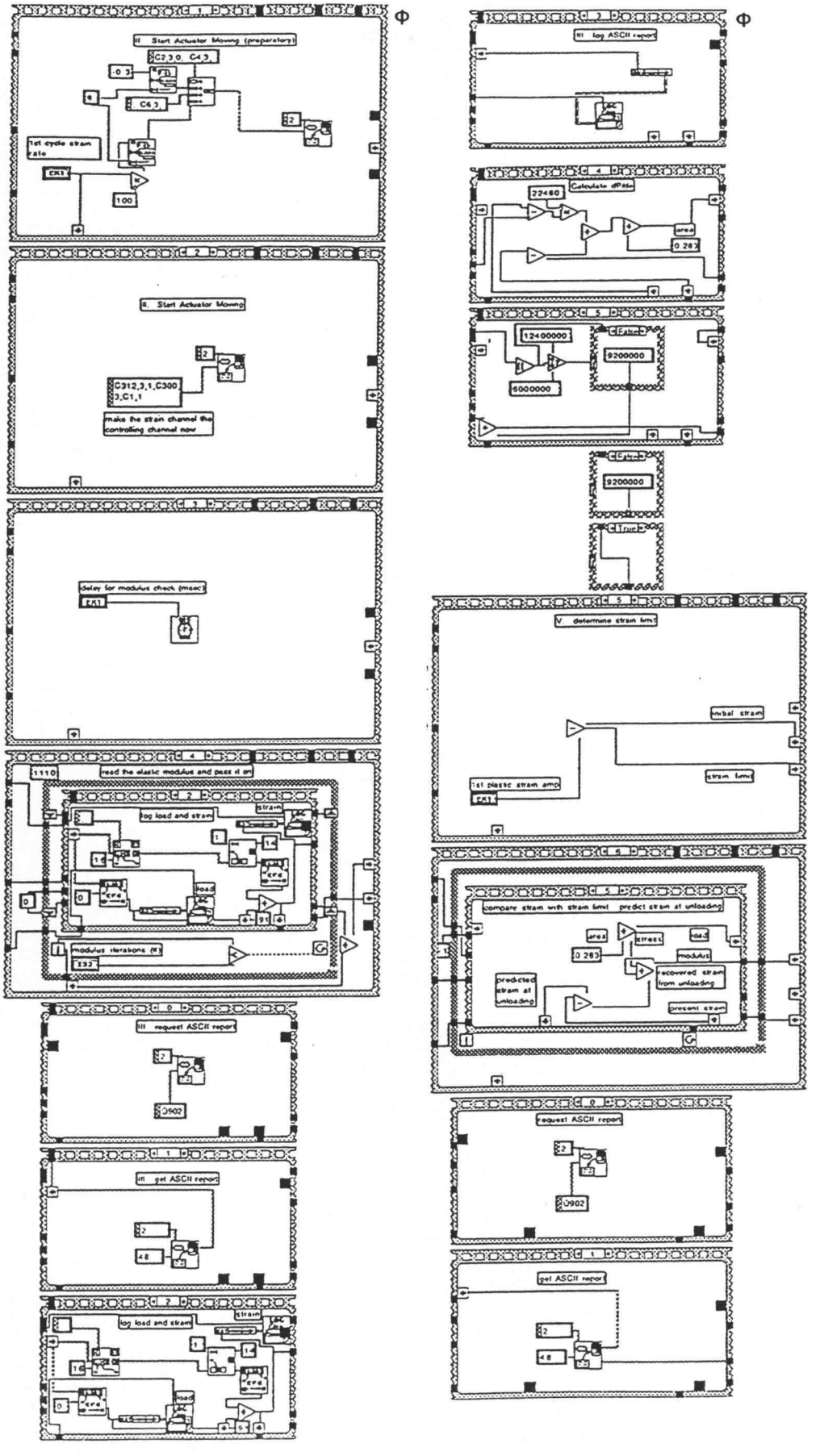
I. Start Actuator Moving (preparatory)
C23,0 C43,
C63,
1st cycle strain rate
CAL
100
II. Start Actuator Moving
C312,3,1,C300
3,C1,1
make the strain channel the controlling channel now
delay for modulus check (msec)
CAL
1110
read the elastic modulus and peak strain
log load and strain
strain
load
modulus iterations (N)
III request ASCII report
0902
IV get ASCII report
48
log load and strain
strain
load
III log ASCII report
22480
Calculate dP/dt
prod
0.283
12400000
9200000
6000000
9200000
True
V. determine strain limit
initial strain
strain limit
1st plastic strain amp
CAL
compare strain with strain limit predict strain at unloading
prod
stress
load
0.283
modulus
predicted strain at unloading
recovered strain from unloading
present strain
request ASCII report
0902
get ASCII report
48

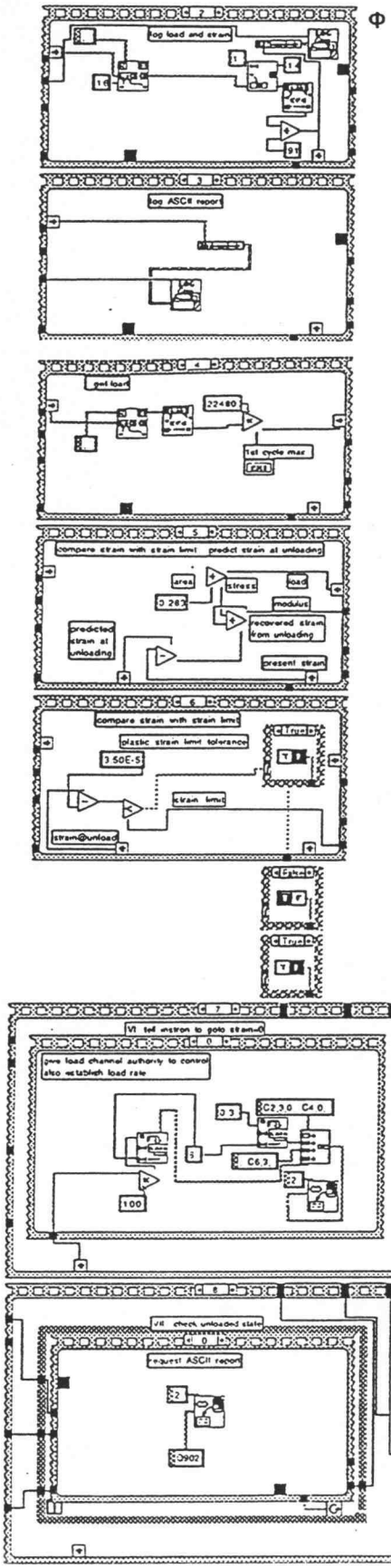
log load and strain
log ASCII report
get load
22480
set cycle max
compare strain with strain limit predict strain at unloading
area
stress
load
0.283
modulus
predicted strain at unloading
recovered strain from unloading
present strain
compare strain with strain limit
plastic strain limit tolerance
3.50E-5
strain limit
strain@unload
True
False
VI set motron to goto strain-0
pwm load channel authority to control
also establish load rate
0.3
C2,3,0 C4 0
C6 3
100
request ASCII report
0902

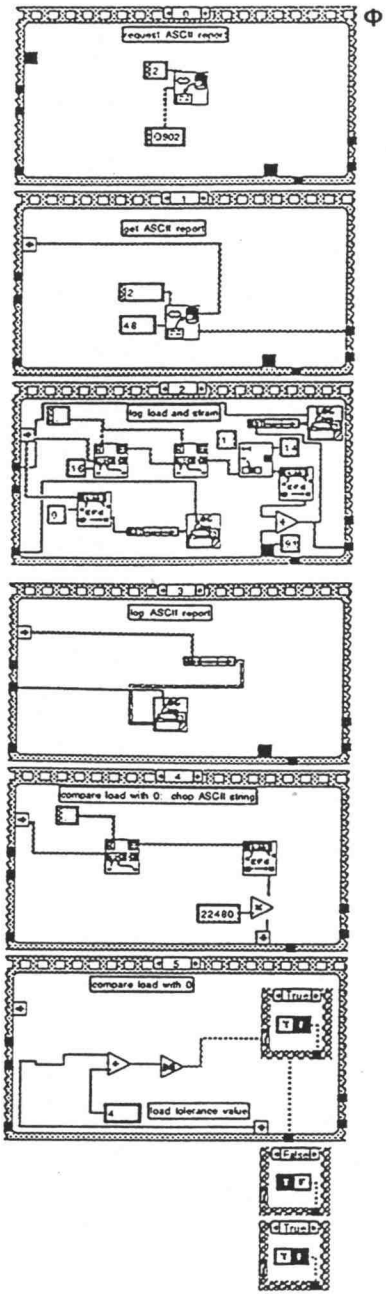
request ASCII report
0902
get ASCII report
32
48
log load and strain
log ASCII report
compare load with 0: chop ASCII string
22480
compare load with 0
load tolerance value
True
False

APPENDIX G

Thin Foil Buckling Calculation

Given: A thin foil of aluminum with some measured angle of bend θ measured relative to the foil surface.

Required: What is the maximum shear stress in the material due to the bend alone?

Solution:

assumptions:
* to keep this simple, let's model the thin foil as an isotropic, elastically deforming, prismatic beam
* the beam bends uniformly
* small angle approximation can be used

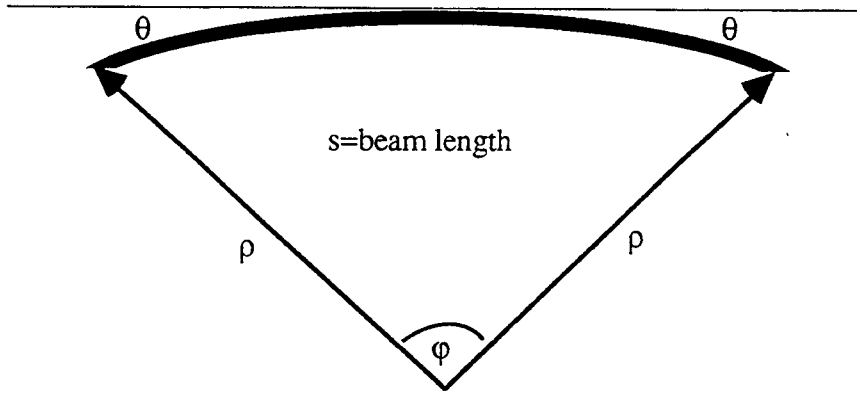

If there is an angle of bend θ, then there is an associated radius of curvature ρ. Geometry then dictates that

$$\rho \cdot \varphi = s \qquad \text{and} \qquad 2 \cdot \theta = \varphi$$

combining these yields:

$$\rho = \frac{s}{2 \cdot \theta} \qquad \text{eq 1}$$

where s is the segment length.

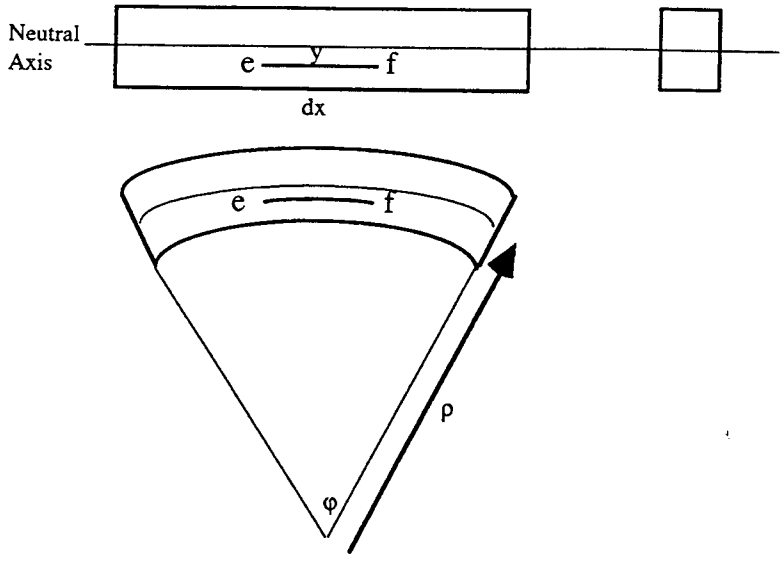

where y is the distance from the neutral axis (plane of zero stress) to the plane of interest (e-f); dx is the original length of segment e-f and L is the length of e-f after the bending.

From geometry, we know that the length of segment e-f after bending will be:

$$L = d\varphi(\rho - y) \qquad \text{eq 2}$$

If we factor out a ρ we have:

$$L = \rho \cdot d\varphi(1 - \frac{y}{\rho}) \qquad \text{eq 3}$$

and since $\rho \cdot d\varphi = dx$, we have:

$$L = dx(1 - \frac{y}{\rho}) \qquad \text{eq 4}$$

Now, distribute the dx:

$$L = dx - dx\frac{y}{\rho} \qquad \text{eq 5}$$

We calculate the elongation from the final length by subtracting the original length from the final length, or L-dx:

$$\textit{elongation:} \quad L - dx = -dx\frac{y}{\rho} \qquad \text{eq 6}$$

The strain is simply the elongation divided by the original length, or

$$strain\,(\varepsilon)=\frac{elongation}{original\ length}=\frac{-dx\frac{y}{\rho}}{dx}\Rightarrow-\frac{y}{\rho}$$

$$\varepsilon=-\frac{y}{\rho} \qquad \text{eq 7}$$

From basic mechanics, we have the 1-D Hooke's Law (for elastic deformation with small strains):

$$\sigma=E\varepsilon \qquad \text{eq 8}$$

Now, we combine equations 7 and 8:

$$\sigma=-\frac{E\cdot y}{\rho} \qquad \text{eq 9}$$

Substituting equation 1 into equation 9 for ρ:

$$\sigma=-\frac{Ey\cdot 2\theta}{s} \qquad \text{eq 10}$$

If t is the thickness of the foil, we know that the maximum (normal) bending stress occurs where $y=\pm\frac{t}{2}$, so the maximum normal stress is:

$$\sigma_{max}=\mp\frac{Et\cdot\theta}{s} \qquad \text{eq 11}$$

and the maximum shear stress τ_{max} will be $\sigma_{max}/2$:

$$\tau_{max}=\left|\frac{Et\cdot\theta}{2s}\right| \qquad \text{eq 12}$$

Insert Values To Determine Bending Stress

For our aluminum thin foils we have E=70GPa, t=5μm, and s=30μm. From Honeycombe, we know that the critical resolved shear stress in aluminum, at room temperature, 99.999% pure, for (111) oriented single crystal, is 0.54-0.98 MPa.

Substituting values yields:

θ (degrees)	0.50	0.25	0.10	0.05	0.025	0.005
τ_{max} (MPa)	51	25	10	5.1	2.5	0.5

If the thickness changes, then the maximum stress changes proportionately for the same angle of bend. For example, with an angle of 0.04 degrees, a thickness of 5 microns has a max. shear stress of 0.04 MPa, while a thickness of 15 microns would have a maximum shear stress of 0.12 MPa. So, the thicker parts of a foil (or thicker foils) would tend to have greater stresses in them for the same angle of bend.

Even with the conservative nature of this simple analysis we find that there may be high enough stress present to move dislocations (due to foil buckling with bend in the thin foil of as little as 0.005 degrees). In other words, 0.005 degrees of bend may be enough of a bend in the foil to cause dislocations to move.